New insights into the halide-related reactions on platinum surfaces - an electrochemical investigation

BMS Mogwase

orcid.org 0000-0002-3865-6676

Thesis submitted in fulfilment of the requirements for the degree *Doctor of Philosophy in Chemistry* at the North-West University

Promoter:	Prof RJ Kriek
Co-promoter:	Prof SW Vorster

Graduation July 2019

16864204

Declarations

I, Boitumelo Mogwase, declare that the thesis entitled: **"*New insights into the halide-related reactions on platinum surfaces – an electrochemical investigation*"**, submitted in fulfilment of the requirements for the degree *Philosophiae Doctor* in Chemistry, is my own account of research, unless otherwise stated. It contains as its main content, work which has not previously been submitted for a degree at any tertiary institution.

Signed at North-West University

Signature: …  …… Date: …16 – 11 – 2018……

Preface

I Boitumelo Mogwase, state that I have chosen the full-thesis format for submitting this thesis.

Conference poster presentations

- **B.M.S. Mogwase**, R.J. Kriek and S.W. Vorster**.** Calibration of an Electrochemical Quartz Crystal Microbalance by the electrodeposition of silver on a platinum quartz electrode, *CATSA Conference*, Cape Town, South Africa, November **2015**.

- **B.M.S. Mogwase**, R.J. Kriek and S.W. Vorster**.** An electrochemical comparative study of glassy carbon and carbon/quartz electrodes in hexachloroplatinic acid, *CATSA Conference*, Champagne Sports Resort, Drakensberg, Kwazulu Natal South Africa, November **2016**

- **B.M.S. Mogwase**, S.W. Vorster and R.J. Kriek. The Formation of Anodic Oxide Films on Pt in 0.5 M H_2SO_4, 4^{th} *International Symposium of Electrochemistry, "Pure and Applied Electrochemistry"*, School of Hospitality and Tourism, University of Johannesburg (UJ), South Africa, April **2018**

Acknowledgements

Firstly, I would like to give thanks to The Almighty, Your Glory surpasses all. I would like to say thank you with the Bible scripture from the Book of Exodus 33: 18-23 NIV.

- I would like to greatly acknowledge my supervisor, Prof. R.J. Kriek, for his guidance, supervision, motivation, and for making sure that I always reach my full potential and think outside the box.

- To my co-supervisor and also proof editor, Prof. S.W. Vorster, I am out of words, no amount of 'Thank You' can compensate my gratitude to you. I will forever be grateful. Sir Isaac Newton wrote,

  "If I have seen further it is by standing on the shoulders of giants"

  Thank you for allowing me to stand on your shoulders and for living this dream with me.

- To my colleagues, Mr. Neels le Roux, Dr. Vasillica Badets, Dr. Zafar Iqbal, Mr. Zach Sehume, Mr. Romanus Uwaoma, Miss Huguette Kishinkwa, Mr. De Wet Coertzen, Mr. Lizwi Gule and Dr Anzel Falch, thank you, be it in a scientific or personal capacity. I would like to also thank Mrs Hestelle Stoppel and Mrs Lara Kroeze for administration and ordering of chemicals.

- To my family and friends, thank you all for the love and support. *"Le Boitumelo jwa me"*

- I would like to thank Dr. Anine Jordaan in the Laboratory for Electron Microscopy of the CRB, NWU (Potchefstroom Campus) For SEM-EDX analysis.

- Additionally, I acknowledge the Microscopy and Microanalysis Unit (MMU) of the Witwatersrand University for AFM analysis.

- Also, acknowledge the Central Analytical Facility (CAF) of the University of Stellenbosch for ICP-MS analysis.

- Moreover I would like to greatly acknowledge the Hydrogen South Africa Infrastructure Center of Competence (HySA CoC) and the National Research Foundation (NRF) for funding.

- Lastly I would like to acknowledge the Chemical Resource Beneficiation (CRB) Focus Area for admissions for the degree in Chemistry.

ABSTRACT

The results of an electrochemical investigation of polycrystalline platinum are presented. The aim of the study was the elucidation of aspects of the electrochemistry of polycrystalline platinum in 0.5 M sulphuric acid solution and differing concentrations of halides (chloride, bromide and iodide). Conventional cyclic voltammetry (CV) (both single cycle and multicycle techniques) formed the cornerstone of the study, while a variety of supplementary experimental techniques were also employed, namely the electrochemical quartz crystal microbalance (EQCM), ICP-analyses, X-ray diffraction (XRD), scanning electron microscopy (SEM) and atomic force microscopy (AFM). Both glassy carbon and platinum metal electrodes were employed.

By studying eight linked potential peaks in the CVs it was ascertained that the reduction of $[PtCl_6]^{2-}$ to $[PtCl_4]^{2-}$ occurred between 0.15 and 0.03 V (SHE), followed by the incomplete reduction of $[PtCl_4]^{2-}$ to Pt. Furthermore, the simultaneous adsorption and desorption reactions of (H_2^+) and (H_3O^+) could be identified in the CVs and correlated with published results. A notable observation is the occurrence, under certain experimental conditions, of an isopotential point in the CVs. The interplay between the reduction of $[PtCl_6]^{2-}/[PtCl_4]^{2-}$ and the reduction/oxidation of hydrogen-containing species perfectly fit the H_2^+/H_3O^+ model, and supports the mechanism for the HER to proceed via the adsorbed molecular hydrogen ion $(H_2^+)_{ads}$ as intermediate. The formation of oxide films from oxygen species was viewed from a metal passivation perspective and led to a new model for the oxidation process which, *inter alia* suggests that the frequently reported "place exchange" process involve oxygen species entering the platinum subsurface lattice by occupation of tetrahedral and octahedral interstices, rendering them electrochemically inert, thereby explaining the phenomenon of hysteresis associated with the reduction of platinum anodic oxide films.

By interrupting the positive-going CV potential scans for a specified time (100 s) at specific holding potentials, followed by the reduction cycle, the electrochemical reactions occurring at those potentials could be amplified, leading to a better understanding of the processes involved. Another innovation was to graphically represent Pt mass loss at different potentials together with mass gains as determined by EQCM. Valuable information on the adsorption/desorption and reactions of species at the different holding potentials was obtained, especially when halide ions were present. The influence of the halide ions (Cl^-, Br^- and I^-) on the Pt oxidation was studied in electrolytes containing 6, 60 and 600 μM ions. Regarding hydrogen evolution a clear tendency was observed in going from Cl^-, to Br^-, to I^-, in that hydrogen adsorption/desorption diminishes with two peak pairs being evident for Cl^-, one peak pair for Br^-, and no peaks for I^-.

Keywords: *Platinum, oxide, electrochemical quartz crystal microbalance (EQCM), chloride, bromide, iodide, electrodes, glassy carbon, hydrogen, cyclic voltammetry, holding potential*

TABLE OF CONTENTS

LIST OF FIGURES

LIST OF TABLES

LIST OF ABBREVIATIONS

A	Ampere
AR	Analytical reagent
AFM	Atomic force microscopy
AES	Auger electron spectroscopy
CA	Chronoamperometry
CE	Counter electrode
CV	Cyclic voltammetry
DL	Double layer
EQCM	Electrochemical quartz crystal microbalance
EQCN	Electrochemical quartz crystal nanobalance
EASA	Electrochemically active surface area
EDX	Energy dispersive x-ray
GC	Glassy carbon
HCPA	Hexachloroplatinic acid
HER	Hydrogen evolution reactions
HOR	Hydrogen oxidation reactions
ICP-MS	Inductively coupled plasma mass spectroscopy
ML	Monolayer of atoms
NHE	Normal hydrogen electrode
ORR	Oxygen reduction reactions
Pt	Platinum
PEM	Proton exchange membrane
PEMFCs	Proton exchange membrane fuel cells
RE	Reference electrode
RHE	Reversible hydrogen electrode
SCE	Saturated calomel electrode
SEM	Scanning electron microscopy
SOEC	Solid oxide electrolysis cells
SHE	Standard hydrogen electrode
UPD-H	Underpotentially deposited hydrogen
WE	Working electrode
XRD	X-ray diffraction

LIST OF SYMBOLS

Å	Angstrom	m	Mass
N_A	Avogadro's constant	μ	Micro
cm	Centimeters	m	Milli
ΔQ	Change in charge	ml	Milliliters
Δm	Change in mass	mm	Millimetre
Δ*f*	Change in resonance frequency	M	Molarity
Q	Charge	mol	Mole
$Q_{ox,form}$	Charge of oxide formation	M_W	Molecular weight
$Q_{ox,red}$	Charge of oxide reduction	n	Number of moles of atoms
C	Coulomb	n	Order of harmonic
i	Current	i_{pa}	Peak current anodic
^oC	Degrees centigrade	i_{pc}	Peak current cathodic
ρ	Density	E_{pa}	Peak potential anodic
e	Electron Charge	E_{pc}	Peak potential cathodic
E_f	Flade potential	d_m	Planar density of the surface material
g	Grams	*f*	Resonance frequency
Hz	Hertz	s	Seconds
E_p	Holding potential	C_f	Sensitivity factor
t_p	Holding time	μ	Shear modulus
H_{ads}	Hydrogen adsorption	V	Voltage
H_{upd}	Hydrogen underpotentially developed	wt %	Weight percentage

CHAPTER 1

BACKGROUND TO THE INVESTIGATION

1.1 Introduction

The main reasons for the pursuit of hydrogen technologies are climate change and fossil fuel depletion.[1] The global demand for electricity is forever increasing with no indication of stabilising or decreasing (Figure 1-1).[2] By far the greatest portion of the electricity supply technologies is based on fossil fuels (coal, oil and natural gas) with the amount of carbon dioxide (CO_2) having been emitted in 2015 being double that of fourty years prior (Figure 1-2 (A) and Figure 1-2 (B)).[2]

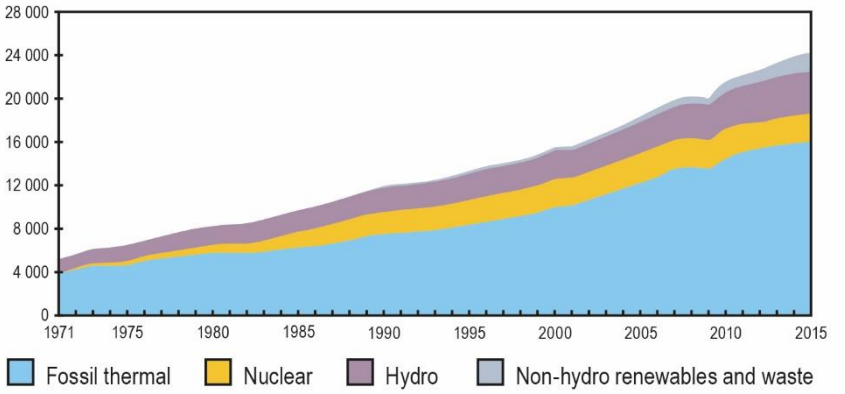

Figure 1-1: Global electricity generation from 1971 to 2015 by fuel (TWh) (Redrawn from[2])

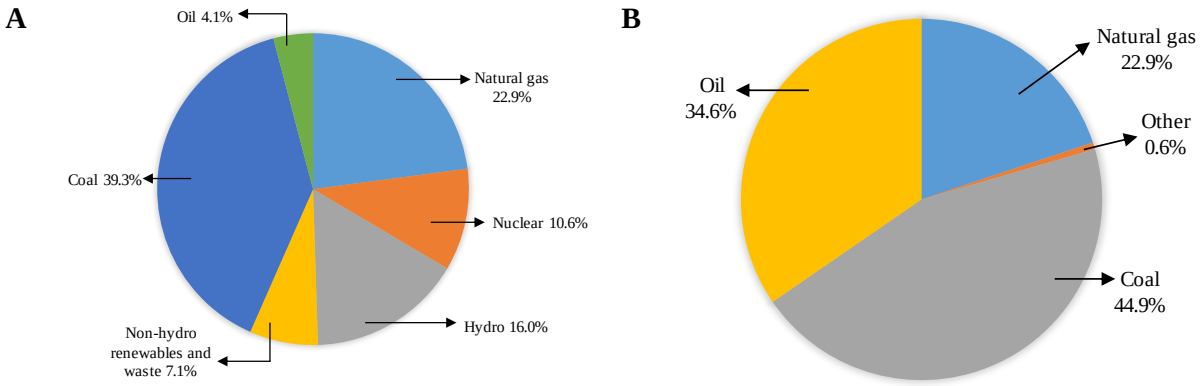

Figure 1-2: A. Fuel share (24255 TWh total), and B. CO_2 source (32294 Mt total), for the production of electricity in 2015 (Redrawn from[2])

If renewable energy sources are used for its production, hydrogen will be the cleanest energy carrier that could be used by mankind. H_2 is used in internal combustion engines, turbines, cookers, gas boilers and fuel cells. Currently around the world hydrogen is produced from three main sources, namely natural gas, coal and water by utilizing nuclear, biomass, solar and wind energy.[1] A promising technique for water splitting is electrolysis,[3] which currently supplies 4-5% of hydrogen produced on a global scale.[1,4] The energy requirement is, however, high due to the endothermic splitting reaction.[4] All electrolysers consists of a cathode and an anode (frequently made of platinum) immersed in an electrolyte (which may be acidic or alkaline), and when direct electrical

current is applied water is split into hydrogen at the cathode and oxygen at the anode (Equation 1-1). Inefficiencies and losses, however, result in an energy requirement in excess of 285.8 kJ.mol^{-1}.[5]

$$H_2O + 285.8\ kJ.mol^{-1} \rightarrow H_2 + ½O_2 \quad (1\text{-}1)$$

The most common electrolysis technologies are based on proton exchange membrane (PEM), and alkaline and solid oxide electrolysis cells (SOEC). Water is introduced into the PEM electrolyser in the anode compartment where it is split into hydrogen ions, H^+ and oxygen. The hydrogen ions move to the cathode, through a membrane, where it is reduced to form H_2. In the SOEC and alkaline processes water is introduced in the cathode area to form H_2, with the separation of H_2 from water occurring external to the cell. Hydroxide ions (OH^-) migrate through the aqueous electrolyte to the anode where oxygen is produced. A certain amount of the electrical energy used in the SOEC is actually substituted with thermal energy. In both acidic and alkaline electrolysers the oxygen evolution reaction (OER) is the rate limiting step, and in acidic electrolysers platinum (Pt) is used to increase the rate of water splitting and thereby the efficiency of the electrolyser.

A renewable non-polluting source of electric energy is provided by fuel cells powered by the electrochemical reactions involving the oxidation of hydrogen and the reduction of oxygen. However, successful commercialization still requires further research.[6] The oxygen reduction reaction (ORR) is about six orders of magnitude slower than the anodic hydrogen oxidation reaction (HOR).[6,7] Pt catalysts play an indispensable role in both the production and application of hydrogen, e.g. in polymer electrolyte membrane fuel cells (PEMFCs). To increase the efficiency of electrolytic hydrogen production and application technologies, it is imperative to gain more insight into the surface processes occurring on Pt. It is furthermore imperative to reclaim Pt from spent platinum-containing materials, such as catalysts, to conserve resources with a view to future demand.[8]

Specifically adsorbed anions on platinum have an adverse effect on its efficiency as a catalyst.[9] It has been proposed that the Pt oxide does not appreciably influence the adsorption energy of reaction intermediates, but that it blocks active sites for the ORR.[10] Pt oxide has been shown to play a role in promoting Pt dissolution during the oxidation of Pt and reduction of Pt oxides.[11] It has been shown, with regard to PEMFC electrocatalyst degradation, that platinum dissolution and subsequent re-deposition of platinum is of great importance in limiting the lifetime of the electrocatalyst. Even though the anodic formation of Pt oxides has been studied for many years, understanding their exact electrochemical behaviour is still largely lacking.[12,13] For example, it is unknown whether or not anodic platinum dissolution takes place in competition to its oxide formation, during the cathodic reduction of the oxide, or through chemical dissolution of the produced platinum oxide.[14]

In contrast to other metals that show active dissolution behaviour, Pt dissolution differs fundamentally in that it is a transient process occurring only when the surface state is changed by changes in the potential.[14] The dissolution of platinum can therefore not be explained through a model that assumes the existence of reaction

equilibria between the oxidized and reduced surfaces, as well as the dissolved species.[15] Consequently, entrenched theories will have to be changed to describe the mechanism of dissolution of platinum at fixed potential.[14]

The full commercialization of fuel cells is largely impeded by the durability of the cell compartments, especially the electrocatalysts. Apart from dissolution via Pt oxides, corrosive degradation of the platinum components of fuel cells may be caused by chloride impurities, originating from airborne salts.[16] Cl^- adsorption was reported to occur in two stages, one associated with H_{upd} desorption, and the second, occurring at more positive potentials, associated with concurrent OH_{ad} formation.[17] It is now generally accepted that the adsorption strength follows the order $F^-_{ad} < Cl^-_{ad} < Br^-_{ad} < I^-_{ad}$.[17] In 0.5 M H_2SO_4 I^-, Br^-, and Cl^- poison the Pt surface with halide ad-atoms that result in the decrease of hydrogen adsorption/desorption in the lower potential region (0.06–0.4 V) and electro-oxidation of Pt in the 0.6–1.2 V potential region. Above a concentration of about 5×10^{-6} M, I^- ions strongly adsorbs and mask the H_{upd} features, while Br^- and Cl^- ions change the peak characteristics in the H_{upd} region. At potentials above about 1.2 V the simultaneous evolution of the halogen (in gaseous form), the evolution of oxygen, and the oxidation of platinum, are observed.[9] It has been reported that Cl^- blocks the initial OH monolayer selectively on the platinum surface, while the formation of the surface oxides is blocked non-selectively by Br^- and I^- over a wide potential range, which point to a difference in the charged state of adsorbed Br^- and I^-.[18] The adsorption of iodine atoms occurs in a nonuniform fashion in which only about 60% of the electrode surface seems to be available. It is thought that the rest of the surface may be covered in platinum oxide.[19,20] A survey of the literature has shown that while extensive research is being done on the influence of the chloride ion, comparatively little work has been published on the influence of Br^- and I^-.

1.2 Motivation for this investigation

From the above discussion it is clear that the challenge at hand is to improve the stability of platinum and platinum-based electrocatalysts for fuel cell applications as well as other electrochemical energy applications. In this regard a comprehensive and quantitative understanding of the mechanism of dissolution of platinum and the influence that the applied operational conditions have, is demanded.[14,16] Therefore, the main practical problem can be identified as a need for clarification of a number of issues that adversely affect the optimum application of Pt in technologies such as the splitting of water to produce hydrogen and the efficient utilization of Pt's catalytic properties. These many-faceted problems have to be, of necessity, studied initially using conventional electrochemical techniques. The main areas of interest are best described with the aid of a generic cyclic voltammogram (CV) of Pt in an acidic medium (Figure 1-3):

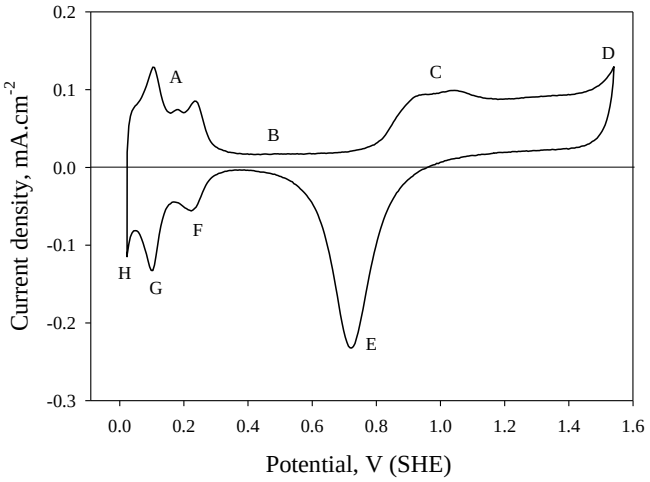

Figure 1-3: CV for platinum in acidic media

The main regions of interest are divided into 7 as follows:

A Hydrogen desorption

B Double layer charging

C Oxide formation

D Gas evolution

E Reduction

F Underpotential hydrogen development

G Hydrogen adsorption

H Hydrogen evolution

Areas A, F, G and H involve reactions pertaining to the evolution of hydrogen. Areas C, D and E are of interest when studying surface films on Pt, for example oxides.

1.3 The objectives of the study

- The first objective is to investigate platinum metal that is deposited in situ on glassy carbon electrodes from a hexachloro-platinic acid (H_2PtCl_6) electrolyte.
- The second objective of this study is to provide new insights into the reactions pertaining to the electrochemistry of platinum in acidic media with and without the presence of chloride, bromide and iodide ions.

1.4 Scope of the study

A thorough literature study was conducted regarding the following topics:

- Electrodeposition of platinum from hexachloroplatinic acid on glassy carbon electrodes.
- Nature of surface films formed during anodic polarization in acidic media together with halide ions.

This project entails:

a. The hydrogen evolution reaction in the context of electrochemical interaction between H_2PtCl_6 and H_2O/H_3O^+
b. Anodic oxide growth on platinum in sulphuric acid electrolytes.
c. Anodic oxide growth on platinum in sulphuric acid electrolytes containing chloride, bromide and iodide ions.

1.5 Methodology

1.5.1 Electrochemical investigation

- A three-electrode system was employed across different potential points (E_p) to generate either single or multiple cyclic voltammetry, and where necessary, chronoamperometry in order to study the materials under investigation.
- A quartz crystal microbalance (QCM) coupled with a potentiostat to form an electrochemical quartz crystal microbalance (EQCM) wase used to determine the mass changes of the materials under investigation.

1.5.2 Dissolution

- The inductively coupled plasma mass spectroscopy (ICP-MS) was used to determine the amount of the material dissolved in the electrolyte subsequent to subjecting the materials under investigation to various chemical and electrochemical procedures.

1.5.3 Characterisation

- X-ray diffraction (XRD) was employed to determine the preferred orientation of the material under investigation.
- Scanning electron microscopy (SEM-EDX) coupled with an electron dispersive x-ray spectroscopy was used to determine the surface morphology and composition of the materials under investigation.
- Subsequent to subjecting the materials under investigation to various chemical and electrochemical procedures, atomic force microscopy (AFM) was employed to determine the surface roughness of the material under investigation.

1.6 Thesis outline

In this thesis Chapter 2 provides an overview of the experimental investigations. Chapter 3 contains the results obtained with Pt/glassy carbon electrodes in an electrolyte containing H_2PtCl_6 with a view to study the hydrogen evolution reaction. Chapter 4 shows the results pertaining to the anodic oxidation of Pt in 0.5 M H_2SO_4, while Chapter 5 describes the role of Cl^- ions in Pt oxidation at the anode. Chapter 6 treats the results

obtained with electrolytes containing Br^- ions and in Chapter 7 the role of electrolytes containing I^- ions is reported. Chapter 8 contains the main conclusions and proposed future work.

Each of chapter 3, 4, 5, 6 and 7 has the following outline:

- Introduction, which presents the background and a literature survey.
- Experimental, which refers back to Chapter 2 (Experimental Section).
- Results and discussions
- Conclusions
- References

1.7 References

1 Nikolaidis, P. & Poullikkas, A. A comparative overview of hydrogen production processes. *Renewable and sustainable energy reviews* **67**, 597-611 (2017).

2 International Energy Agency, World Energy Statistics, https://doi.org/10.1787/world-energy-stats-2017-en, (2017).

3 Bamberger, C. & Richardson, D. Hydrogen production from water by thermochemical cycles. *Cryogenics* **16**, 197-208 (1976).

4 Mazloomi, S. & Sulaiman, N. Influencing factors of water electrolysis electrical efficiency. *Renewable and Sustainable Energy Reviews* **16**, 4257-4263 (2012).

5 Carmo, M., Fritz, D.L., Mergel, J. & Stolten, D. A comprehesive review on PEM water electrolysis. *International Journal of Hydrogen Energy*, **38**, 4901-4934 (2013).

6 Debe, M. K. Electrocatalyst approaches and challenges for automotive fuel cells. *Nature* **486**, 43 (2012).

7 Rinaldo, S. G., Lee, W., Stumper, J. & Eikerling, M. Mechanistic principles of platinum oxide formation and reduction. *Electrocatalysis* **5**, 262-272 (2014).

8 Jha, M. K., Lee, J. C., Kim, M. S., Jeong, J., Kim, B. S. & Kumar, V. Hydrometallurgical recovery/recycling of platinum by the leaching of spent catalysts: A review. *Hydrometallurgy* **133**, 23 (2013).

9 Devivaraprasad, R., Kar, T., Leuaa, P. & Neergat, M. Recovery of Active Surface Sites of Shape-Controlled Platinum Nanoparticles Contaminated with Halide Ions and Its Effect on Surface-Structure. *Journal of The Electrochemical Society* **164**, H551-H560 (2017).

10 Sugawara, S., Tsujita, K., Mitsushima, S., Shinohara, K. & Ota, K.-i. Simultaneous Electrochemical Measurement of Oxygen Reduction and Pt Oxide Formation/Reduction on Pt Nanoparticle Surface. *Electrocatalysis* **2**, 60-68 (2011).

11 Alsabet, M., Grden, M. & Jerkiewicz, G. Comprehensive study of the growth of thin oxide layers on Pt electrodes under well-defined temperature, potential, and time conditions. *Journal of Electroanalytical Chemistry* **589**, 120-127 (2006).

12 Topalov, A. A., Cherevko, S., Zeradjanin, A. R., Meier, J. C., Katsounaros, I. & Mayrhofer, K. J. J. Towards a comprehensive understanding of platinum dissolution in acidic media. *Chemical Science* **5**, 631-638 (2014).

13 Cherevko, S., Zeradjanin, A. R., Keeley, G. P. & Mayrhofer, K. J. A comparative study on gold and platinum dissolution in acidic and alkaline media. *Journal of The Electrochemical Society* **161**, H822-H830 (2014).

14 Topalov, A. A., Katsounaros, I., Auinger, M., Cherevko, S., Meier, J. C., Klemm, S. O. & Mayrhofer, K. J. J. Dissolution of platinum: limits for the deployment of electrochemical energy conversion? *Angewandte Chemie International Edition* **51**, 12613-12615 (2012).

15 Darling, R. M., Meyers & Jeremy P. Kinetic model of platinum dissolution in PEMFCs. *Journal of the Electrochemical Society* **150**, A1523-A1527 (2003).

16 Geiger, S., Cherevko, S. & Mayrhofer, K. J. J. Dissolution of Platinum in Presence of Chloride Traces. *Electrochimica Acta* **179**, 24-31 (2015).

17 Marković N. M. & Ross Jr. P. N. Surface science studies of model fuel cell electrocatalysts. *Surface Science Reports* **45**, 117-229 (2002).

18 Novak, D. & Conway, B. Competitive adsorption and state of charge of halide ions in monolayer oxide film growth processes at Pt anodes. *J. Chem. Soc., Faraday Trans. 1* **77**, 2341-2359 (1981).

19 Newson, J. & Riddiford, A. The kinetics of the iodine redox process at platinum electrodes. *Journal of the Electrochemical Society* **108**, 699-706 (1961).

20 Vetter, K. J. Der Einstellungsmechanismus des Jod-Jodid-Redoxpotentials an Platin auf Grund von Wechselstrompolarisation. *Zeitschrift für Physikalische Chemie* **199**, 285-299 (1952).

CHAPTER 2

EXPERIMENTAL METHODS

2.1 Introduction

Chapter 2 discusses the instrumentation and experimental methods that were used in this investigation. While conventional cyclic voltammetry (both single cycle and multicycle techniques) formed the mainstay of the study, a variety of supplementary experimental techniques were also employed in an effort to elucidate various experimental observations and provide additional insight. These techniques included cyclic voltammetry (CV), chronoamperometry (CA), electrochemical quartz crystal microbalance (EQCM), inductively coupled plasma mass spectroscopy (ICP-MS), X-ray diffractometry (XRD), scanning electron microscopy with electron dispersive x-ray spectroscopy (SEM-EDX) and atomic force microscopy (AFM).

2.2 Electrodes and electrolyte preparation

2.2.1 Glassy carbon electrodes

The electrodes, consisting of 0.5 cm diameter glassy carbon (GC) discs (SIGRADUR® G, HTW, Germany), were embedded in Teflon, with an exposed area of 0.196 cm^2, and were mechanically polished with diamond grit down to 1 µm (Strauss & Co., Industrial diamonds Ltd), followed by a final polish with 0.05 µm alumina (Gamma Micropolish II, Buehler), subsequent to which they were rinsed with ethanol (Merck), isopropanol (Merck), followed by Milli-Q water under ultrasonication and dried with nitrogen (Afrox, 99.999%). The electrodes were finally anodically oxidised at 2 V in a 0.1 M NaOH (Promark Chemicals) solution for 30 seconds in order to dislodge any polishing debris and remove oxide films from the surface. They were subsequently thoroughly rinsed with Milli-Q water before proceeding with the recording of multiple cycle voltammograms.

2.2.2 Platinum electrodes

To obtain reproducible and clean electrode surfaces, the platinum electrodes were preconditioned in 0.5 M H_2SO_4 (prepared from 98% AR (Analytical grade) H_2SO_4 from Rochelle Chemicals) by cycling between 0.021 and 1.5 V at least 20 times at a scan rate of 50 mV s^{-1}, or until there were no further changes in the voltammograms. In order to ascertain that the electrode surface was clean and the results were reproducible, the voltammogram (illustrated in Figure 2-1 below) had to show well-defined hydrogen desorption (A) and adsorption peaks (E), the double layer region (B), oxide formation peak(s) (C), the oxide reduction peak (D), and finally a baseline (at i = 0) that separates the anodic and the cathodic regions. In order to render the electrode oxide-free, the electrode was cycled five times in the region 0.021 V to 0.6 V in 0.5 M H_2SO_4 at a scan rate of 50 mV s^{-1}.

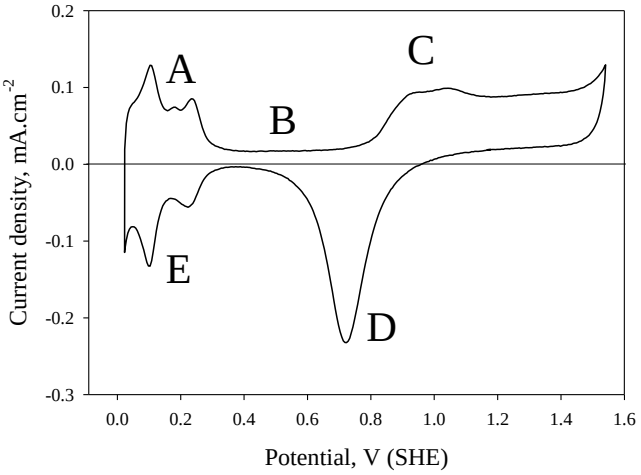

Figure 2-1: Voltammogram of a platinum electrode preconditioned in 0.5 M H_2SO_4 at a scan rate of 50 mV s^{-1}

2.2.3 Preparation of electrolytes

Three types of electrolyte were used in different stages of the investigation.

2.2.3.1 Electrolytes containing Hexachloroplatinic acid (HCPA)

The 2 mM H_2PtCl_6 electrolyte was prepared by dissolving the required weight of 99.995% $H_2PtCl_6.6H_2O$ (Sigma-Aldrich) in Milli-Q water. The pH of the electrolyte was 0.53 and was found to remain unchanged during polarization runs. A volume of 100 ml electrolyte was placed in the electrochemical cell and was deoxygenated by nitrogen (Afrox, 99.999 %) bubbling for at least 30 minutes before commencement of a run. A blanket of nitrogen was maintained above the electrolyte in the cell during execution of the run in order to minimize ingress of oxygen.

2.2.3.2 Electrolyte containing 0.5 M H_2SO_4

The electrolyte containing 0.5 M H_2SO_4 was prepared from 98% AR H_2SO_4 (Rochelle Chemicals) and Milli-Q.

2.2.3.3 Electrolytes containing halide ions

Sodium salts (99% AR sodium chloride, sodium bromide and sodium iodide, purchased from Associated Chemical Enterprises (Pty) Ltd) were prepared in 0.5 M H_2SO_4 with concentrations of 6, 60 and 600 µM of chloride, bromide and iodide ions.

2.3 Instrumentation and their application

2.3.1 The electrochemical cells

Two types of electrochemical cells were used. For the experiments with GC electrodes in electrolytes containing HCPA a two-compartment, three electrode system as illustrated in Figure (2-2) was employed inside a 100 ml jacketed reaction vessel (Pine Research) with the temperature fixed at 25 °C in all instances,

employing a Julabo F12-ED temperature controller. The working electrode (WE), consisting of a 0.5 cm diameter GC disc, a platinum wire helix counter electrode (CE) (Pine Instrumentation; total area of 0.477 cm^2), and a Ag/AgCl reference electrode (RE) from Radiometer were all connected to a Bio-Logic VMP3 potentiostat.

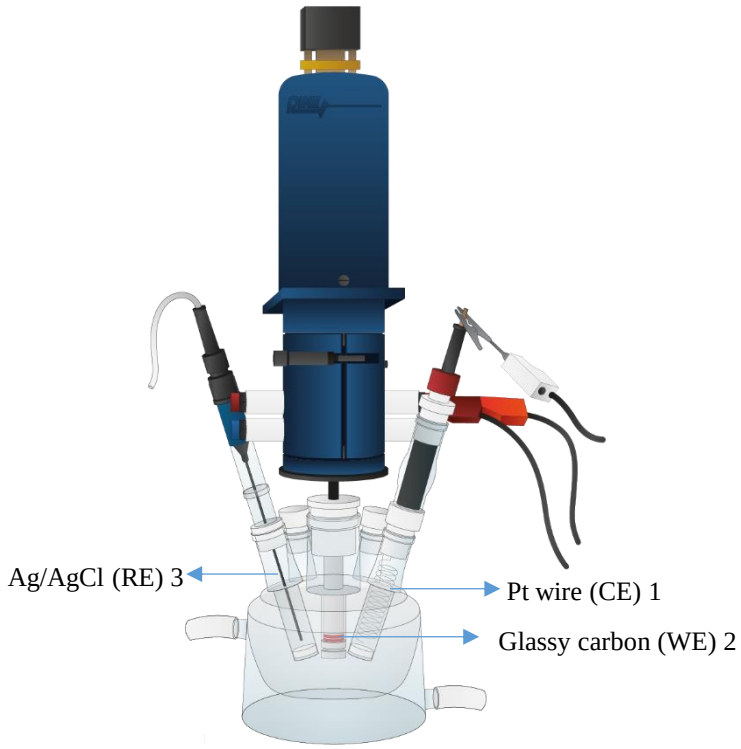

Figure 2-2: A two-compartment, three-electrode system

All experiments employing Pt quartz working electrodes were carried out in an in-house manufactured set-up as illustrated in Figure 2-3. The in-house manufactured double walled cell consisted of three electrodes. The working electrode (WE) which was a Bio-Logic AT cut quartz crystal resonator covered by a uniformly sputtered Pt layer (~300 nm) on top of a 100 nm substrate of titanium. The vibrational frequency was ~9 MHz in air and the electrode's geometric area was 0.196 cm^2. The Pt deposit was characteristically polycrystalline Pt, as evidenced by CVs and X-ray diffraction. The counter electrode (CE) was a platinum wire helix (Pine Instrument) situated in a glass tube, with a total area of 0.477 cm^2, and the reference electrode was a Radiometer Analytical saturated calomel electrode from Bio-Logic, positioned near the WE by means of a Luggin capillary. The working electrode holder is shown schematically in Figure 2-4, where it is firmly held by the two O-rings to avoid any electrolyte entering the electrode connection.

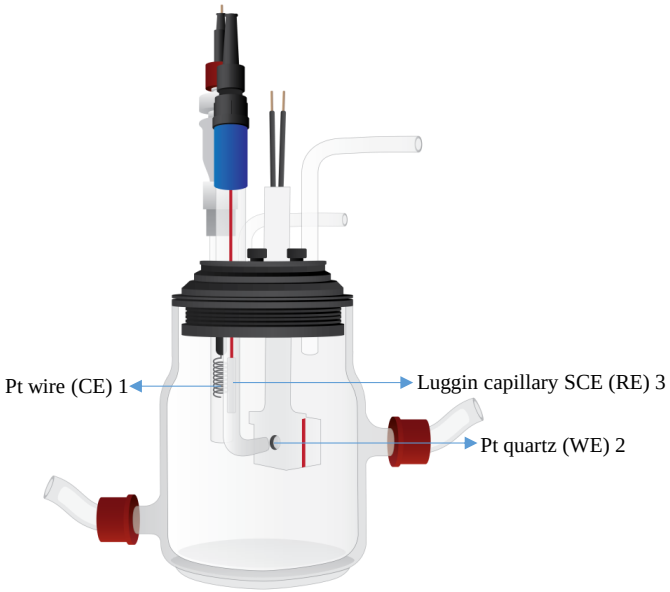

Figure 2-3: In-house constructed double walled cell used for experiments in Chapter 4, 5, 6, and 7

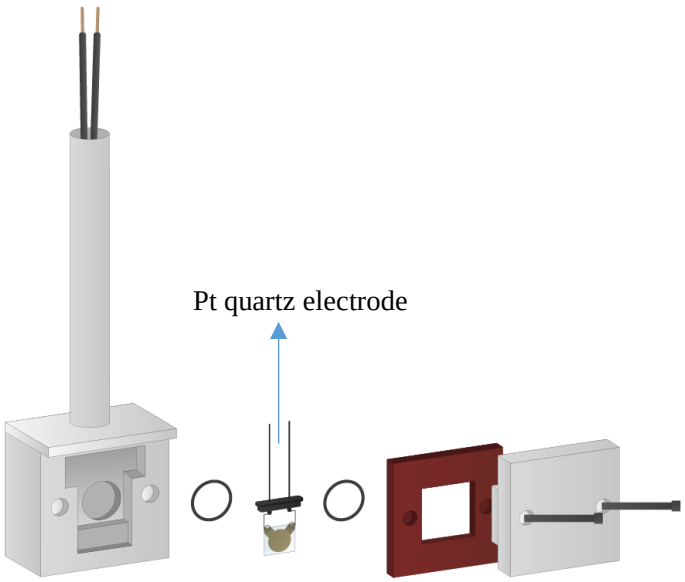

Figure 2-4: Schematic of working electrode holder

2.3.2 The potentiostat/electrochemical quartz crystal microbalance

For the Pt quartz electrode experiments, the Bio-logic model VMP3 potentiostat was coupled with a quartz crystal microbalance (SEIKO EG&G Quartz Crystal Analyzer QCA922) purchased from Bio-logic which, when placed in the electrolyte, is referred to as an EQCM. This arrangement forms a powerful tool in mechanistic studies of chemical or electrochemical processes at electrode surfaces. From the potentiostat there are two cables, one connects the quartz crystal microbalance to the potentiostat and the other one connects the electrodes (Figure 2-5). All electrochemical potentials were converted to Standard Hydrogen Electrode (SHE).

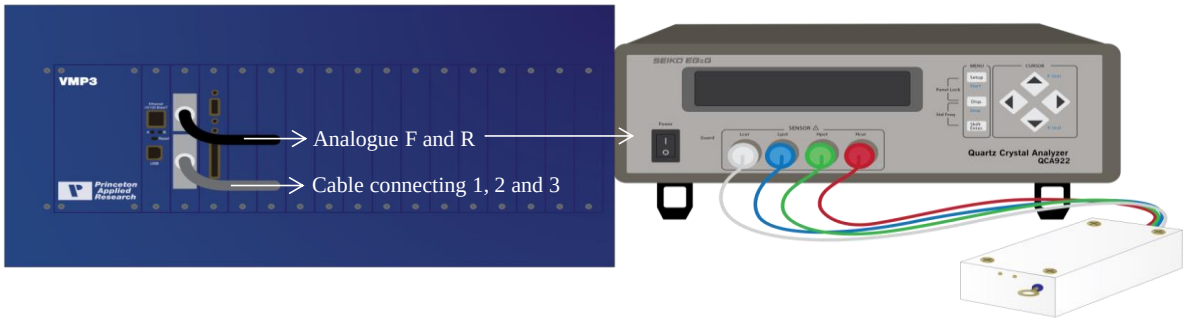

Figure 2-5: Schematic of the VMP3 potentiostat and SEIKO EG&G Quartz Crystal Analyser QCA922

2.3.3 The Faraday cage

In order to block electromagnetic fields which could influence measured currents and potentials a Faraday cage was made from aluminium sheet and a copper mesh, earthed and placed on top of a slate. In experiments requiring the use of the EQCM the electrochemical cell was placed inside the cage before recording voltammograms and mass changes.

2.4 ELECTROCHEMICAL TECHNIQUES USED

2.4.1 Cyclic voltammetry

Cyclic voltammetry is a prominent and widely used electroanalytical technique applied in many fields of chemistry to follow redox processes, reaction intermediates and the stability of reaction products at the working electrode by applying potentials in both the reverse and the forward directions while monitoring the current.[1] A redox system, for example platinum cycled in acidic electrolytes (Figure 2-6), gives rise to potential (E_{pa}, E_{pc}) and current (i_{pa}, i_{pc}) peaks of the anodic (oxide formation) and cathodic (oxide reduction) regions, which are very important parameters in cyclic voltammetric analysis.[1]

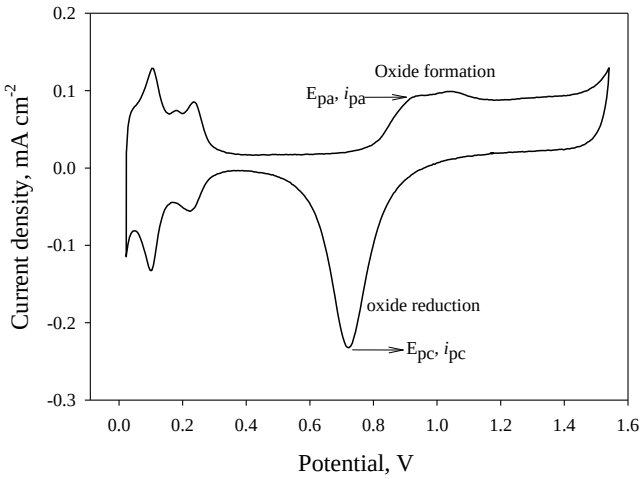

Figure 2-6: CV of platinum quartz electrode in 0.5 M H_2SO_4 at a scan rate of 50 mVs^{-1}

2.4.2 Chronoamperometry (CA)

Chronoamperometry is a technique used to measure the current of the working electrode while controlling the potential for a certain time interval. This plot of current (or current density) against time can be integrated to calculate the amount of charge, denoted by Q, that passed during the experiment. Also, depending on the reaction taking place, the current can be in the anodic or cathodic region. An example of a CA in the anodic region is shown in Figure 2-7 for a Pt quartz electrode in 0.5 M H_2SO_4. The potential applied was 0.8 V with the aim to grow an oxide layer for 300 s.

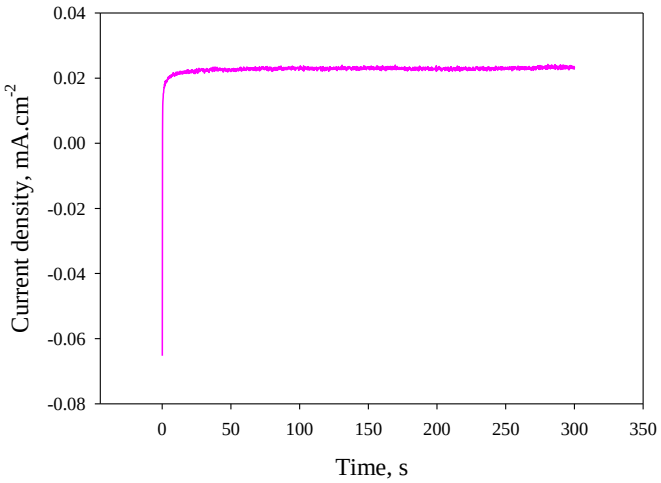

Figure 2-7: CA of a Pt quartz electrode in 0.5 M H_2SO_4 held at 0.8 V for 300 s

2.4.3 Multiple cycle voltammetry

In the investigations involving GC electrodes the potentiostat was set to generate a series of superimposed voltammograms in the potential range 0.5 to -0.023 V as demonstrated in Figure 2-8 below. This resulted in the deposition of Pt crystallites on the GC surface, initially on a few electrochemically active sites, but with each cycle deposition also occurred on the newly formed platinum crystallites. In the interpretation of the different reactions it was assumed that the glassy carbon substrate did not play an active role.

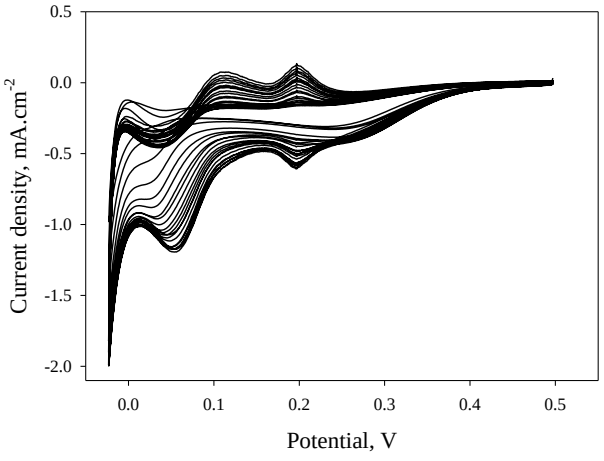

Figure 2-8: Multiple scan CV of a GC electrode in 2 mM HCPA with pH adjusted to 0.53 with HCl at a scan rate of 10 mV s^{-1}

2.4.4 Linear sweep voltammetry in the anodic region for oxide growth

For oxide growth, the experiments were performed inside an in-house manufactured faraday cage employing an in-house manufactured double-walled electrochemical cell incorporating a three electrode setup. Platinum oxide layers were grown in a two-stage process by linear sweep voltammetry starting at a scan of 0.6 V, scanning in the anodic direction to different maximum potential points (E_p) and holding the potential there for a time (t_p) of 100 s to allow further oxide growth at a scan rate of 50 mV s^{-1}. Subsequent to this holding time a 15 ml sample was taken for ICP-MS analysis so as to determine the concentration of Pt in solution. An example of a linear sweep voltammetry in the anodic region for the oxide growth is illustrated in Figure 2-9 below.

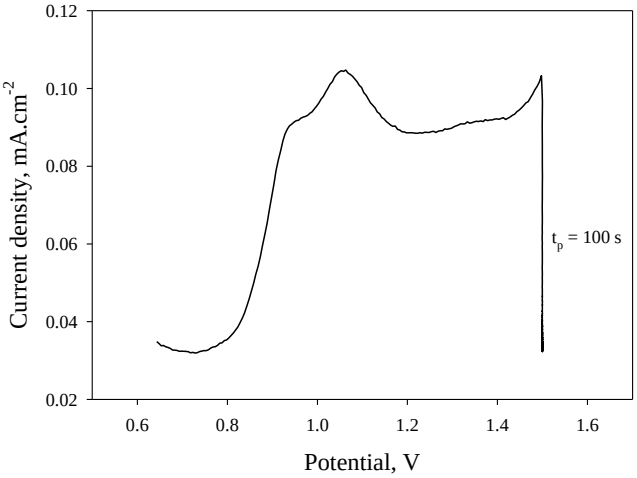

Figure 2-9: A linear sweep voltammetry of platinum electrode in 0.5 M H_2SO_4 at holding potential E_p = 1.5 V at holding time t_p = 100 s

This procedure was also followed for electrolytes containing 6, 60 and 600 μM of chloride, bromide and iodide in 0.5 M H_2SO_4.

2.4.5 Anodic linear sweep voltammetry to E_p followed by oxide growth for t_p and reduction

A similar procedure was followed as in Section 2.4.4, however, this was immediately followed by a semi cycle voltammogram sweeping in the cathodic direction in order to reduce (at about 0.7 V) any oxide that had formed. After completion of this reduction scan, scanning was continued to the hydrogen desorption and adsorption peaks with the scan terminating in the anodic direction at 0.6 V. A 15 ml sample was also taken for ICP-MS analysis to determine the amount of Pt in solution. A typical scan that followed this procedure is shown in Figure 2-10.

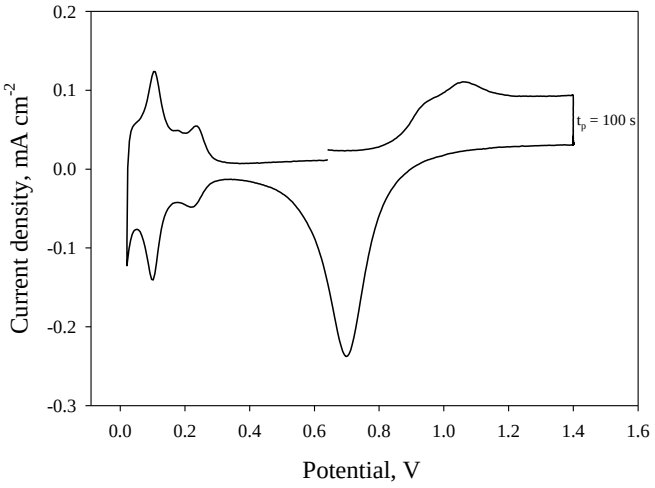

Figure 2-10: A linear scanning voltammetry coupled with a semi cyclic voltammogram of platinum electrode in 0.5 M H_2SO_4 at holding potential E_p = 1.4 V at holding time t_p = 100 s at a scan rate of 50 mV s^{-1}

This procedure was also followed for electrolytes containing 6, 60 and 600 μM halide ions of chloride, bromide and iodide in 0.5 M H_2SO_4.

2.4.6 Electrochemical Quartz Crystal Microbalance

A quartz crystal electrode (Bio-logic), covered on both sides with platinum, was inserted into an in-house manufactured Teflon holder (Figure 2-4) so that only one side faced the electrolyte. A small change of mass of the exposed area, which will cause a change in the resonant frequency of the quartz crystal, is related to a change in mass by the Sauerbrey equation (Equation 2-1):[2]

$$\Delta f = \frac{2f^2}{nA\sqrt{\mu\rho}}\Delta m = -C_f \Delta m \qquad (2\text{-}1)$$

where f is the resonance frequency of the unloaded quartz crystal, n is the order of the harmonic of the oscillating quartz, ρ is the density (2.648 g cm^{-3}) of the quartz crystal, μ is the shear modulus of the quartz crystal (2.947 x 10^{11} g cm^{-1} s^{-2}), A is the piezo-electric active area, which is the same as the geometric area (cm^2), Δf (Hz) is the change in resonance frequency, Δm is the change in mass per unit surface area (μg cm^{-2}), and C_f is the experimental sensitivity factor (Hz μg^{-1} cm^2). A wide-range of different commercial quartz crystals exhibit different sensitivities due to differences in resonant frequency, the material deposited, and the shear modulus of the quartz crystal. It is therefore necessary to determine the calibration constant C_f of the quartz crystal microbalance.[3]

2.4.6.1 Calibration of the EQCM

In this work, the method of calibration was adapted from Ratieuville *et al.*[2] The quartz/platinum was pre-treated according to the method described in Section 2.2.2, subsequent to which silver was electrodeposited onto the quartz crystal from a solution of 0.5 M H_2SO_4 containing 10^{-3} M 66.50% AR $AgNO_3$ (Promark Chemicals). The deposition was performed using chronoamperometry by holding the potential at 0.5 V for

time intervals ranging from 10 to 300 s. It has to be noted that in this study, after every deposition run, stripping of the deposited silver was performed at 1.041 V to allow re-use of the electrode during deposition, but to avoid contamination, all experiments were performed on a new platinum quartz electrode that had been pretreated.

The chronoamperometric plots were integrated to obtain the charge (Q) involved for each deposition run, which was then plotted against the associated change in frequency (Figure 2-11). From the slope of this graph, C_f was determined through a modified Sauerbrey equation (Equation 2-2) according to Faraday laws.[2]

$$\Delta f = -\frac{C_f M}{nF} Q \qquad (2\text{-}2)$$

Where C_f is the experimental sensitivity factor (Hz μg^{-1} cm^2), M is the molar mass of the silver deposited (g/mol), n is the number of electrons involved in the deposition reaction, Δf (Hz) is the change in frequency, and Q is the charge (C). The experimental C_f was found to be 182.8 Hz μg^{-1} cm^2, which is very close to the theoretical value of 183.2 Hz μg^{-1} cm^2 and can therefore be deemed to be accurate with percentage relative difference of 0.22%. The experimental C_f obtained was used to calculate the mass changes in Chapters 4, 5, 6 and 7 for comparison and accuracy.

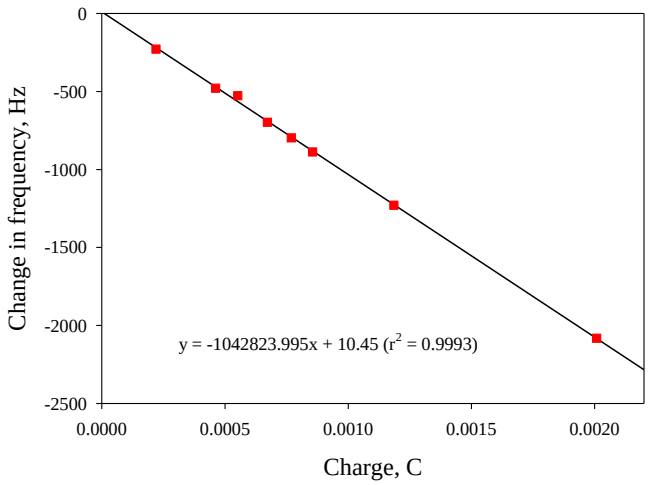

Figure 2-11: A plot of change in frequency vs silver deposition charge to obtain the slope

2.4.6.2 Data processing of the frequency changes

The frequency shift readings were mostly very noisy, which required smoothing, and were therefore filtered using the EC-Lab® software. For example, cyclic voltammetry of a platinum electrode in 0.5 M H_2SO_4, swept from 0.6 V to a holding potential (E_p) of 1.5 V and held there for 100 s, followed by reduction at about 0.7 V, moving through the hydrogen region again to 0.6 V, is shown below (Figure 2-12(A)) together with the accompanying shift in frequency (Figure 2-12(B)). The noise associated with the change in frequency (Figure 2-12(B)), in the absence of filtering, is clearly evident.

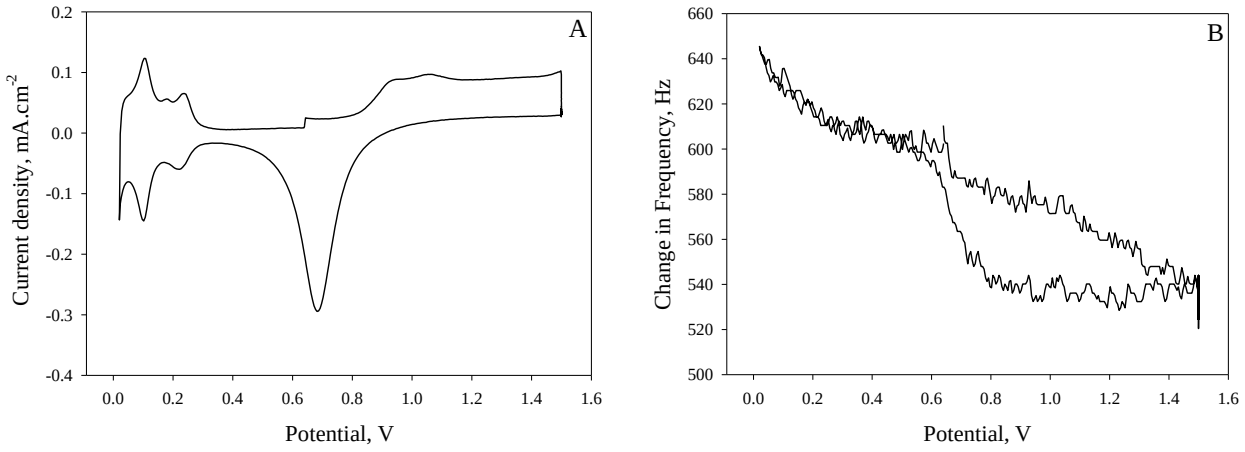

Figure 2-12: (A) A linear sweep voltammogram coupled with a semi cycle voltammogram of Pt in 0.5 M H_2SO_4 (B) Frequency change of graph (A) in 0.5 M H_2SO_4 at a scan rate of 50 mV s^{-1}

It can be seen how moving average points of 11 (Figure 2-13 (A)) and 51 (Figure 2-13 (B)) smooths the associated frequency readings respectively. It was subsequently decided to use 51 moving average points for the treatment of data, as the application of 51 was showing the important features clearly.

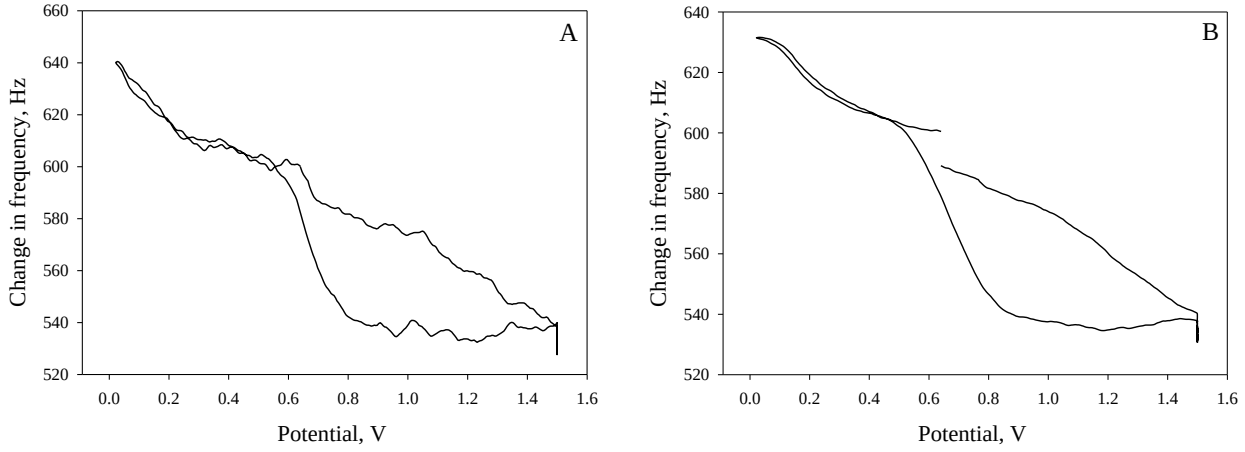

Figure 2-13: (A) Frequency change filtered with 11 average points (B) Frequency change filtered with 51 average

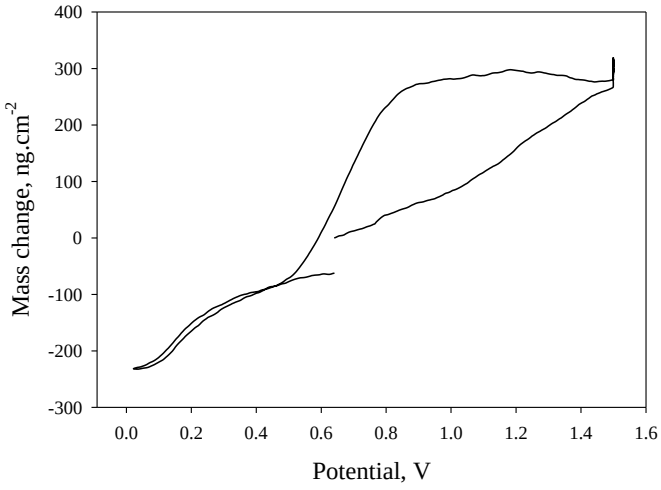

Figure 2-14: After filtering with 51 moving average points, and mass change was calculated using the experimentally C_f obtained from the calibration

Subsequent to applying 51 average points the change in frequency was zeroed, divided by the experimentally obtained C_f-value (to flip the curve), and converted to mass change (Figure 2-14).

2.5 Execution of experiments (general overview)

Conventional cyclic voltammetry (both single cycle and multicycle) was the key electrochemical technique employed for this study, complemented with EQCM studies. It was nevertheless necessary to augment these electrochemical techniques by the use of appropriate physical characterisation techniques to provide further useful information. ICP-MS is an extremely sensitive analytical technique, and was used to quantify the dissolved platinum in the electrolytes studied. XRD provided information regarding the physical state of the Pt electrodes used in this study, e.g. the orientation of the dominant Pt surface crystals present. The AFM technique provided detailed surface topography and is a useful tool to establish surface roughening after subjecting a polished metal surface to chemical and/or electrochemical attack. SEM was used to study surface features of electrodes (e.g. presence of deposited material), while EDX was used to provide information about the elemental composition of the electrode surfaces.

2.6 Post-electrochemical examination of electrodes

2.6.1 Inductively Coupled Plasma Mass Spectrometry

At the end of the experiments investigating oxide growth in electrolytes of 0.5 M H_2SO_4 and in the absence and presence of halide ions, a 15 ml solution was taken and analysed with an ICP-MS for platinum content.

2.6.2 X-Ray Diffraction

A clean platinum quartz electrode was mounted on modelling clay using a zero background holder (silicon crystal cut) and was analysed for crystal orientation using Powder X-ray diffractometry (PXRD). A Bruker D2 phaser desktop diffractometer was used to detect the preferred orientation of the crystals on the surface of the platinum samples in the 2θ range of 20^o to 110^o employing a sealed tube Co X-ray source equipped with a Bruker Lynxeye PSD detector. The spectrogram shown confirmed the (111) phase to be the preferred orientation of the platinum quartz electrode surface (Figure 2-15).

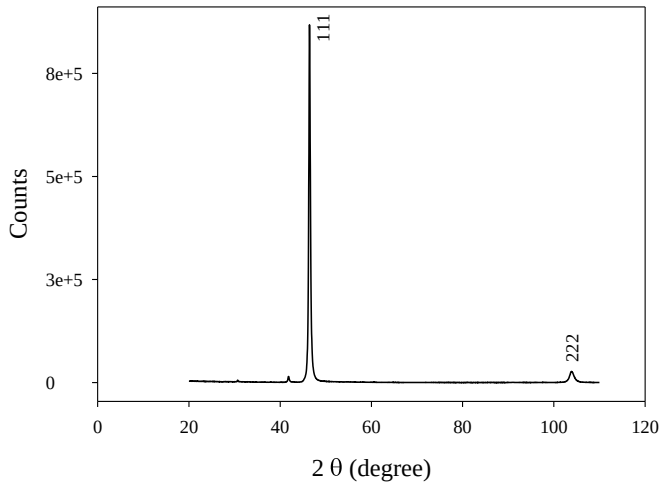

Figure 2-15: XRD diffractogram of a platinum quartz electrode

2.6.3 Atomic Force Microscopy

The platinum quartz electrodes were kept in nitrogen atmosphere for later analysis by means of atomic force microscopy (AFM) to investigate surface roughness. The operating principle of the AFM is the cantilever/tip assembly, which can be used in either contact or tapping mode and that interacts with the sample, thereby tracking the vertical and lateral motion of the probe. A Dimension 3100 AFM was used in tapping mode. The up/down and side to side motion of the tip as it scans along the surface is related to the root mean square roughness of the surface.

2.6.4 Scanning Electron Microscopy

Surface micrographs were obtained using a FEI Quanta 250 FEG SEM and analyses of the electrode during the electrodeposition of platinum from HCPA was carried out using an Oxford X-MAX20 EDX system. A FEI 2003 electron gun was used to produce secondary and backscattered electrons, as well as photons and X-ray signals from the surface of the sample. The scattered electrons were converted to an image of the surface. The X-ray signal was analysed by an Oxford X-MAX20 energy dispersive X-ray (EDX) system to determine the elemental distribution of the sample surface.

2.6.5 Calculation of surface coverage

The number of atoms on the surface of platinum was calculated using Equation 2-3

$$n = \frac{m}{M_w}.N_A \qquad (2\text{-}3)$$

where n is the number of atoms accumulated on electrode surface ($atoms^{-1}$), m the maximum mass change ($ng.cm^{-2}$) recorded by the EQCM from the cyclic voltammogram of Pt quartz electrodes at time t_p = 100s, M_w the atomic mass of the atom in question ($g\ mol^{-1}$), and N_A being Avogadro's constant (mol^{-1}). The number of monolayers (ML) is obtained by dividing n by the planar density of Pt (111) (1.5×10^{15} atoms

cm^{-2}).

2.6.6 Calculation of charge density

The charge involved in the formation of various substances on the Pt electrode was calculated.[4] From the EC-Lab® software the cyclic voltammetry in the hydrogen desorption region, for example, is shown in Figure 2-16 and was integrated as follows:

$$q = \int_{t_1}^{t_2} I.\ d\tau = \frac{1}{V_b} \int_{E_1}^{E_2} I.\ dE \qquad (2\text{-}4)$$

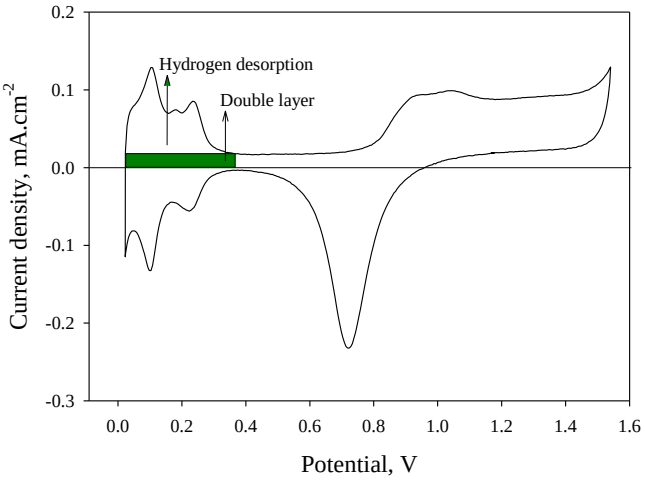

Figure 2-16: Integration of hydrogen desorption region for charge calculations and exclusion of a double layer

where V_b is the scan rate. The double layer region was subtracted manually, since EC-Lab® software also includes the double layer portion as part of the integrated area. Following the above procedure, the oxide formation and reduction regions can also be integrated to obtain the charge involved.

2.7 References

1 Kounaves, S. P. *Voltammetric techniques*. (Prentice Hall, Upper Saddle River, NJ, USA, 1997).

2 Ratieuville, Y., Viers, P., Alexandre, J. & Durand, G. A new electrochemical cell adapted to quartz crystal microbalance measurements. *Electrochemistry communications* **2**, 839-844 (2000).

3 Gu, N., Niu, L. & Dong, S. Simultaneous determination of both the calibration constant in an electrochemical quartz crystal microbalance and the active surface area of a polycrystalline gold electrode. *Electrochemistry communications* **2**, 48-50 (2000).

4 Bio-logic. (http://www.bio-logic.net/wp-content/uploads/20101105-application-note-11.pdf).

CHAPTER 3

The hydrogen evolution reaction in the context of electrochemical interaction between H_2PtCl_6 and H_2O/H_3O^+

3.1 Introduction

Hexachloroplatinic acid (HCPA) is frequently used as a precursor in the manufacturing of supported platinum catalysts and in the recovery of platinum from spent catalysts, be it through employing wet chemistry techniques or electrodeposition.[1-3] The electroplating of platinum from HCPA is furthermore frequently used to study reduction mechanisms at the cathode involving platinum chloride complexes.[4-7] It is generally accepted that Pt(IV), in the form of $[PtCl_6]^{2-}$, is first reduced to Pt(II), i.e. $[PtCl_4]^{2-}$, subsequent to which Pt(II) is reduced to Pt^0 (reactions 3-1 and 3-2).

$$[PtCl_6]^{2-} + 2e^- \rightleftharpoons [PtCl_4]^{2-} + 2Cl^- \qquad (E° = 0.680\ V)^8 \qquad (3\text{-}1)$$

$$[PtCl_4]^{2-} + 2e^- \rightleftharpoons Pt^0 + 4Cl^- \qquad (E° = 0.755\ V)^8 \qquad (3\text{-}2)$$

The above has indeed been shown by, for example, Hagihara *et al.*[9] during their study of the electrodeposition of platinum employing an electrochemical quartz crystal microbalance, with the evolution of hydrogen only being initiated at potentials negative to the electrodeposition of platinum.[9,10] It is generally accepted that the evolution of hydrogen in acidic electrolytes proceeds according to reactions 3-3 – 3-5, known as the Volmer, Heyrovsky, and Tafel reactions, respectively.[11]

$$H_3O^+ + e^- \rightleftharpoons H_{ads} + H_2O \qquad (3\text{-}3)$$

$$H_3O^+ + H_{ads} + e^- \rightleftharpoons H_2 + H_2O \qquad (3\text{-}4)$$

$$2H_{ads} \rightleftharpoons H_2 \qquad (3\text{-}5)$$

At potentials positive to the evolution of hydrogen it has been observed that the adsorption of halogen species on the electrode surface inhibits the continued electrodeposition of platinum.[9,10,12] It is therefore to be expected that the interfacial behaviour of platinum chloride species, and their interplay with hydrogen-containing species, is of considerable importance.[13,14]

In this regard, by employing cyclic voltammetry, it is the aim of this chapter to provide further insight into the hydrogen evolution reaction (HER) and its role related to the interplay between the electrochemistry of HCPA and hydrogen-containing species, i.e. H_2O/H_3O^+.

3.2. Experimental

Please refer to chapter 2 for a description of the appropriate techniques employed as part of this investigation. The electrochemical cell that was employed is described in section 2.3.1 (Figure 2-2). The glassy carbon pre-treatment is discussed in section 2.2.1. The electrolyte of HCPA was prepared following section 2.2.3.1. The electrochemical procedures followed section 2.4.3 and the potentiostat was a VMP3 model as shown in section

2.3.2 without a QCM. The SEM image and weight percentage from EDX were analyzed according to section 2.6.4.

3.3. Results and discussion

Starting with a clean glassy carbon (GC) surface a series of superimposed voltammograms in the potential range 0.5 to -0.023 V was obtained as shown below in Figure 3-1 at a potential scan rate of 10 mV s^{-1} in 2 mM HCPA (pH adjusted to 0.53 with HCl). Continued cycling resulted in the deposition of Pt crystallites (about 50 to 150 nm in diameter) on the GC surface, shown in Figure 3-1 (A) insert, initially on a few electrochemically active sites, but with each cycle also on the previously formed platinum crystallites, which in turn resulted in continually increasing prominence of the peaks that developed. By using this technique current peaks, which could go unnoticed in single cycle voltammograms, were made much more conspicuous. The interpretation of the resulting cyclic voltammograms involved the consideration of two intertwined redox systems, i.e. the water/hydronium ion/hydrogen system and the platinum(II, IV) chloride system.

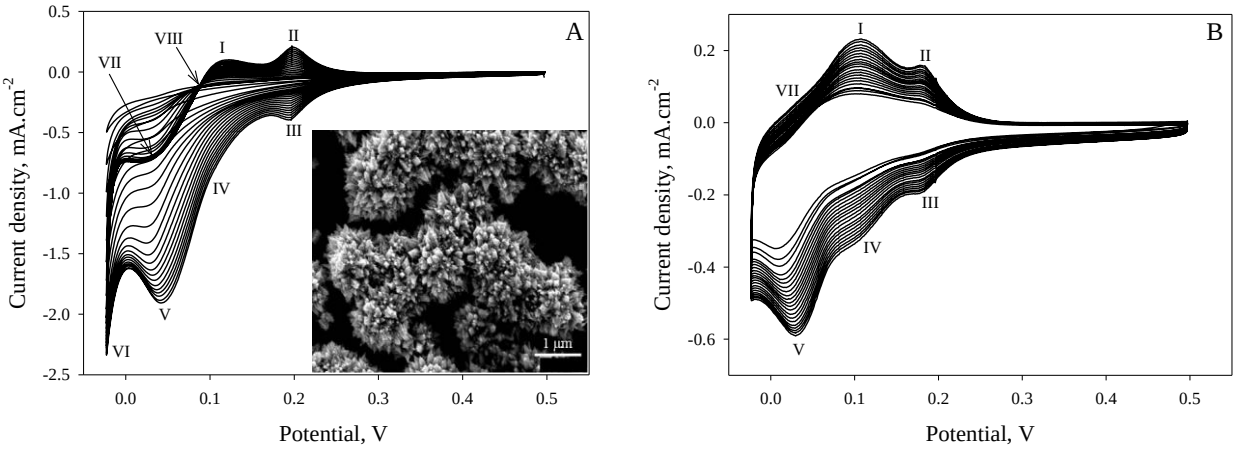

Figure 3-1: Voltammograms recorded with a stationary glassy carbon electrode with platinum electrodeposited during 20 cycles (A) Limited hydrogen evolution was allowed to occur, and (B) hydrogen evolution interrupted by early commencement of the return cycle. (Insert in (A): Electron micrograph of Pt crystal clusters on glassy carbon after 50 CV cycles in 2 mM HCPA at a pH of 0.53)

It is well documented that adsorbed or chemisorbed hydrogen, underpotentially deposited hydrogen (UPD-H) and/or protons[4,10,15,16] as well as chloride ions[10,17-19] play definite (but still frequently debated) roles during the deposition of platinum in acidic chloride electrolytes. It has been observed that the presence of chloride results in the reduction of $[PtCl_4]^{2-}$ to occur at potentials negative enough to allow for the simultaneous reduction of the solvent/electrolyte.[20]

As the number of cycles increased the voltammograms developed certain prominent features, indicated as potentials E_I to E_{VIII}. A notable feature is the development, under hydrogen evolution conditions, of an isopotential point (E_{VIII}) at about 0.08 V (Figure 3-1 (A)). However, when the evolution of hydrogen is interrupted by the early commencement of the return cycle, the isopotential point disappears (see Figure 3-1 (B)).

A common intersection potential can occur in a family of current-potential curves of an electrode when the potential is scanned through a certain point. There is still some debate as to the exact reason for the development of isopotential points. A model developed by Untereker and Bruckenstein[21] that describes the conditions necessary for the occurrence of isopotential points, suggests a surface that is seemingly composed of at least two electrochemically independent regions allowing reactions in these regions to occur isopotentially. In work conducted by Wasberg[22] on a rhodium-covered platinum electrode, it was proposed that the isopotential point was due to adsorption competition of two independent species.

The presence of peaks E_{II} and E_{III} (at about 0.2 V), in the presence and absence of previous hydrogen evolution (Figures 3-1 (A) and 3-1 (B)), is indicative of rapid reversible oxidation/reduction reactions involving species in which the reaction products remain on the surface.[23]

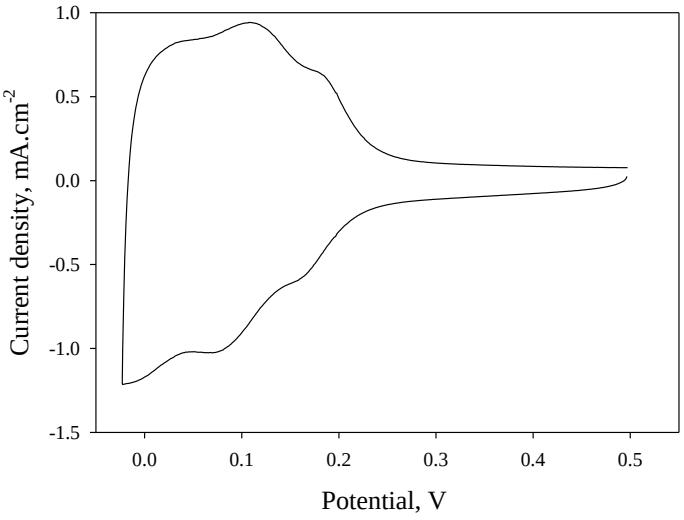

Figure 3-2: Second cycle of a Voltammogram obtained in 0.1 M HCl after previously deposited Pt on a GC electrode in a 2 mM HCPA electrolyte at pH 0.53, followed by rinsing

Comparison with a CV obtained in an electrolyte not containing HCPA (Figure 3-2) confirmed that the development of peaks E_{II} and E_{III} as observed in Figure 3-1 (A) and 3-1 (B) do not involve the participation of platinum species because the oxidation of platinum does not occur at potentials below 0.85 to 1.1 V.[24,25] The participation of chloride ions in the formation of these peaks therefore has to be considered. It has been reported that chloride ions begin to adsorb specifically already in the hydrogen region.[18,26] In the potential range $0.2 < E < 0.3$ V chloride ions and hydrogen ions adsorb simultaneously and competitively.[27] With the potential progressing in the anodic direction adsorbed hydrogen is increasingly displaced by Cl^- and the adsorption of OH blocked[27], thereby retarding PtO/PtO_2 film formation.[18,28,29] Chloride ions are expelled from the electrode surface due to the evolution of chlorine at potentials above about 1 V.

With any participation of Pt species and chloride ions discounted in the formation of current peaks at E_{II} and E_{III} it is postulated that the formation of the current peaks has to be ascribed to the desorption and adsorption of H_3O^+ ions, respectively.

In order to understand the further development of the CV it is important to consider possible reactions at potential point E_{IV} (not present in Figure 3-1 (A) and weakly developed in Figure 3-1 (B)), namely the reduction of H_3O^+ and the reduction of platinum-containing species, such as $[PtCl_6]^{2-}$.

In order to establish the potential for the onset of Pt deposition, cleaned GC electrodes were exposed to the electrolyte at different potentials for 30 minutes and the surface concentration of platinum determined by means of EDX. The weight percentages of platinum observed at the different potentials are shown in Table 3-1.

Table 3-1: Surface wt% Pt (average of 2 repeats) deposited on GC electrodes at different potentials

E (V,)	Pt (wt%)
0.237	0.0
0.155	0.0
0.145	0.15
0.117	0.20
0.079	1.30
0.047	5.65

The potential at which the first deposited Pt was detected was found to be ~0.15 V due to the reduction of $[PtCl_4]^{2-}$ (reaction 3-2) at E_V, which was found to be postponed to a relatively more negative potential in the presence of Cl^-.[10] As the concomitant reduction of Pt and other species is not uncommon in chloride electrolytes[10] attention is now drawn to the possible simultaneous reduction of $(H_3O^+)_{ads}$ and $[PtCl_6]^{2-}$at ~0.15 V. In this regard it is necessary to invoke the role of the molecular ion H_2^+. The existence of this ion, which has thus far been largely ignored by electrochemists, was originally proposed by Hirota and Horiuti[30] and entails that the adsorbed molecular hydrogen ion, $(H_2^+)_{ads}$, exists in equilibrium with adsorbed hydrogen ions, $(H^+)_{ads}$, and electrolytic bulk hydrogen ions, H^+, according to reaction 3-6.

$$(H^+)_{ads} + H^+ + e^- \rightleftharpoons (H_2^+)_{ads} \qquad (3\text{-}6)$$

In order to account for the different peaks in the voltammograms generated in the present study, and taking cognizance of previously published results, the following model is put forward:

3.3.1 Proposed model

A summary of the adsorption/desorption and reduction/oxidation processes, as proposed by Juodkazis *et al.*[31], involving H_2O, H_3O^+, H_2^+, and H_2, is presented in Figure 3-3. This proposed model is employed to elucidate aspects of the present work by comparing certain features exhibited in Figures 3-1 (A) and 3-1 (B) to that of Figure 3-3.

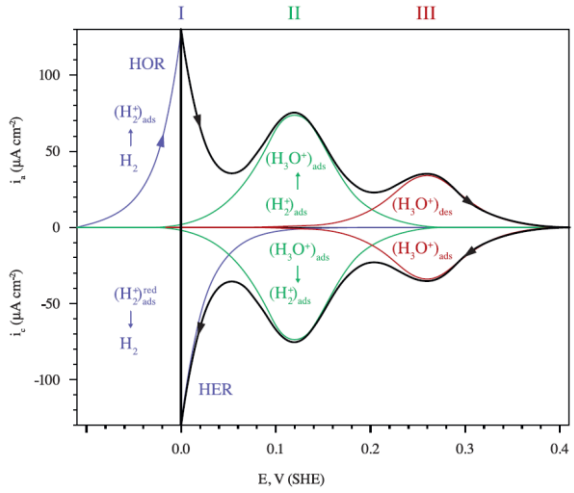

Figure 3-3: Theoretical voltammograms for the reversible adsorption/desorption and oxidation/reduction of H_3O^+ and H_2^+ and the hydrogen evolution reaction, (redrawn and adapted from Juodkazis *et al.* [31])

During the potential sweep in the cathodic direction, the first prominent electrochemical process is the dissociation of surface H_2O (reaction 3-7, E_{III} in Figures 3-1 (A) and 3-1 (B) at 0.175 V), with the subsequent adsorption of H_3O^+ (a non-faradaic charge build-up process) as per cathodic region III in Figure 3-3. The second electrochemical process, following from the first, is the reduction of $(H_3O^+)_{ads}$ to the molecular hydrogen ion, H_2^+, followed by the adsorption of the latter onto the Pt surface (reaction 3-8), E_{IV} in Figure 3-1 (B) at 0.16 V as per cathodic region II in Figure 3-3.

$$2(H_2O)_{surf} \rightleftharpoons (H_3O^+)_{ads} + OH^- \quad (3\text{-}7)$$

$$2(H_3O^+)_{ads} + e^- \rightleftharpoons (H_2^+)_{ads} + 2H_2O \quad (3\text{-}8)$$

The adsorbed molecular hydrogen ion, $(H_2^+)_{ads}$ can, in turn, be reversibly reduced to H_2 molecules according to reaction 3-9 (E_{VI} in Figure 3-1 (A)) as per cathodic region I in Figure 3-3. The adsorbed molecular hydrogen ion, $(H_2^+)_{ads}$, therefore acts as an intermediate in the reversible overall electrochemical reaction for the production of hydrogen (reaction 3-9).

$$(H_2^+)_{ads} + e^- \rightleftharpoons H_2 \quad (3\text{-}9)$$

Additionally, reduction of $[PtCl_6]^{2-}$ at potential E_{VI} is effected by $(H_2^+)_{ads}$ at E_{IV} according to equation 3-10.

$$[PtCl_6]^{2-} + (H_2^+)_{ads} \rightarrow [PtCl_4]^{2-} + 2H^+ + 2Cl^- \quad (3\text{-}10)$$

The $[PtCl_4]^{2-}$ complex is an intermediate in the reduction of $[PtCl_6]^{2-}$ to Pt^0. The reduction of $[PtCl_4]^{2-}$ to Pt^0 was found to be a slow process by Lau and Hubbard[32] who reported that the rate constant of the electro-reduction of $[PtCl_4]^{2-}$ was about an order of magnitude lower than that of $[PtCl_6]^{2-}$ reduction at equal chloride concentrations. The initiation of $[PtCl_4]^{2-}$ reduction is at ~0.08 V (E_V) with the maximum rate of $[PtCl_4]^{2-}$ reduction occurring at 0.027 V. At potentials more cathodic than 0.027 V the reduction of $[PtCl_4]^{2-}$ is increasingly inhibited by the adsorption of H_2^+, as per cathodic region II (Figure 3-3), until reduction of $[PtCl_4]^{2-}$ ceases upon the commencement of hydrogen evolution (Figure 3-1 (A) at ~0.005 V between E_V and E_{VI}, or when the potential is reversed to initiate the sweep in the anodic direction (Figure 3-1 (B)) at the point

where hydrogen evolution is initiated. This is confirmed through the work done by Liu *et al.*[10] who found that the quenching of platinum electrodeposition coincided with the hydrogen evolution reaction. Study of the development of the cathodic part of the CVs in the potential range 0.050 to 0.010 V shows that the 'passivation' of the platinum surface becomes more pronounced in successive CVs (indicating incomplete reduction and surface accumulation of $[PtCl_4]^{2-}$). According to Liu *et al.*[10] platinum electrodeposition overlaps with hydrogen adsorption, albeit termed, H_{upd}, in line with the monatomic hydrogen mechanism. It would therefore seem probable that, between E_V and E_{VI}, competition for the available adsorption sites develops between $[PtCl_4]^{2-}$ and $(H_2^+)_{ads}$ with the latter dominating adsorption and ultimately leading to hydrogen gas evolution at E_{VI} (according to reaction 3-9), and the cessation of $[PtCl_4]^{2-}$ reduction[10] with the formation of a film of 'passivating' unreduced $[PtCl_4]^{2-}$ on the surface at E_{VI} (Figure 3-1 (A)).

Turning the attention now to the potential sweep in the anodic direction a clear reduction peak is observed at E_{VII} (Figure 3-1 (A)). This is attributed to the continued reduction of $[PtCl_4]^{2-}$ as a result of the 'cleansing' action of hydrogen evolution, i.e. the removal of $(H_2^+)_{ads}$ from the surface in the form of molecular hydrogen (H_2), which opens up active sites on the platinum surface, allowing the reduction of $[PtCl_4]^{2-}$. In the case of hydrogen evolution having been prevented (Figure 3-1 (B)) this reduction peak is not evident and becomes less prominent with continued cycling, which directly correlates with a build-up of $(H_2^+)_{ads}$ on the surface. This is evident in E_I being much more prominent in Figure 3-1 (B) than in Figure 3-1 (A). In the absence of this 'cleansing' action, i.e. hydrogen evolution, the surface is saturated with $(H_2^+)_{ads}$, which is evident in the pronounced peak at E_{IV} being visible (Figure 3-1 (B)) in contrast to the masking of this peak by the reduction of $[PtCl_4]^{2-}$ in Figure 3-1 (A). This $(H_2^+)_{ads}$-saturated surface results in no reduction of $[PtCl_4]^{2-}$ occurring during the return sweep at E_{VII} (Figure 3-1 (B)), which results in increased oxidation of $(H_2^+)_{ads}$ and subsequent adsorption of H_3O^+ at E_I. Under these conditions, i.e. the absence of hydrogen evolution, the isopotential point between the reduction of $[PtCl_4]^{2-}$ and the oxidation of $(H_2^+)_{ads}$ disappears. In Figure 3-1 (A) the limited 'cleansing' action of hydrogen evolution has removed some of the $(H_2^+)_{ads}$ from the surface, leaving a surface partly covered with $[PtCl_4]^{2-}$ and $(H_2^+)_{ads}$ and which gives rise to the isopotential point. In Figure 3-1 (B), however, the absence of this 'cleansing' action results in the surface being totally covered with a single entity, i.e. $(H_2^+)_{ads}$, resulting in the obvious absence of the previously observed isopotential point. It is furthermore quite clear that the 'poisoning' of the surface by $(H_2^+)_{ads}$ results in a limited amount of $[PtCl_4]^{2-}$ reduction to occur (at E_V), which is evident in the reduced current densities being observed in Figure 3-1 (B). Under hydrogen evolution conditions the current density for E_V, associated to $[PtCl_4]^{2-}$ reduction, is 1.9 $mA.cm^{-2}$, while it is only 0.58 $mA.cm^{-2}$ in the absence of hydrogen evolution.

3.4 Conclusions

By employing glassy carbon electrodes to generate multiple voltammetric scans for the reduction of $[PtCl_6]^{2-}$ in HCPA electrolytes new insights into the different reactions occurring could be obtained. Eight interrelated potential peaks and areas were studied in the CVs. It was found that the reduction of $[PtCl_6]^{2-}$ to $[PtCl_4]^{2-}$ occurred between 0.15 and 0.03 V, followed by the incomplete reduction of $[PtCl_4]^{2-}$ to Pt. The simultaneous

adsorption and desorption reactions of (H_2^+) and (H_3O^+) could be identified in the CVs and correlated with published results. The occurrence, under certain experimental conditions, of an isopotential point in the CVs is a notable observation in this research and to the knowledge of the author has not previously been reported for the electrolyte in question. The experimental observation of the interplay between the reduction of $[PtCl_6]^{2-}/[PtCl_4]^{2-}$ and the reduction/oxidation of hydrogen-containing species perfectly fits the model developed by Juodkazis *et al*.[31] and supports the mechanism for the HER to proceed via the adsorbed molecular hydrogen ion $(H_2^+)_{ads}$ as intermediate.

3.5 References

1 Barakat, M. & Mahmoud, M. Recovery of platinum from spent catalyst. *Hydrometallurgy* **72**, 179-184 (2004).

2 Jha, M.K., Lee, J.C., Kim, M.S., Jeong, J., Kim, B.S. & Kumar, V. Hydrometallurgical recovery/recycling of platinum by the leaching of spent catalysts: A review. *Hydrometallurgy* **133**, 23 (2013).

3 Van Rheenen, P., McKelvy, M. & Glaunsinger, W. Synthesis and characterization of small platinum particles formed by the chemical reduction of chloroplatinic acid. *Journal of Solid State Chemistry* **67**, 151-169 (1987).

4 Marrese, C. A. Preparation of strongly adherent platinum black coatings. *Analytical Chemistry* **59**, 217-218 (1987).

5 Kravtsov, V. I. Platinum electrodeposition mechanism during the reduction of platinum chloride complexes. *Russian Journal of Electrochemistry* **36**, 1209-1215 (2000).

6 Yasin, H. M., Denuault, G. & Pletcher, D. Studies of the electrodeposition of platinum metal from a hexachloroplatinic acid bath. *Journal of Electroanalytical Chemistry* **633**, 327-332 (2009).

7 Pobelov, I. V., Borzenko, M. I., Tsirlina, G. A. & Petrii, O. A. Reduction of an ensemble of chloride aquacomplexes of platinum (II): An analysis in the framework of phenomenological approach. *Russian Journal of Electrochemistry* **37**, 233-243 (2001).

8 *CRC Handbook of Physics and Chemistry*. (2011-2012).

9 Hagihara, T., Yaori, K., Iwakura, K., Fukumuro, N. & Shinji, Y. Electrochemical quartz crystal microbalance study of the electrodeposition of platinum. *Electrochimica Acta* **176**, 65-69 (2015).

10 Liu, Y., Gokcen, D., Bertocci, U. & Moffat, T. P. Self-Terminating Growth of Platinum Films by Electrochemical Deposition. *Science* **338**, 1327-1330 (2012).

11 Koper, M. T. Activity volcanoes for the electrocatalysis of homolytic and heterolytic hydrogen evolution. *Journal of Solid State Electrochemistry* **20**, 895-899 (2016).

12 Plyasova, L.M., Molina, I.Y., Gavrilov, A.N., Cherepanova, S.V., Cherstiouk, O.V., Rudina, N.A., Savinova, E.R. & Tsirlina, G.A. Electrodeposited platinum revisited: Tuning nanostructure via the deposition potential. *Electrochimica Acta* **51**, 4477-4488 (2006).

13 Shelimov, B. N., Lambert, J. F., Che, M. & Didillon, B. Molecular-level studies of transition metal-support interactions during the first steps of catalysts preparation: platinum speciation in the hexachloroplatinate/alumina system. *Journal of Molecular Catalysis A: Chemical* **158**, 91-99 (2000).

14 Spieker, W. A., Liu, J., Miller, J. T., Kropf, A. J. & Regalbuto, J. R. An EXAFS study of the co-ordination chemistry of hydrogen hexachloroplatinate(IV) 1. Speciation in aqueous solution. *Applied Catalysis A: General* **232**, 219-235 (2002).

15 Georgolios, N., Jannakoudakis, D. & Karabinas, P. Pt electrodeposition on PAN-based carbon fibres. *Journal of Electroanalytical Chemistry and Interfacial Electrochemistry* **264**, 235-245 (1989).

16 Łosiewicz, B., Jurczakowski, R. & Lasia, A. Kinetics of hydrogen underpotential deposition at polycrystalline platinum in acidic solutions. *Electrochimica Acta* **80**, 292-301 (2012).

17 Lu, G. & Zangari, G. Electrodeposition of platinum on highly oriented pyrolytic graphite. Part I: electrochemical characterization. *Journal of Physical Chemistry B* **16**, 7998-8007 (2005).

18 Patil, R. S., Juvekar, V. A. & Naik, V. M. Oxidation of Chloride Ion on Platinum Electrode: Dynamics of Electrode Passivation and its Effect on Oxidation Kinetics. *Industrial & Engineering Chemistry Research* **50**, 12946-12959 (2011).

19 Sherstyuk, O. V., Pron'kin, S. N., Chuvilin, A. L., Salanov, A. N. & Savinova, E. R. Platinum electrodeposits on glassy carbon: The formation, mechanism, morphology and adsorption properties. *Russian Journal of Electrochemistry* **36**, 741-751 (2000).

20 Feltham, A. & Spiro, M. Platinized platinum electrodes. *Chemical Reviews* **71**, 177-193 (1971).

21 Untereker, D. F. & Bruckenstein, S. Interpretation of isopotential points. Common intersection in families of current-potential curves. *Analytical Chemistry* **44**, 1009-1020 (1972).

22 Wasberg, M. Isopotential point: A singularity in the voltammetric behaviour of platinum metal electrodes characterising adsorption competition (Preliminary note). *Journal of Electroanalytical Chemistry* **379**, 541-544 (1994).

23 Pletcher, D. *A First Course in Electrode Processes*. Vol. Second 204 (RSC Publishing, 2009).

24 Angerstein-Kozlowska, H., Conway, B. & Sharp, W. The real condition of electrochemically oxidized platinum surfaces: Part I. Resolution of component processes. *Journal of Electroanalytical Chemistry and Interfacial Electrochemistry* **43**, 9-36 (1973).

25 Conway, B. E. Electrochemical oxide film formation at noble metals as a surface-chemical process. *Progress in surface science* **49**, 331-452 (1995).
26 Kuhn, A. T. & Wright, P. M. A study of the passivation of bright platinum electrodes during chloride evolution from concentrated sodium chloride solutions. *Electroanalytical Chemistry and Interfacial Electrochemistry* **38**, 291-311 (1972).
27 Garcia-Araez, N., Climent, V., Herrero, E., Feliu, J. M. & Lipkowski, J. Determination of the Gibbs excess of H adsorbed at a Pt(111) electrode surface in the presence of co-adsorbed chloride. *Journal of Electroanalytical Chemistry* **582**, 76-84, doi:http://dx.doi.org.nwulib.nwu.ac.za/10.1016/j.jelechem.2005.01.031 (2005).
28 Gilman, S. Electrochemical surface oxidation of platinum. *Electrochimica Acta* **9**, 1025-1046, doi:http://dx.doi.org.nwulib.nwu.ac.za/10.1016/0013-4686(64)85049-0 (1964).
29 Wang, Z., Tada, E. & Nishikata, A. In Situ Analysis of Chloride Effect on Platinum Dissolution by a Channel-Flow Multi-Electrode System. *Journal of The Electrochemical Society* **161**, F845-F849 (2014).
30 Hirota, K. & Horiuti, J. The Mechanism of the Hydrogen Electrode Process. II. The Electrochemical Mechanism. The Existence of Hydrogen Molecule Ions on the Surface of the Electrode. *Bulletin of the Chemical Society of Japan* **13**, 228-233 (1938).
31 Juodkazis, K., Juodkazytė, J., Šebeka, B. & Juodkazis, S. Reversible hydrogen evolution and oxidation on Pt electrode mediated by molecular ion. Applied Surface Science **290**, 13-17, doi:10.1016/j.apsusc.2013.10.164 (2014).
32 Lau, A. L. & Hubbard, A. T. Study of the kinetics of electrochemical reactions by thin-layer voltammetry: III. Electroreduction of the chloride complexes of platinum (II) and (IV). *Journal of Electroanalytical Chemistry and Interfacial Electrochemistry* **24**, 237-249 (1970).

CHAPTER 4

Anodic oxide growth on platinum in sulphuric acid electrolytes

4.1 Introduction

The high catalytic activity, as well as stability, of platinum results in it being an indispensable electrode material for electrochemical energy conversion. During the 1960s to 1970s, the use of platinum as an essential catalyst material for the hydrogen oxidation reaction (HOR) and the oxygen reduction reaction (ORR), in the advancement of fuel cells, prompted investigations into the mechanism for noble metal (anodic) oxidation. The possible roles of oxygen-containing and other species on the platinum surface receive much attention due to their possible inhibition/poisoning of the catalyst surface and their possible enhancement of platinum dissolution under harsh operational conditions.[1] Loss of platinum is a major, and growing, problem, especially in view of the tendency to lower the platinum content of fuel cell catalysts, making platinum stability even more crucial.[1-5] It has been ascertained that the development of a platinum oxide film is essential for the subsequent evolution of oxygen on these platinum surfaces,[6] and is known to degrade the performance of the ORR.[7,8] Understanding the oxygen-platinum interaction during electro-oxidation is therefore of considerable importance.[9] In spite of the extensive literature on platinum oxide growth and reduction, the details of the oxide structure and the reduction kinetics are still not fully understood.[10]

New insights gained on the formation and reduction of oxide thin films on a polycrystalline Pt surface, as well as on the electrochemical Pt loss in halide-free 0.5 M H_2SO_4, is presented here.

4.2 The nature of surface films formed during anodic polarization

Recent experimental work reported in the literature,[11] with a direct bearing on the present results, provides a more detailed view of the processes involved in the formation of surface films on Pt during anodic oxidation. A survey of the development of ideas concerning the formation of anodic oxide layers on platinum show that convincing arguments have been put forward by both the "phase oxide" and "adsorbed oxygen" schools. In 1973 Appleby[12] reported results based on the notion that the first anodic step is OH formation from water dissociation, followed by very rapid O formation associated with a rearrangement of the surface film. In the cathodic direction, the position and shape of the peak was governed by the kinetic parameters of O reduction, whereas OH reduction was rate-determining. Many workers maintained that, in view of the controversy, thin anodic oxide/oxygen films on platinum are best represented by surface Pt:O ratios rather than by chemical formulae and considered it inappropriate to assign stoichiometric formulae to the oxide films until they reach “bulk” thicknesses.[11] However, with the advent of modern physical analysis techniques such as ellipsometry, SEM, electrochemically active surface area (ECSA), Auger spectroscopy, X-ray photo-electron spectroscopy (XPS) and other X-ray techniques, EQCM, and many others, the existence of surface oxides became indisputable.

On the grounds of ellipsometric measurements, a technique that monitors the optical behaviour of a substrate, Reddy *et al.*[13] came to the conclusion that an oxide film and a partial layer of oxygen (two different forms of oxygen) existed on the platinum surface. At about 0.95 V they observed a drastic change in the electrode (platinum) surface, evidenced from the kinetics of the oxidation of hydrogen and a number of hydrocarbons, which could only occur if a new phase, i.e. platinum oxide, was present on the surface. They found that less than a monolayer of oxygen (in the form of platinum oxide) caused inhibition of these reaction rates, which could be ascribed to steric hindrances in the event of the oxide being formed uniformly over the surface or due to a change in the work-function brought about by oxide formation. Reddy *et al.*[13] therefore suggested the following growth mechanism, based on the concept of place exchange.

The mechanism for oxide formation is suggested to be:[13]

$$Pt + H_2O \rightleftharpoons PtOH + H^+ + e^- \quad (4\text{-}1)$$

$$PtOH \xrightarrow[\text{exchange}]{\text{place}} HOPt \quad (4\text{-}2)$$

$$HOPt \rightarrow PtO + H^+ + e^- \quad (4\text{-}3)$$

Reaction (4-2) involves place exchange first proposed by Lanyon and Trapnell[14] and is rate determining.

The over-all rate of place exchange then is:

$$\frac{dq_{ox}}{dt} = n\,\Pi\,pi = nk\,\exp[\Sigma\left(\frac{\Delta G_i^*}{RT}\right)] \quad (4\text{-}4)$$

where dq_{ox} is the rate of place exchange, dt is the time, p_i is the probability of a given row being in the "activated state", n = number of rows of atoms normal to the surface which are in the "activated state", k = rate constant, ΔG^* = the free energy of activation for a single atom (with the exception of the first layer), R = gas constant and T = absolute temperature.

Although Angerstein-Kozlowska *et al.*[15] at first suggested that an intermediate OH_{ads} was formed on Pt at low potential, before O_{ads} development, later EQCM results by Birss *et al.*[16] established that no moderate change of oxide species takes place, and that in all likelihood Pt oxidation continues specifically to O_{ads} without OH_{ads} as an intermediate.

Gomez-Marin *et al.*[17] suggest that oxide growth on Pt(111) is initiated by the dissociation of water to OH_{ads}, which in turn is electrochemically oxidized to O_{ads} at higher potentials, with O_{ads} transforming to a Pt oxide structure. There are therefore two processes related to the growth of the surface oxide layer (two states of oxide films), i.e. the O_{ads} layer and a Pt oxide layer.

There seems to be wide agreement that the formation of a surface oxide on Pt in acidic electrolytes occurs according to the direct logarithmic rate law:

$$x = k_l \log(bt + c) \quad (4\text{-}5)$$

where x is the direct logarithmic rate law, k_l is the rate constant, t the time, and b and c are constants.

The following steps are involved: (i) dissociation of H_2O with release of two hydrated protons (H^+_{aq}) and a chemisorbed O (O_{ads}); and (ii) formation of a quasi-3D lattice comprising Pt^{2+} and O^{2-} through a place-exchange process.[9,16,18-20] These reactions are summarized in Equations 4-6 and 4-7.

$$Pt + H_2O \xrightarrow{\text{electroadsorption}} Pt^{\delta+} - O^{\delta-}_{ads} + 2H^+_{aq} + 2e^- \quad (4\text{-}6)$$

$$Pt^{\delta+} - O^{\delta-}_{ads} \xrightarrow{\text{quasi-3D layer}} Pt^{2+} - O^{2-} \quad (4\text{-}7)$$

Ellipsometric studies[15] have shown that the oxidation/reduction hysteresis in the formation and reduction of the oxygen films on Pt is due to "place-exchange", as the cathodic reduction profile can be resolved into reversible and irreversible components. In voltammograms the asymmetry between Pt oxide formation peaks and reduction peaks is indicative of irreversibility of the oxide reactions.[10] Hysteresis refers to an irreversible process whereby (in this instance) the oxide formation peak(s) form, but does not reduce immediately on the return cycle (at the same potential as oxide formation, which would have pointed towards a reversible process). This process of irreversible potential shift is illustrated by a series of CVs in Figure 4-4 on page 38. Hysteresis, pointing to a separation between the anodic and cathodic i–E profiles, is therefore a consequence of a change of state of the surface oxide film, with the irreversible component thought to arise from a rearrangement of the surface oxide and has already been formed well below the “PtOH” monolayer. The irreversible component is reduced at more negative potentials, which results in the characteristic hysteresis between oxide formation and the reduction processes on the Pt surface. Because place-exchange is thought to be initiated above 1.05 V, the reaction below 1.05 V would just be the simple adsorption of OH or O.[10]

Using CV and EQCN measurements, Jerkiewicz *et al.*[8] determined the molecular weights of the interfacial species, which were identified as chemisorbed O (O_{chem}) at $0.85 \leq E \leq 1.10$ V and as O^{2-} in the form of surface PtO at $1.20 \leq E \leq 1.40$ V. Yadav[21] found that in the 1.3 to 1.4 V region the platinum metal is fully covered by a protective PtO film. This film can undergo further oxidation at 1.5 V to form PtO_2.[22] The potential region between ~0.27 V (point of zero charge) and ~0.80 V can be regarded as the region in which physisorption of water molecules on the Pt surface occurs.[8,11,15,23] This region is therefore characterized by non-faradaic current flow, which is utilized for the maintenance of the double layer. In the further development of surface oxygen-containing species with increasing potential the involvement of OH_{ads} as an intermediate has been discounted by Jerkiewicz *et al.*[8]. McMath *et al.*[23] hypothesized that between ~0.83 V and ~1.00 V the first half of a monolayer of chemisorbed oxygen (O_{chem}) is formed by the splitting of water molecules, followed by the formation of the second half monolayer. This monolayer has an electrical conductivity comparable to that of platinum metal.[24] A critical value of the coverage with oxygenated species is reached when the enthalpy of the repulsive interactions between the O adatoms gradually reduce that of chemisorption until it equals the

enthalpy of oxide formation.[1] This process seems to be associated with a potential of ~0.95 V (see Figure 4-3), which is marked by a very slight decrease in the anodic current, probably due to some rearrangement activity on the surface (e.g. place-exchange between O_{chem} and surface Pt atoms, to form "buried" (subsurface) oxygen atoms ("dermasorbed oxygen"[25]), and charge transfer to form Pt-O on the Pt surface. The growth of the Pt-O layer leads to a notable current decrease, and the consolidation and stabilization of the anodic current between ~1.05 V and ~1.35 V, followed by dynamic maintenance of the (transient) oxide layer, which renders the platinum "passive". An important point is that a continuous flow of current is required to maintain passivity of the oxide layer. Due to the high ionic conductivity of platinum in Pt(IV) oxide, Redmond *et al.*[26] proposed a mechanism involving the initial formation of PtOH, which is then converted stepwise to PtO_2 via a single transition state by the place-exchange process, leading to a heterogeneous oxide layer. On the basis of Auger electron spectroscopy measurements, Jerkiewicz *et al.*[8] found that oxygen-containing species residing on the platinum surface at potentials below ~1.10 V are incorporated into the surface lattice of the Pt at higher potentials.

A steep increase in the current at ~1.5 V can be ascribed to the oxidation of Pt-O to PtO_2, followed by the evolution of oxygen gas from water oxidation. [19,22] When the potential of a metal exceeds the equilibrium potential that exists between the metal and one of its oxides, an oxide or hydroxide can be expected to form on the metal surface. Such a film will protect the metal from rapid dissolution, rendering the metal "passive"[27] (See Figure 4-3 on page 37).

The upshot of the above appraisal of some relevant literature on the electrochemical oxidation of platinum is that any further advancement of the understanding of the phenomenon will have to provide new insights (adequate explanation for) into the following key aspects (Section 4.4).

4.3 Experimental

Please refer to chapter 2 for a description of the appropriate techniques employed as part of this investigation. For this investigation, an in-house cell was employed as described in section 2.3.1 (Figure 2-3). The electrode holder was shown in Figure 2-4. The platinum quartz electrodes were pre-treated as discussed in section 2.2.2. The electrolyte of 0.5 M H_2SO_4 was prepared accordingly following section 2.2.3.2. The potentiostat and the QCM were connected as discussed in section 2.3.2. The QCM was calibrated as discussed in section 2.4.6.1. In order to determine the time to grow an oxide film on the platinum quartz, chronoamperometry was performed as discussed in section 2.4.2. The electrochemical procedures followed section 2.4.5. The preferred orientation of the platinum quartz electrode was determined according to section 2.6.2. The charge density of the oxide formation and reduction was calculated following section 2.6.6. The mass changes were recorded with a QCM and analysed as discussed in section 2.4.6.2. The physical characterization of the Pt quartz after subjected to electrochemical procedures, ICP-MS was used to determine Pt content in the electrolyte as discussed in section 2.6.1 and the surface roughness was determined with AFM as described in section 2.6.3. The number of atoms of oxygen absorbed on Pt(111) were calculated as described in section 2.6.5.

4.4 Results and discussion

4.4.1 Rate of oxidation

In order to establish the time required to form oxide layers on Pt, chronopotentiometry at 0.8 V was used, with the results shown in Figure 4-1.

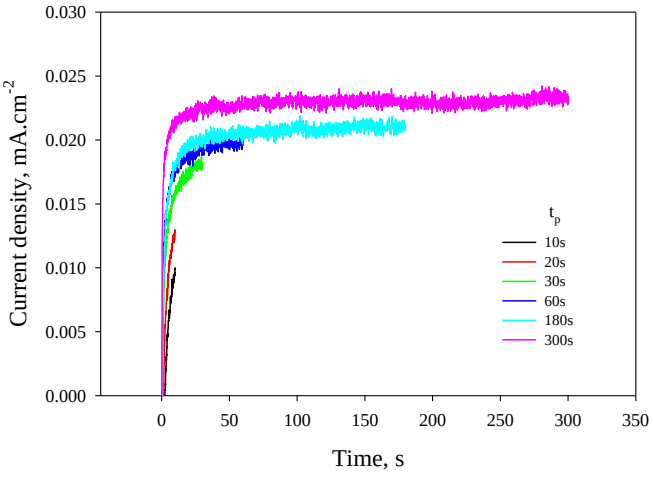

Figure 4-1: Chronopotentiometric curve of Pt showing current (j_p) resulting from anodic polarization at a holding potential (E_p) of 0.8 V in 0.5 M H_2SO_4

The results show that the charging of the double layer and the greatest part of the equilibrium oxide growth are completed within a relatively short time, (between 10 and 15 seconds after application of the current) with equilibrium reached in ~60 to 100 s. This finding agrees with results obtained by Imai *et al*.[19] Extension of the oxidation time, t_p, beyond 100 s in an effort to grow "thick" oxide film is not necessary, especially above ~1.3 V. Reports[9] of "oxide growth" during periods of up to 10 000 s are based on the assumption that the growth of the "oxide" will continue as long as a potential is maintained in a "passive" potential region. Platinum oxides are ionic conductors[24] and will allow Pt ions to pass into the electrolyte once the equilibrium thickness is reached. If exchange current density (j_p) is prolonged the charge required for "oxide formation" is largely the charge required to continuously generate Pt, which leaves the electrolyte/"oxide" interface to be complexed, by e.g. water molecules.

4.4.2 Charge density

The objective was to establish the amount of charge required to form and to reduce surface oxide films at the different holding potentials (E_ps). This is achieved by integrating the anodic formation curves and the cathodic reduction curves. It was consistently found that the charges for the reduction of oxides, $Q_{ox,red}$, were in each instance lower than that for the associated oxidation process, $Q_{ox,form}$, as is shown in Figure 4-2, with the observation being consistent with published results.[23] The values shown in Figure 4-2 seem to suggest that two types of surface films have to be considered: those existing up to ~1.05 V, and those above ~1.05 V showing appreciably higher values of Q. It is also of interest to note that the difference between $Q_{ox,form}$ and $Q_{ox,red}$, i.e.

ΔQ, at each value of the holding potential (E_p) reaches a maximum at 1.2 V, a potential associated with the onset of passivity of platinum (see Figure 4-6A on page 39).

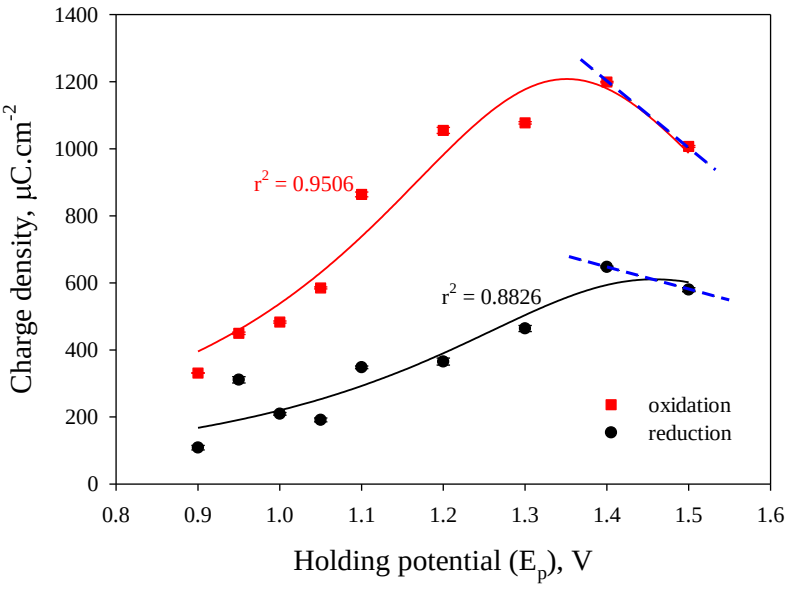

E_p (V)	ΔQ (μC.cm^{-2})
0.90	222.45
0.95	139.03
1.00	274.19
1.05	394.08
1.10	515.69
1.20	689.19
1.30	613.34
1.40	551.36
1.50	427.15

Figure 4-2: Charge density for oxide formation and reduction at different holding potentials (E_p) in 0.5 M aqueous H_2SO_4 recorded at 50 mV s^{-1} (Average of three repeats)

Taking the charge required to form 1 monolayer (ML) of PtO as 420 μC cm^{-2} [23], it appears that above ~1.1 V 2 to 3 monolayer (ML) of Pt-O are formed. However, the charge expended in the oxidation region will also include the charge associated with the formation of platinum ions continuously required to maintain an equilibrium thickness of oxide. The relatively large differences between $Q_{ox,red}$ and $Q_{ox,form}$, and especially the fact that less charge is required for reduction than to form an oxide at a particular E_p, has a direct bearing on the phenomenon of irreversibility, which receives attention in Section 4.4.5.2.

4.4.3 The formation and reduction of platinum oxides

Figure 4-3 provides an overview of the different potential regions within which the current research was focused.

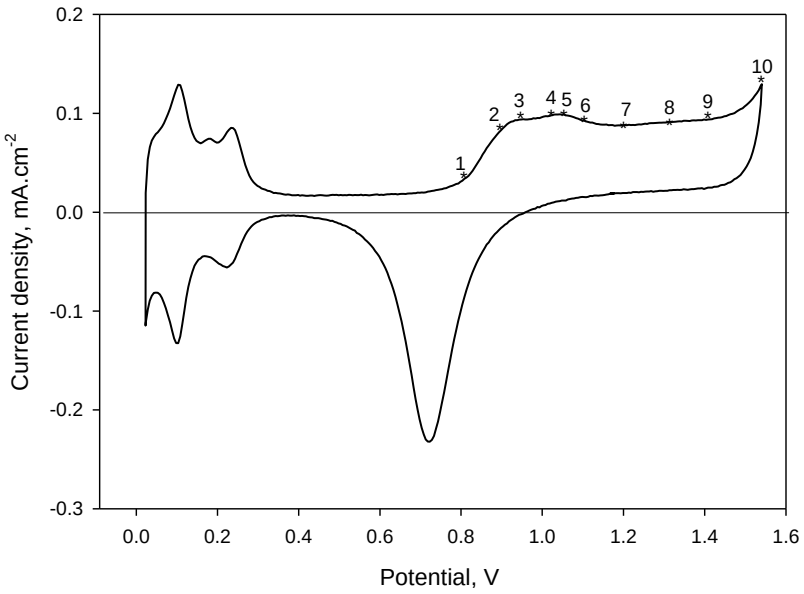

No.	E_p (V)
1	0.80
2	0.90
3	0.95
4	1.00
5	1.05
6	1.10
7	1.20
8	1.30
9	1.40
10	1.50

Figure 4-3: Typical cyclic voltammogram of Pt in deoxygenated 0.5 M H_2SO_4 recorded at a scan rate of 50 mVs^{-1} showing the potentials in the regions of focus

The main regions of interest of the current investigation were (a) the anodic region, in which the different surface films formed on Pt, and (b) the cathodic region, in which surface films were subsequently reduced with a view of determining the characteristics of the preceding anodic films. The voltammogram is characterized by the oxygen-related surface reactions (oxidation and reduction) in the range ~0.3 to ~1.5 V, and the adsorption/desorption of hydrogen in the range ~0.012 to ~0.3 V.

Figure 4-4 displays a series of CVs in which the electrode potential was increased to specific potentials in the range $0.8 \leq E_p \leq 1.5$ V and reactions allowed to proceed for a time t_p (= 100 s) at E_p, followed by reduction of surface films during a negative-going cycle. Figure 4-4 is a graphical representation of the voltammetric procedures carried out.

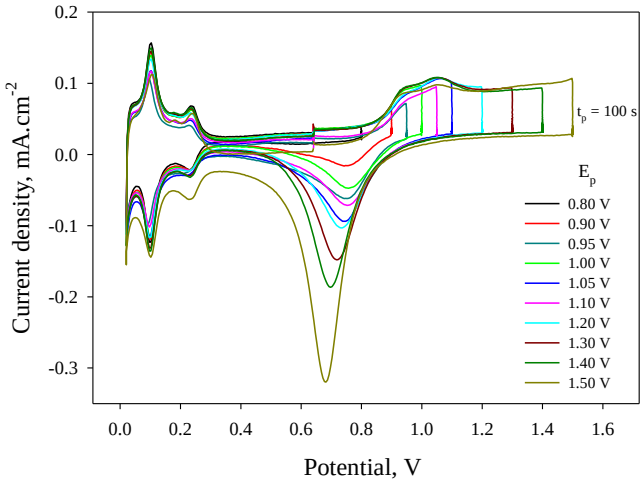

Figure 4-4: Series of CVs for Pt at different holding potentials (E_ps) in 0.5 M H_2SO_4 for t_p = 100 s recorded at 50 mV s^{-1} (scan direction = 0.6 V - E_p's - 0.7 V - 0.01 V – 0.6 V)

The mass changes obtained by using electrochemical quartz crystal microbalance (EQCM) for the CVs in Figure 4-4 at different holding potentials (E_ps) are shown in Figure 4-5 below.

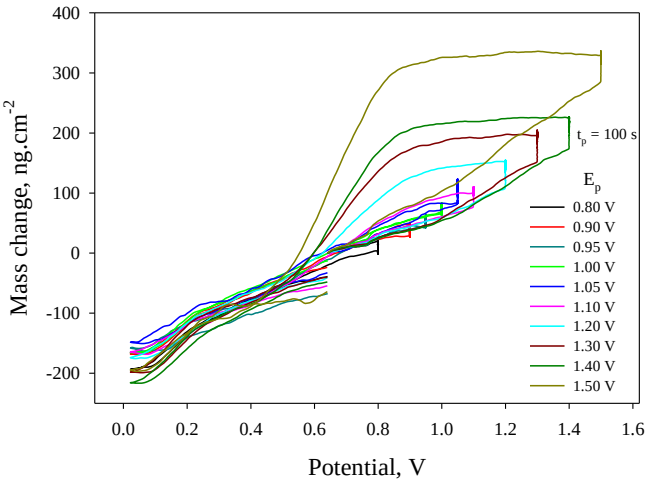

Figure 4-5: Series of mass changes for Pt at different holding potentials (E_ps) in 0.5 M H_2SO_4 for t_p = 100 s recorded at 50 mV s^{-1} (scan direction = 0.6 V - E_p's - 0.7 V - 0.01 V – 0.6 V)

Potentials below ~0.80 V can be regarded as the region of physisorption of water molecules on the Pt surface.[8,11,15,23] Jerkiewicz *et al.*[8] identified chemisorbed O (O_{chem}) at $0.85 \leq E \leq 1.10$ V and reacted O (O^{2-}) in the form of surface PtO at $1.20 \leq E \leq 1.40$ V. At 1.4 V Imai *et al.*[19] found evidence of PtO_2.

Three features of the curves shown in Figure 4-5 are important: Firstly, the extent of the hysteresis increases with the potential of formation E_p, indicating a greater measure of irreversibility of the species the higher the potential of formation. Secondly, no hysteresis is displayed in the range below ~0.8 V. Thirdly, the potential at which reduction takes place, is shifted to lower (more cathodic) values as E_p is increased (clearer in Figure 4-4). These observations are in line with results reported by Jerkiewicz *et al*[8] and Yadav.[21]

The slopes of the different oxidation curves do not differ appreciably and appear to cluster around about 0.5 ng/s cm^2. Further addition of oxygen-containing species during the holding time t_p of 100 s is significantly slower. At E_p = 1.4 V oxygen-containing species are added at a rate of ~0.02 ng/s cm^2, which is twenty-five times slower than at a potential of 0.8 V. This points to fundamentally different reactions that involve the O species.

4.4.4 Chemical and physical characteristics of anodic oxide films on Pt

Figure 4-6 is a comprehensive composite that integrates a large number of results pertaining to the chemical and physical characteristics of anodic oxide films on Pt in 0.5 M H_2SO_4.

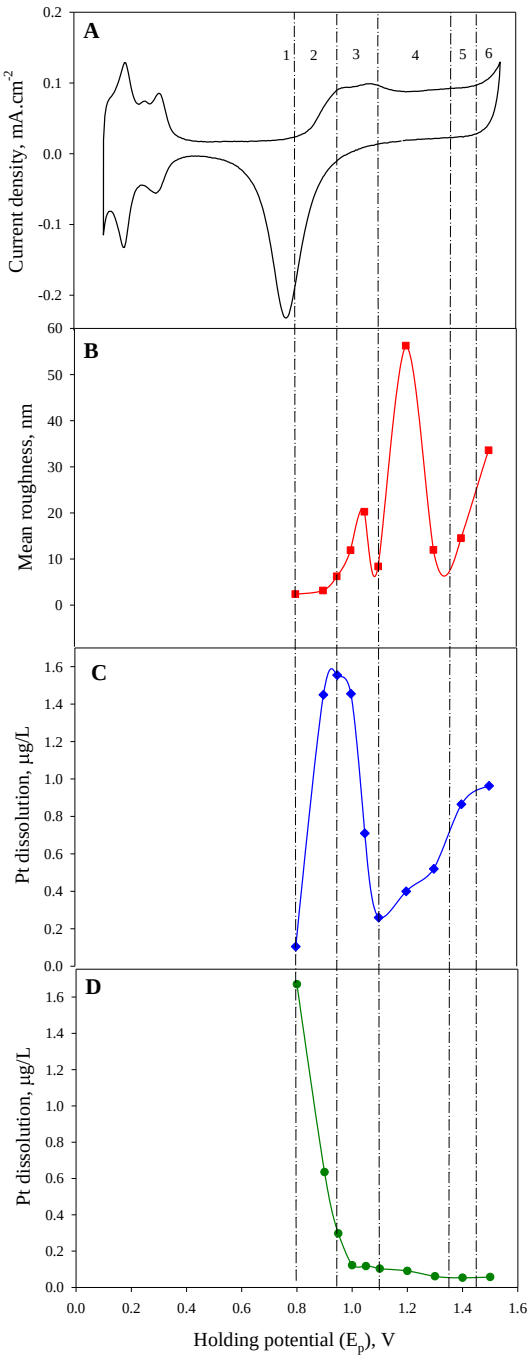

Figure 4-6: **A: Cyclic voltammetric curve of Pt used to select the potential regions of interest as already shown in (Figure 4-3) B: AFM surface roughness after oxidation at different E_ps followed by reduction, C: ICP results for Pt dissolution after different holding potentials (E_ps) and subsequent reduction, and D: ICP results for Pt dissolved at different E_ps without reduction**

A brief summary of the observations relating to Figure 4-6 is given in Table 4-1, while a more detailed discussion of certain issues is given in Section 4.4.5.

Table 4-1: Summary of results of anodic oxide formation at E_p prior to reduction (Figure 4-6 (B) and (C)) and of anodic oxidation without reduction (Figure 4-6 (D))

Nr	Potential range (V)	Description relating to current research	Observations reported in literature ***Current findings***
1	0.27 – 0.8	Physisorption of water molecules	Point of zero charge = ~0.27 V. Physisorption[8,11,15,23] Rapid adsorption (within ~10 s) of OH at ~0.8 V.[19] Normal Pt-Pt bond length 2.7 Å.[11]
2	0.8 – 0.95	Corrosion and beginning of film formation. Start of incorporation of O in Pt lattice.	Increase in the anodic current. Pt-O bond length 2.2 Å.[11] *Slight increase in surface roughness. Pt concentration in surface film increasing.*
3	0.95 – 1.1	Oxide (PtO) film on surface	Probably some rearrangement on surface at ~1.0 V.[1] *Film contains high concentration of Pt. Surface roughness increases due to etching during anodic cycle and/or Pt deposition during cathodic cycle.*
4	1.1 – 1.35	Passivity	PtO forms.[15,16]. Pt-O bond length 2 Å.[11] *Large increase in surface roughness due to oxide formation. Pt concentration in oxide film rising with potential. Flade potential ~1.1 V (see Section 4.4.5.1).*
5	1.35 – 1.45	PtO_2 formation. Transpassivity. Incorporation of interstitial O in Pt (see Section 4.4.5.2)	Pt-O bond length 3.5 Å.[11] *Surface roughness increases due to PtO_2 formation and Pt dissolution. Pt content of film levelling off.*
6	1.45 +	Oxygen evolution	*Pt content of film levelling off. Surface roughness increases due to pitting. Oxide film destroyed.*

4.4.5 Comments with respect to Table 4-1 and Figure 4-6

4.4.5.1 Passivity

Figure 4-7 shows a plot of a passivatable metal in an acid electrolyte.

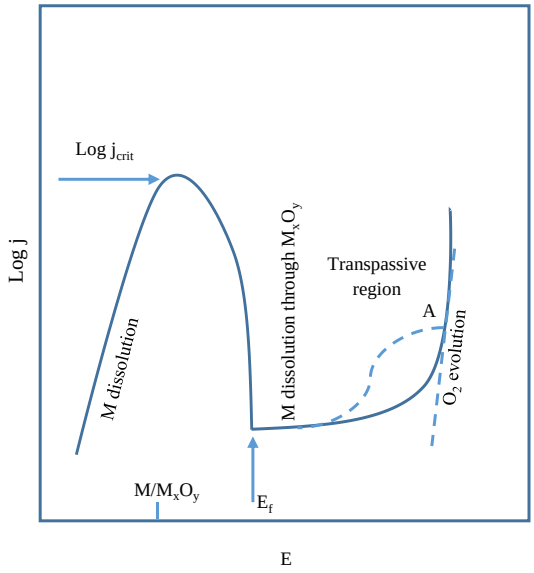

Figure 4-7: Schematic anodic polarization curve of a passivatable metal (Redrawn from West[27])

When a passivatable metal is anodically polarized the current starts to deviate from the rectilinear Tafel line and passes through a maximum value, referred to as the critical passivating current density, j_{crit}, before dropping to a minimum value. The potential at which the minimum current density is reached, when full passivity sets in, is known as the Flade potential (E_f) and corresponds to the onset of the maintenance of the surface film, at a limiting thickness, by a minimal flow of current. In the potential region just above the Flade potential the metal dissolves rapidly, causing the surface to become etched, thereby increasing its roughness. Hoar and Mowat's solid film concept, dating back to 1950[28], in which the formation of a compact solid anodic films on some metals, dissolving at its outer surface as fast as it is formed anodically from the metal, is now fairly generally accepted, although frequently modified.[29] Electrochemical passivation, while having been actively researched for application in base metals, is not generally associated with noble metals. West[27], however, alluded to a platinum Flade potential of ~0.87 V (NHE, Normal Hydrogen Electrode), based on the Pt/PtO couple in H_2SO_4 at a pH of 1.

In the context of the anodic oxidation of platinum, an approach from a passivation viewpoint is instructive, and by comparing the curves shown in Figure 4-6 (A), (B) and (C) the following conclusions can be reached in the context of this passivation process(es):

The flow of the dissolution current causes dissolution of the platinum anode, thereby leading to an increase in the surface roughness and the electrochemically active surface area (EASA), inevitably influencing the results obtained with multi-scan CVs. The significance of this aspect is not generally appreciated, as can be inferred from the work of, for example, Alsabet *et al.*[9]. Prior to the commencement of the oxide-growth experiments,

the Pt working electrodes were subjected to a process referred to as "electrochemical annealing" which involved that the electrode was cycled 200 times between 0.05 and 1.50 V to release any stress.[9] This treatment is bound to roughen the surface due to metal dissolution and ideally should be followed by measuring the EASA by hydrogen adsorption/desorption.

- Within the potential-range of ~1.0 V to ~1.1 V etching of the Pt-surface seems to occur, which in turn seems to be interrupted by some surface occurrence at ~1.1 V, the potential at which full coverage with O adatoms is reached.[1,30] This result seems to agree generally with findings of Jerkiewicz *et al*.[8] and Sugavara *et al*.[8,31], namely that a maximum amount of Pt dissolves between 1.0 and 1.2 V. It is, however, important to note that dissolution of Pt occurs throughout the potential range from 0.8 to 1.4 V. This finding has a bearing on results obtained during long-term polarization in the oxidation region. At slightly higher potentials anodic etching of Pt occurs, leading to maxima in both the dissolution and surface roughness curves at 1.2 V, as shown in Figure 4-6 (B) and (C).
- At ~1.1 V (the Flade potential) the Pt is rendered "passive", with a concomitant drop in the Pt dissolution rate. The range of passivity is, however, very limited. At a potential of 1.4 V significant increases in Pt dissolution and surface roughness are evident in Figure 4-6 (B) and (C).

Figure 4-6 (D) refers to the concentration of Pt in the electrolyte before reduction. It illustrates the concentration of Pt in the electrolyte as a function of the holding potential E_p. At a holding potential of 0.80 V (which is below the potential required for anodic film formation) a relatively large amount of Pt in the electrolyte is evident).

Pt is known to be oxidised at room temperature:[32]

$$Pt + O_2 \rightarrow PtO_2 \qquad (4\text{-}8)$$

With a heat of formation, ΔH, of -134 kJ mol^{-1} at 25°C for PtO_2, the reaction between platinum and oxygen (reaction 4-8) is therefore exothermic. Although PtO_2 is in all likelihood present on platinum surfaces at room temperature, the presence of PtO cannot be discarded.[32,33] If it is assumed that air-formed oxide is PtO_2, the potential would seem to be low enough so as to allow protons to reach the anode surface for the following chemical reaction to take place (reaction 4-9):

$$PtO_2 + 4H^+ + 6H_2O \rightarrow Pt(H_2O)_6^{2+} + 2H_2O \qquad (4\text{-}9)$$

However, as the holding potential is increased to 0.90 V, (reaction 4-9) becomes less efficient as the number of protons approaching the Pt surface is diminished, and subsequently less Pt is detected in the electrolytes. At a potential of 1.0 V reaction (4-9) is prevented. At this potential electrochemical anodic oxide formation starts. It would seem that earlier work largely ignored the possible adsorption of OH or O species before anodic oxidation commences.[34-36] This aspect is important in determining the kinetics of the initial stages of anodic oxide formation.

An important conclusion that can be reached from Figure 4-6 (D) is that relatively small amounts of Pt are dissolved in the electrolyte during the anodic part of a voltammographic cycle.

4.4.5.2 Irreversibility and the interstitial dissolution of oxygen

Gómez-Marín *et al.*[17] suggest that oxide formation on Pt (111) planes starts by the dissociation of water to form OH_{ads}, followed by electrochemical oxidation of OH_{ads} to O_{ads} upon further increase of the potential until a stable adlayer is formed. Simultaneously, an initial Pt oxide structure is formed by an electrochemical reaction between O_{ads} and Pt. The conclusion is that there are at least two types of processes involved in the early growth of the surface oxide layer, as is made clear by the separation of the anodic and cathodic CV curves, reflecting hysteresis arising from a change in the surface oxide film. According to Conway[11] the formation of anodic oxide films, beyond the initial sub-monolayer, is always found to be irreversible on noble metals. This phenomenon, variously referred to as hysteresis or irreversibility, has not been explained adequately. While results by Jerkiewics *et al.*[8] support the incorporation of O atoms in the potential region 1.10 to 1.20 V through a interfacial "place-exchange" mechanism, they visualize this process as the building of a surface PtO lattice. The initial process in the formation of anodic oxide films on Pt is the formation of a complete or partial oxygen-containing monolayer (ML). Beyond the level of the sub-monolayer (incomplete monolayer) the reactions leading to the films are found to be irreversible.[15] In the case of oxide film formation and reduction on Pt the process of place-exchange could provide a different pathway for formation from that in reduction of the oxide film.[11] Consequently, the reduction curve typically found at 0.7 – 0.8 V (see Figure 4-3) probably does not account for the reduction of all the "oxide" formed in the oxidation regime, due to slow kinetics in the reduction stage, or, as is suggested below, due to the physical state of the oxygen contained in the reaction zone. The reduction potential was found to be ~0.74 V for E_p = 0.9 V, dropping to ~0.68 V for E_p = 1.4 V as shown in Figure 4-8.

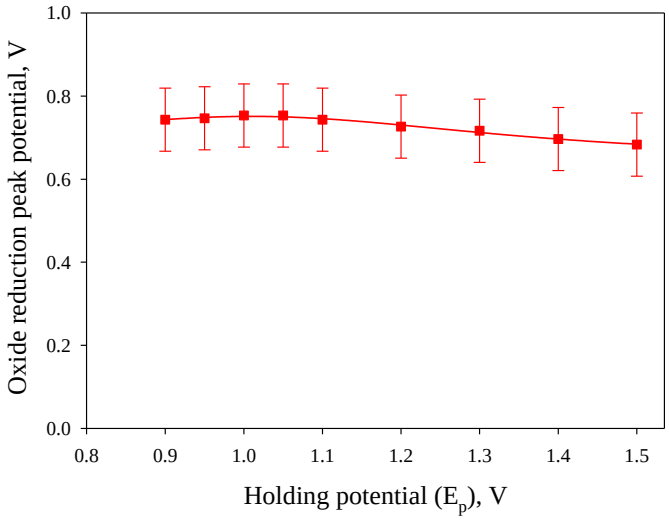

Figure 4.8: Cathodic reduction peak position of Pt from the growth of oxide at different E_ps in 0.5 M H_2SO_4 at a scan rate of 50 mV s^{-1} (see Figure 4-4)

These values are in reasonable agreement with published reduction potentials.[8-10,21,23,37] The reversibility of the reduction peak can help in understanding the reaction mechanism. Angerstein-Kozlowska *et al.*[15] concluded that the irreversibility of the oxide reduction is related to E_p and that the occurrence of reversibility can be attributed to a mechanism involving an irreversible reaction of PtO to PtOH and an irreversible reaction from

PtOH to Pt. This is an example of the unusual mechanisms that have been, and still are, being proposed in an effort to come to grips with the phenomenon of irreversibility. The geometry of the platinum surface determines the transition from reversible to irreversible oxide formation and it seems that the OER is favoured by oxide films on the platinum surface and occurs above 1.0 V.[38]

The absorption of oxygen atoms into dislocations, grain boundaries and into two interstitial sites, namely tetrahedral and octahedral sites, in the platinum lattice has been mooted. However, this has not been established *unequivocally* and the consequences of such a situation has not been fully recognised.

A cutaway view of the unit cell of a face centred cubic metal (such as platinum) and the atomic arrangement around two interstitial sites, namely tetrahedral and octahedral sites is shown in Figure 4-9. A tetrahedral site is developed when triangular voids made by three touching spheres in one layer having contact with spheres in an adjacent layer. In octahedral sites the void is surrounded by six closely packed spheres.

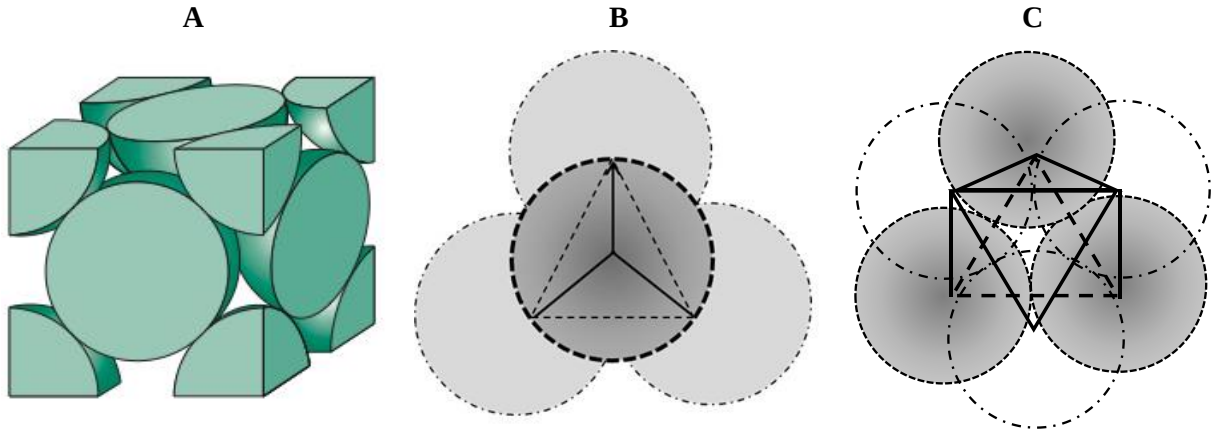

Figure 4-9: (A) Cutaway view of the face centred cubic (FCC) crystal structure. (B) Tetrahedral sites (C) Octahedral sites

The sizes of tetrahedral and octahedral cites can conveniently be expressed in terms of the radii of the inscribed spheres of the defects and the host metals. By simple geometry it can be shown that for tetrahedral interstitial sites r/R = 0.2247 and for octahedral sites r/R = 0.4142, where r is the radius of the dissolved atom and R the radius of the solvent ions. With the radius of the Pt atom = 1.388 Å and the radius of the oxygen atom = 0.600 Å,[39] the radius ratio is 2.31; it is therefore clear that from a geometrical point of view oxygen can be accommodated easily in both interstitial sites. X-ray structural analyses conducted on Pt (111) by Imai *et al.*[19] confirmed a sequence of events starting with the rapid adsorption (within ~10 s) of OH at ~0.8 V. Adsorption of Pt atoms occurs, resulting in a Pt-O bond length of 2.2 Å, followed by further oxidation to atomic oxygen which moves from top sites to energetically more stable 3-fold interstitial spaces – in the process forming shorter Pt-O bonds with a bond length of 2.0 Å *a*t ~1.0 V (20 to 30 s after the potential step). Next, two-dimensional oxides form at ~1.2 V (within 30 to 120 s) and enter the octahedral sites of the platinum lattice, stretching the Pt-Pt bond lengths to ~3.1 Å (compared to the normal Pt-Pt bond length of ~2.7 Å). At ~1.4 V (after about 100 to 120 s and ~1.5 ML of O), quasi-3D oxide with a bond length of ~3.5 Å (indicating the formation of PtO_2) is detected. This exposition offered by Imai *et al.*[19] is useful in interpreting some of the

features shown in Figure 4-6 (B) and (C). The slight drop in current at a potential of ~0.95 V can probably be best described by the "place-exchange" process in which atomic oxygen moves from top sites to interstitial spaces in the Pt lattice just below the surface to form a layer of Pt-O. Between ~1.0 and ~1.2 V a two-dimensional array of Pt-O is established and at ~1.45 V further oxidation leads to OPtO formation. This representation of the oxidation process does not, however, take note of the dissolution of Pt, which is evident from potentials more positive than ~0.9 V. It seems reasonable to assume that these results point towards the possibility that oxygen atoms might easily leave the "oxide" layer at the oxide/platinum interface to be accommodated in the Pt structure in energetically favourable tetrahedral and octahedral cites, as well as in grain boundaries. The important upshot of such an occurrence is that the oxygen atoms will then partly, and as E_p increases eventually totally be disabled from taking part in any electrochemical reduction process.

The physical absorption of oxygen atoms in Pt will therefore present as "irreducible oxide". It is furthermore clear that the unwitting application of the direct logarithmic oxide growth rate law leads to fallacious results, as it will predict oxide thicknesses which have no empirical meaning. The number of oxygen atoms (or monolayers) on the electrode surface can be determined either by the use of EQCM techniques as described in Section 2.6.5 or by calculating the charge density by integrating voltammetric curves. Figure 4-10, which is based on mass change determinations in the EQCM, shows how the number of atoms of oxygen on the electrode surface increase with E_p, with a total coverage of platinum increasing to at least nine monolayers. However, in reported research[8] the number of ML found on the surface rarely exceeds 1 to 2. *Ex situ* AES and EQCN measurements enabled Jerkiewicz *et al.*[8] to conclude that the molecular weight of surface oxides formed in the region 0.85 to 1.4 V is 15.8 g mol^{-1}, which corresponds to the addition of one ML of oxygen, with the charge density involved in this process being 372 μC cm^{-2}. In recent work, employing a range of techniques, coverage of 1 to 2 ML of PtO was found.[1,8,21] In Figure 4-2, which is based on integration of the CV curve, a charge density of ~1 200 μC cm^{-2} at 1.4 V is reported, which, when using the Jerkiewicz figure for the charge density involved, will translate to 3.2 ML.

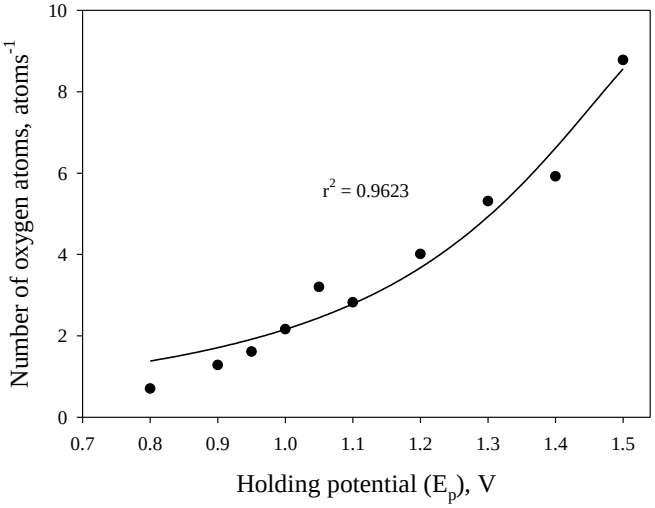

Figure 4-10: Number of oxygen atoms adsorbed on Pt (111) at different E_ps with t_ps = 100 s, determined from the maximum mass changes in Figure 4-5

4.5 Conclusions

Recent literature was used to establish the current state of the knowledge of anodic oxidation of Pt. A new model based on a passivation perspective of the anodic oxidation process of Pt is presented. The build-up of a passive film of the surface of the platinum gives rise to a decrease in the dissolution rate as the potential is increased.[5] The high rate of dissolution preceeding oxide formation can be explained by classic metal passivation.[5] This model accounts for the changes in the surface morphology and chemical species that determine the characteristics of oxidized Pt surfaces. The possibility of oxygen entering the platinum lattice to form a solid solution was used in an attempt to cast new light on the phenomenon of hysteresis in the oxidation/reduction cycle. The continuous movement from the oxide at the oxide/Pt interface to the Pt lattice during logarithmic growth to a limiting thickness at the oxide/electrolyte interface is a central hypothesis of the proposed model. It is argued that the locking of oxygen in tetrahedral and octahedral sites and in grain boundaries causes an imbalance in the charge density required to form and to reduce platinum oxide films resulting in these atoms being rendered electrochemically inactive. This is clearly observed in Figure 4-2 on page 36 where the cathodic charge density is always lower than the anodic charge density. The following depiction (Figure 4-11) is therefore proposed to describe the anodic oxidation of Pt occurring in three stages. There is dissociation of water to OH_{ads}[17] and O_{ads} in the first stage, the interstitial oxygen which is adsorbed on the surface penetrates the crystal lattice of platinum, thereby forming a PtO layer. On the second stage, the PtO formed reacts with the adsorbed interstitial oxygen by further disassembling the platinum surface forming PtO_2, proceeding to stage 3, in which PtO_2 becomes dominant.

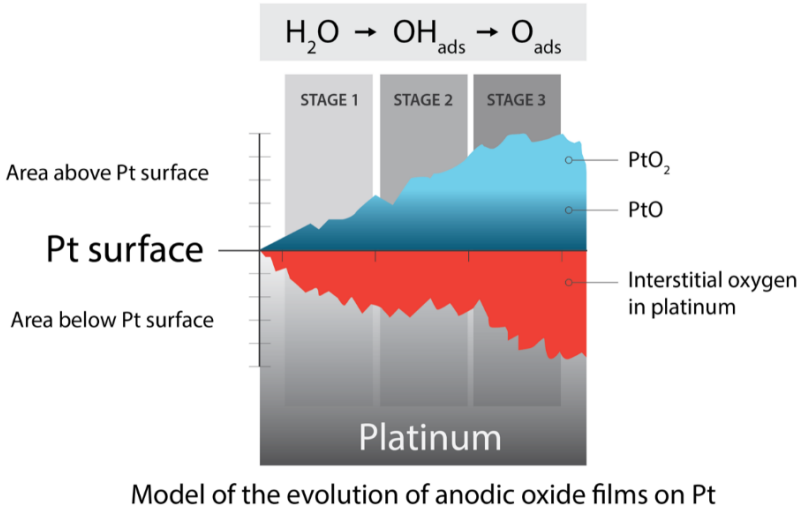

Figure 4-11: A schematic representation of the formation of anodic oxide films on Pt

This postulated model supports the anodic oxidation and dissolution of Pt, as well as the cathodic dissolution of Pt as per reactions 4-10 and 4-11 below.

$$PtO + 5H_2O + 2H^+ \rightarrow Pt(H_2O)_6^{4+} + 2e^- \quad (4\text{-}10)$$

$$PtO_2 + 2H_2O + 4H^+ + 2e^- \rightarrow Pt(H_2O)_4^{2+} \quad (4\text{-}11)$$

This ‘weakening’ and dismantling of the platinum surface through oxidative/reductive dissolution does not preclude subsequent chemical dissolution of platinum (as per reaction 4-12), in fact this ‘weakening’ and dismantling of the platinum surface facilitates chemical dissolution.

$$PtO_2 + 4H_2O + 4H^+ \rightarrow Pt(H_2O)_6^{4+} \quad (4\text{-}12)$$

This would mean that the typical reduction peak that is normally observed for a platinum surface (see Figure 4-3) could incorporate the reduction of the platinum oxide surface, as well as dissolved platinum complexes (reactions 4-8 and 4-9) that still remain in the vicinity of the surface.

4.6 References

1 Topalov, A.A., Cherevko, S., Zeradjanin, A.R., Meier, J.C., Katsounaros, I. & Mayrhofer, K.J.J. Towards a comprehensive understanding of platinum dissolution in acidic media. *Chemical Science* **5**, 631-638 (2014).

2 Hu, C. C. & Wen, T. C. Voltammetric Investigation of Hydrogen Sorption/Desorption at/within Oxide-Derived Pd Electrodes in NaOH and H_2SO_4. *Journal of the Electrochemical Society* **141**, 2996-3001 (1994).

3 Hu, C. C. E. & Liu, K. Y. Voltammetric investigation of platinum oxides. I. Effects of ageing on their formation/reduction behavior as well as catalytic activities for methanol oxidation. *Electrochimica Acta* **44**, 2727-2738 (1999).

4 Shrestha, B. R., Tada, E. & Nishikata, A. Effect of Chloride on Platinum Dissolution. *Electrochimica Acta* **143**, 161-167 (2014).

5 Geiger, S., Cherevko, S. & Mayrhofer, K. J. J. Dissolution of Platinum in Presence of Chloride Traces. *Electrochimica Acta* **179**, 24-31 (2015).

6 Hoare, J. P. Oxygen Overvoltage Measurements on Bright Platinum in Acid Solutions: III . Nitric Acid-Passivated Bright Platinum. *Journal of The Electrochemical Society* **112**, 849-853, doi:10.1149/1.2423709 (1965).

7 Sugawara, Y., Yadav, A. P., Nishikata, A. & Tsuru, T. Dissolution and surface area loss of platinum nanoparticles under potential cycling. *Journal of electroanalytical chemistry* **662**, 379-383 (2011).

8 Jerkiewicz, G., Vatankhah, G., Lessard, J., Soriaga, M. P. & Park, Y.-S. Surface-oxide growth at platinum electrodes in aqueous H_2SO_4: Reexamination of its mechanism through combined cyclic-voltammetry, electrochemical quartz-crystal nanobalance, and Auger electron spectroscopy measurements. *Electrochimica Acta* **49**, 1451-1459 (2004).

9 Alsabet, M., Grden, M. & Jerkiewicz, G. Comprehensive study of the growth of thin oxide layers on Pt electrodes under well-defined temperature, potential, and time conditions. *Journal of Electroanalytical Chemistry* **589**, 120-127 (2006).

10 Qile, G. *Platinum oxide reduction kinetics on polycrystalline platinum electrodes* MSc thesis, Victoria, (2016).

11 Conway, B. E. Electrochemical oxide film formation at noble metals as a surface-chemical process. *Progress in surface science* **49**, 331-452 (1995).

12 Appleby, A. Theory of successive electron transfer steps in cyclic voltammetry: Application to oxygen pseudocapacitance on platinum. *Journal of The Electrochemical Society* **120**, 1205-1214 (1973).

13 Reddy, A., Genshaw, M. & Bockris, J. O. M. Ellipsometric Study of Oxygen-Containing Films on Platinum Anodes. *The Journal of Chemical Physics* **48**, 671-675 (1968).

14 Lanyon, M. H. & Trapnell, B. The interaction of oxygen with clean metal surfaces. *Proc. R. Soc. Lond. A* **227**, 387-399 (1955).

15 Angerstein-Kozlowska, H., Conway, B. & Sharp, W. The real condition of electrochemically oxidized platinum surfaces: Part I. Resolution of component processes. *Journal of Electroanalytical Chemistry and Interfacial Electrochemistry* **43**, 9-36 (1973).

16 Birss, V. I., Chang, M. & Segal, J. Platinum oxide film formation—reduction: an in-situ mass measurement study. *Journal of Electroanalytical Chemistry* **355**, 181-191 (1993).

17 Gómez-Marín, A. M., Clavilier, J. & Feliu, J. M. Sequential Pt (111) oxide formation in perchloric acid: an electrochemical study of surface species inter-conversion. *Journal of Electroanalytical Chemistry* **688**, 360-370 (2013).

18 Harrington, D. A. Simulation of anodic Pt oxide growth. *Journal of Electroanalytical Chemistry* **420**, 101-109 (1997).

19 Imai, H., Izumi, K., Matsumoto, M., Kubo, Y., Kato, K. & Imai, Y. In situ and real-time monitoring of oxide growth in a few monolayers at surfaces of platinum nanoparticles in aqueous media. *Journal of the American Chemical Society* **131**, 6293-6300 (2009).

20 Chao, C., Lin, L. & Macdonald, D. A point defect model for anodic passive films I. Film growth kinetics. *Journal of the Electrochemical Society* **128**, 1187-1194 (1981).

21 Yadav, A. P. Stability of Platinum in Sulfuric Acid Solution Studied by Electrochemical Quartz Crystal Microbalance. *Journal of Nepal Chemical Society* **29**, 24-27 (2013).

22 You, H., Chu, Y.S., Lister, T.E., Nagy, Z., Ankudiniv, A.L. & Rehr, J.J. Resonance X-ray scattering from Pt (111) surfaces under water. *Physica B: Condensed Matter* **283**, 212-216 (2000).

23 McMath, A. A., van Drunen, J., Kim, J. & Jerkiewicz, G. Identification and Analysis of Electrochemical Instrumentation Limitations through the Study of Platinum Surface Oxide Formation and Reduction. *Analytical chemistry* **88**, 3136-3143 (2016).
24 Shibata, S. Conductance measurement of thin oxide films on a platinum anode. *Electrochimica Acta* **22**, 175-179 (1977).
25 Kuhn, A. T. & Wright, P. M. A study of the passivation of bright platinum electrodes during chloride evolution from concentrated sodium chloride solutions. *Electroanalytical Chemistry and Interfacial Electrochemistry* **38**, 291-311 (1972).
26 Redmond, E. L., Setzler, B. P., Alamgir, F. M. & Fuller, T. F. Elucidating the oxide growth mechanism on platinum at the cathode in PEM fuel cells. *Physical Chemistry Chemical Physics* **16**, 5301-5311 (2014).
27 West, J. M. *Electrodeposition and corrosion processes*. First edn, (D van Nostrand & Co, 1965).
28 Hoar, T. & Mowat, J. Mechanism of electropolishing. *Nature* **165**, 64 (1950).
29 Rokicki, R. & Hryniewicz, T. Enhanced oxidation–dissolution theory of electropolishing. *Transactions of the IMF* **90**, 188-196 (2012).
30 Biegler, T. An electrochemical and electron microscopic study of activation and roughening of platinum electrodes. *Journal of the Electrochemical Society* **116**, 1131 (1969).
31 Sugawara, Y., Okayasu, T., Yadav, A. P., Nishikata, A. & Tsuru, T. Dissolution mechanism of platinum in sulfuric acid solution. *Journal of The Electrochemical Society* **159**, F779-F786 (2012).
32 Chaston, J. Reaction of Oxygen with the Platinum Metals I-The oxidation of platinum *Platinum Metals Review* **8**, 50-54 (1964).
33 Brewer, L. Thermodynamic Properties of the Oxides and their Vaporization Processes. *Chemical Reviews* **52**, 1-75 (1953).
34 Chiu, Y.-C. & Genshaw, M. Study of anion adsorption of platinum by ellipsometry. *The Journal of Physical Chemistry* **73**, 3571-3577 (1969).
35 Vetter, K. & Schultze, J. The kinetics of the electrochemical formation and reduction of monomolecular oxide layers on platinum in 0.5 M H_2SO_4: Part I. Potentiostatic pulse measurements. *Journal of Electroanalytical Chemistry and Interfacial Electrochemistry* **34**, 131-139 (1972).
36 Vetter, K. & Schultze, J. The kinetics of the electrochemical formation and reduction of monomolecular oxide layers on platinum in 0.5 M H_2SO_4: Part II. Galvanostatic pulse measurements and the model of oxide growth. *Journal of Electroanalytical Chemistry and Interfacial Electrochemistry* **34**, 141-158 (1972).
37 Jerkiewicz, G., Vatankhah, G., Tanaka, S.-i. & Lessard, J. Discovery of the potential of minimum mass for platinum electrodes. *Langmuir* **27**, 4220-4226 (2011).
38 Lopes, P.P., Strmcnik, D., Tripkovic, D., Connell, J.G., Stamenkovic, V. & Markovic, N.M. Relationships between atomic level surface structure and stability/activity of platinum surface atoms in aqueous environments. *ACS Catalysis* **6**, 2536-2544 (2016).
39 Shannon, R. D., Revised effective ionic radii and systematic studies of interatomic distances in halides and chalcogens. *Acta Crystallographica Setion A: Crystal Physics* **32**, 751-767 (1976).

CHAPTER 5

Anodic oxide growth on platinum in sulphuric acid electrolytes containing chloride ions

5.1 Introduction

The chloride ion forms a strong chemisorption bond with the platinum surface, although the adsorption strength of Cl^- is lower than that of Br^- and I^-.[1] The adsorption involves a redistribution of charge at the interface, with the polarity of the chemisorption bond found to be very small.[2] Halide ions have a strong tendency to be specifically adsorbed on platinum, beginning right from the hydrogen evolution region, with equilibrium coverage of chloride varying linearly with potential.[3,4] It has been demonstrated that the adsorption of chloride and hydrogen has a synergistic character, while chloride and OH_{ad} are in competition for adsorption sites.[2] Chloride ions retard passivating film formation on platinum. Competition between the specifically adsorbed chloride ions and oxygen accounts for the inhibition of platinum oxide film formation.[4] Experimental results show that despite the presence of an overwhelming number of other ions (X), the adsorption of Cl^- ions is not diminished, even if the molar ratio X/Cl^- is as low as 10^{-6}.[5] It was found that Cl^- selectively blocked the initially deposited OH monolayer at Pt.[6] A mechanism has been proposed for the anodic oxidation of platinum and the adsorption of chloride ions.[7] It is suggested that oxide film formation is initiated by the occupation of half of the surface by Pt/O species up to 1.10 V. This process is followed by completion of the monolayer coverage by O species, with simultaneous place-exchange. In this potential region the blocking effect of adsorbed Cl^- is evidenced by the occurrence of an isopotential point at 1.10 V. Beyond this stage the formation of the oxide film resembles that of film growth in the absence of Cl^- for coverage $\theta_o > 0.5$.[7] Recent data obtained by means of sensitive EQCN nanogravimetry measurements on the effect of Cl^- on Pt dissolution showed that adsorption of Br^- leads to net positive mass changes and that of Cl^- to net negative mass changes in the oxide region.[8] At a low chloride ion concentration of 10 ppm Pt (~300 μM) dissolution was induced, however dissolution was enhanced above about 100 ppm Cl^-, with significant mass loss due to Pt dissolution above 1.2 V in a CV anodic scan. Yadav *et al*.[9] illustrated that the CV in 0.5 M H_2SO_4 can be divided into three regions: (i) 0.0 to 0.4 V (hydrogen adsorption and desorption), (ii) 0.4 to 0.75 V (double layer region) and (iii) 0.75 to 1.4 V (dissolution and surface oxidation of Pt). The CV indicates that the oxidation of Pt begins at around 0.75 V in the anodic direction with the accompanying mass growth recorded by the EQCM. The Pt/PtO peaks are suppressed in the presence of chloride ions. In the negative-going scan, a cathodic peak is observed at 0.75 V due to surface oxide reduction, which is reflected in a mass decrease. The cathodic re-deposition of Pt ions is hindered, probably due to increase in the overpotential for the reduction of chloride complex. The H_{upd} and H-adsorption/desorption regions are narrowed and their shapes slightly modified by strong Cl^- adsorption.[9] In the presence of Cl^- increased Pt/PtO solubility in 1.0 M H_2SO_4 and enhanced Pt loss in presence of 10 mg/l Cl^- were found.[9-12] Dissolution of Pt in the form of $[PtCl_4]^{2-}$ occurred below 1.2 V and resulting in the formation of $[PtCl_4]^{2-}$ and $[PtCl_6]^{2-}$ above 1.2 V.[12,13] The dissolution of Pt as Pt^{4+} may proceed through a two-step anodic dissolution sequence given by the following equations:

$$Pt + H_2O \rightarrow Pt{-}O + 2e^- + 2H^+ \quad (5\text{-}1)$$

$$Pt{-}O + 6Cl^- + 2H^+ \rightarrow [PtCl_6]^{2-} + H_2O + 2e^- \quad (5\text{-}2)$$

In some regions, Pt–O may be oxidized to $[PtCl_6]^{2-}$ which, as it detaches from the WE, the underlying Pt atom is quickly oxidized to Pt–O, which may later react with Cl^- to form to $[PtCl_6]^{2-}$.[13] Increased potential during potentiostatic experiments show that the anodic dissolution of platinum can be characterised by active, passive and transpassive regions[14] (*cf.* Chapter 4). Appreciable influence of chlorides can then be seen in the active (0.9 – 1.1 V) and transpassive (>1.5 V), regions. Mass variations and voltammetric charges determined by means of EQCM and cyclic voltammetry were used to study surface occupation after hydrogen desorption.[15] Firstly, a mass increase was observed due to the replacement of UPD H (associated charge density: 210 μC cm^{-2} per monolayer) by 39 ng cm^{-2} of water molecules (about a full monolayer). Secondly, the mass change due to adsorption of hydrated anions occurred in the potential region 0.4 to 0.8 V showed maximum coverages of 7% and 11% for $HSO_4^-.2H_2O$ and $Cl^-.6H_2O$, respectively.[15] It has been demonstrated that, in the potential range $0.2 < E < 0.3$ V hydrogen and chloride adsorb simultaneously on Pt, while at potentials $0.3 < E < 0.7$ V chloride blocked hydrogen and OH adsorption.[16] OH^- adsorption is observed above 0.8 V.[1]

5.1.1 Hydrogen evolution

A review which summarizes the accepted concepts of the fundamental aspects of the development of hydrogen on metal cathodes in aqueous solutions was presented by Jerkiewicz[17], based on the notion of dissociative adsorption of hydrogen on a metal surface, resulting in the chemical splitting of the H_2 molecule into two H atoms that are chemisorbed on the surface. Furthermore, two distinct electro-adsorption phenomena are thought to be involved in the HER, namely the under-potential deposition of H (H_{upd}) and the over-potential deposition of H (H_{OPD}). Only certain noble metals (notably Pt and Pd) display H_{upd}.[17] By adsorbing S onto a Pt electrode Protopopoff & Marcus[18] demonstrated that H_{upd} and H_{opd} occupy different surface sites, with the sites that favour weakly bonded H being completely blocked. Frelink *et al.*[19] identified weak bonding sites as Pt(110) planes with adsorption occurring at ~0.1 V, while hydrogen is adsorbed on strong bonding sites (Pt(100)) at ~0.23 V. Markovic & Grgur[20] reported that the exchange current for hydrogen evolution increases in the order (110)>(100)>(111) for Pt. They concluded that on Pt(110) the reaction follows the Tafel-Volmer (T-V) mechanism, while the Heyrovsky-Volmer (H-V) sequence is followed on Pt(100). Vilekar *et al.*[21] found that the Volmer-Heyrovsky-Tafel (V-H-T) and the Volmer-Heyrovsky (V-H) reaction pathways should be used to describe the HER. These traditionally accepted concepts did not lead to a satisfactory comprehension of hydrogen adsorption and evolution on metal surfaces.

Juodkazis *et al.*[22] made a major contribution to the understanding of the adsorption processes that precede the evolution of hydrogen on Pt electrodes in acid solutions by indicating the possible involvement of the molecular ion H_2^+. This approach is elaborated in Chapter 3 of this thesis and only a brief summary is given here: When the potential is swept in the cathodic direction the first electrochemical process to be considered is the dissociation of surface H_2O, followed by adsorption of H_3O (reaction 5-3). The second electrochemical

process is the reduction of $(H_3O^+)_{ads}$ to the molecular hydrogen ion, H_2^+, followed by the adsorption of the latter onto the Pt surface reversibly where it is reduced to H_2 molecules (reaction 5-4).

$$2(H_2O)_{surf} \rightleftharpoons (H_3O^+)_{ads} + OH^- \quad (5\text{-}3)$$

$$2(H_3O^+)_{ads} + e^- \rightleftharpoons (H_2^+)_{ads} + 2H_2O \quad (5\text{-}4)$$

The adsorbed molecular hydrogen ion, $H_2^+{}_{ads}$, therefore acts as an intermediate in the reversible overall electrochemical reaction for the production of hydrogen (reaction 5-5).[22]

$$(H_2^+)_{ads} + e^- \rightleftharpoons H_2 \quad (5\text{-}5)$$

In the context of the present study the existence of $H_2^+{}_{ads}$ on the Pt surface can be expected to have a pronounced effect on the behaviour of adsorbed Cl, Br and I species.

It is the aim of this chapter to convey and discuss the results of the anodic oxide growth on platinum in sulphuric acid electrolytes containing chloride ions.

5.2 Experimental

Please refer to chapter 2 for a description of the appropriate techniques employed as part of this investigation. The in-house cell employed is described in section 2.3.1 (Figure 2-3) and the electrode holder is shown in Figure 2-4. The platinum quartz electrodes were pre-treated as discussed in section 2.2.2. The electrolyte of 0.5 M H_2SO_4 containing chloride ions were prepared by following section 2.2.3.3. The potentiostat and the QCM were connected as discussed in section 2.3.2. The QCM was calibrated as discussed in section 2.4.6.1. The electrochemical procedures followed section 2.4.5. The mass changes were recorded with a QCM and analyzed as discussed in section 2.4.6.2. The physical characterization of the Pt quartz after subjected to electrochemical procedures, ICP-MS was used to determine Pt content in the electrolyte as discussed in section 2.6.1.

5.3 Results and discussion

5.3.1 CV and EQCM results

Figures 5-1 to 5-3 consist of overlays of CVs for holding potentials (E_ps) of 0.8, 1.2 and 1.5 V for chloride concentrations of 6, 60 and 600 μM, and the corresponding EQCM traces. An important feature of the EQCM curves is the difference in the initial and the final mass of the electrode, indicated by $\Delta w_{(EQCM)}$, and discussed in greater detail in Section 5.3.2.

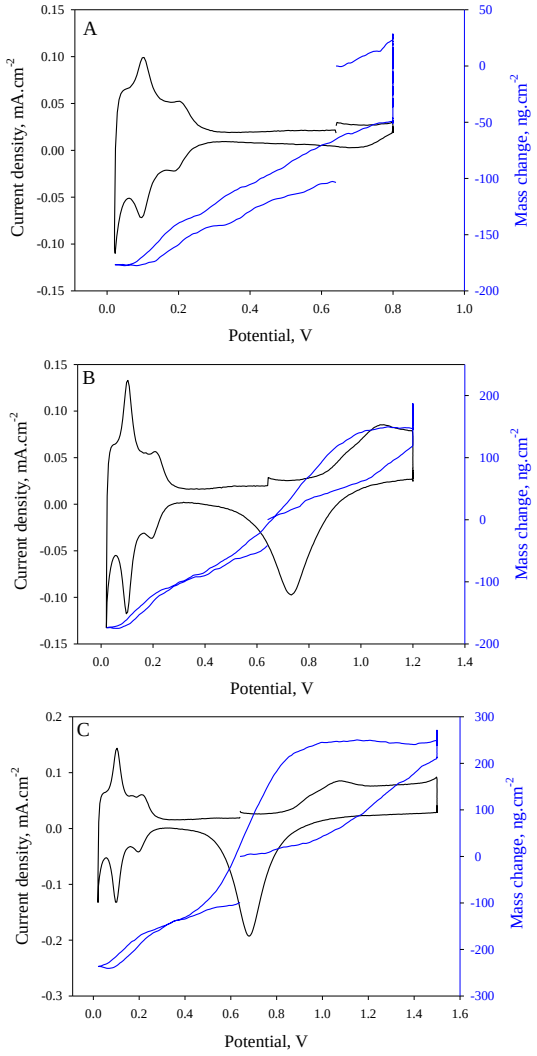

Figure 5-1: CVs and mass changes for 6 µM Cl^- (E_p = (A) 0.80, (B) 1.20 (C) 1.50 V)

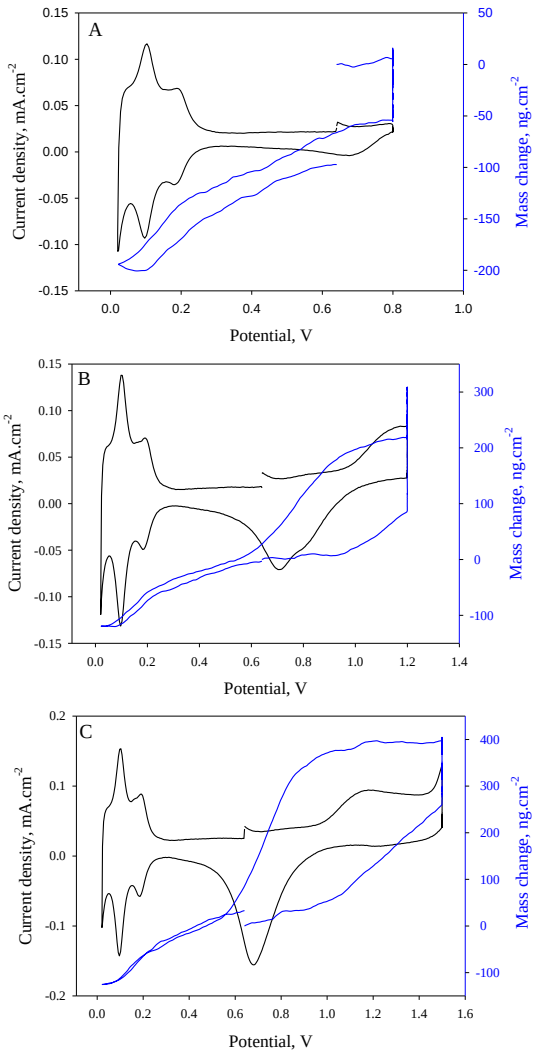

Figure 5-2: CVs and mass changes for 60 µM Cl^- (E_p = (A) 0.80, (B) 1.20 (C) 1.50 V)

Figure 5-1 (A) indicates that an E_p of 0.8 V is below the threshold for oxide formation. The reduction cycle, consequently, does not show the familiar oxide reduction curve at ~0.72 V, and the EQCM curve displays a negative $\Delta w_{(EQCM)}$, indicating a loss of Pt. In Figure 5-1 (B) a change in slope of the EQCM curve in the anodic direction is evident at ~1.1 V, probably due to the adsorption of O species. Figures 5-1 (B) and 5-1 (C) show the reduction of platinum oxide and positive values of $\Delta w_{(EQCM)}$ are found, which may be ascribed to the incomplete reduction of platinum oxide.

Figure 5-2 (A) indicates that an E_p of 0.8 V is just below the threshold for oxide formation. The reduction cycle shows the first sign of the familiar oxide reduction curve at ~0.72 V, and the EQCM curve displays a negative $\Delta w_{(EQCM)}$, indicating loss of Pt. In Figure 5-2 (B) the interference of Cl^- in the oxide formation process becomes apparent. The cathodic reduction peak is somewhat distorted, which probably indicates relative dominance of adsorbed Cl^- ions, preventing full coverage of the electrode by oxygen species. Figure 5-2 (C) shows a situation in which the higher holding potential favours increased adsorption of oxygen species, resulting in a symmetrical reduction curve. The negative $\Delta w_{(EQCM)}$ values in Figure 5-2 (B) and Figure 5-2 (C) indicate that the reduced surfaces were corroded, leading to a loss of platinum.

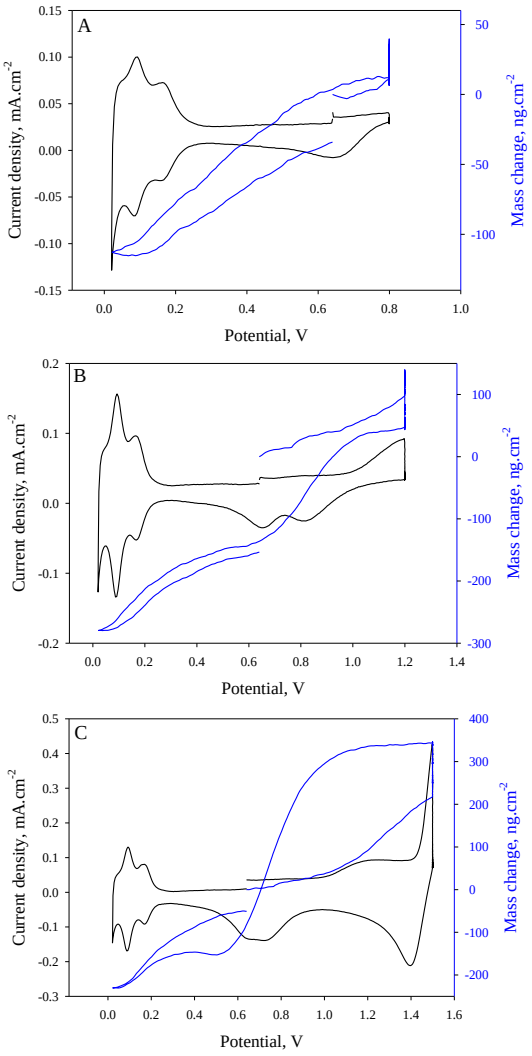

Figure 5-3: CVs and mass changes for 600 µM Cl^- (E_p = (A) 0.80, (B) 1.20 (C) 1.50 V)

The relatively high concentration of 600 µM Cl^- has a pronounced influence on the shape of the CV curves in the oxide region (Figures 5-3 (B) and (C)). Chlorine evolution starts at ~1.36 V in solutions containing 600 µM chloride.[4] Oxide formation is influenced by adsorbed Cl_2 gas as shown the instantaneous drop in current at potential reversal, the appearance of a reduction peak at 1.4 V and the development into a double peak of the usual oxide reduction peak. Moving in the anodic direction an ill-defined peak develops in the potential region of ~1.0 to 1.3 V, which is accompanied by a mass increase of ~140 ng/cm^2 (see Figure 5-3 (C)). The characteristic plateaux formation indicating that the formation of a Pt oxide layer is largely absent indicating an interruption in the oxide forming process. Holding at a potential of 1.5 V leads to an increase of ~135 ng/cm^2, which can be attributed to the adsorption of chlorine. Reversal of the scan after a holding time of 100 s at E_p = 1.5 V (see Figure 5-3 (C)) leads to minimal weight loss up to 1.4 V, accompanied by appreciable flow of charge, which has to be attributed to the reduction of Cl_2 to of Cl^-.

The partial blocking of oxide layer formation by chloride ions is reflected in the shrinking of the oxide reduction peak from ~ 0.19 mA/cm^2 at a Cl^- concentration of 6 µM to ~0.14 mA/cm^2 at a Cl^- concentration of 600 µM at ~0.66 V (Figures 5-1 (C) and 5-3 (C)). The oxide reduction peak (Figures 5-3 (C)) is also ill-defined and partly overlaps a peak at ~0.73 V. As chloride ions are known to attack Pt above 1.2 V the possibility has been raised that there may be some interplay between Cl^- and Pt–O reduction.[13] In the anodic region some Pt–O may be oxidized to $[PtCl_6]^{2-}$, which may be reduced to Pt at ~0.73 V, followed by Pt–O reduction at ~0.65 V.

Comparison of the CVs in Figures 5-1 to 5-3 with Figure 4-3 in Chapter 4 confirms that chloride ions do not appreciably modify the H-adsorption/desorption peaks at ~0.1 and ~0.2 V, even at the relatively high chloride concentration of 600 µM. It has been mentioned in Chapter 3 that chloride ions absorbs simultaneously with hydrogen. The other observation is that the third peak of hydrogen in the hydrogen desorption region disappears, which at this moment is not fully understood.

5.3.2 Combination of ICP and EQCM results

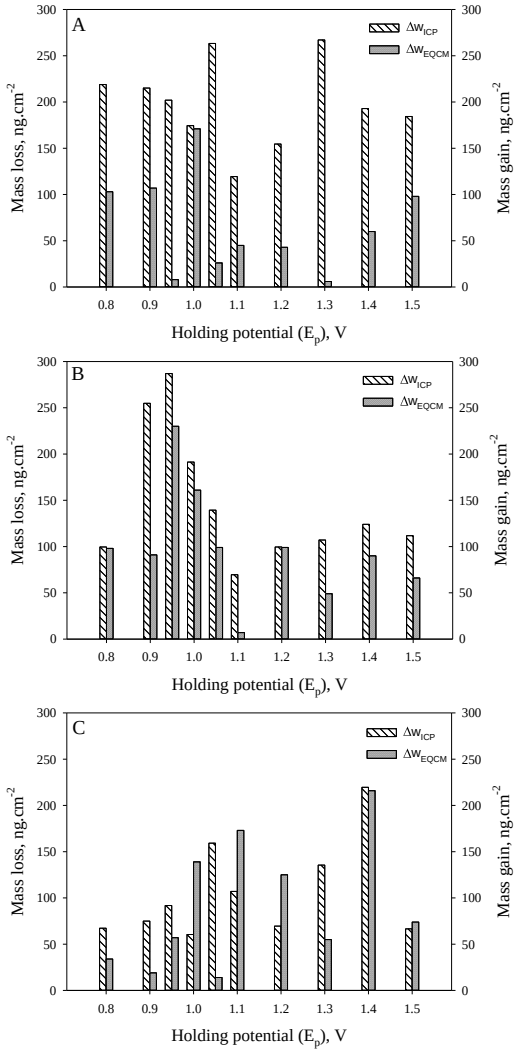

Figure 5-4: Values of mass loss $\Delta w_{(ICP)}$ and mass gain $\Delta w_{(EQCM)}$ as a function of E_p's at Cl^- of (A) 6 µM (B) 60 µM and (C) 600 µM

A feature of the EQCM curves obtained during full cycle CV scans is that the final mass of the platinum as determined by the quartz microbalance, in general, was less than the initial mass by an amount $\Delta w_{(EQCM)}$ (see Figures 5-1 to 5-3). Furthermore, the concentration of Pt in the electrolyte also represents mass lost from the electrode, as indicated by $\Delta w_{(ICP)}$ (see Figure 5-4 where the $\Delta w_{(EQCM)}$ was calculated from Figure 2A (A), (B) and (C) in Appendix A). Generally, $\Delta w_{(ICP)}$ is larger than $\Delta w_{(EQCM)}$. They represent different facets of the history of an electrode as it develops during a voltammetric cycle. Ideally these two values will be equal, but adsorption of ions in the double layer region will cause a difference in mass. At holding potentials that are favourable for adsorption of ions, $\Delta w_{(ICP)}$ will exceed $\Delta w_{(EQCM)}$ by an amount dependent on the extent of adsorption. In these cases, unreduced Pt oxide (e.g. interstitially bound oxide) may also play a role. The ions which are considered actively adsorbing in the double layer region are thought to be chloride and O.

The latter has been suggested initially to be bound in the form of the dipole $(Pt–Pt)^{\delta+}–O^{\delta-}$), which during place exchange converts to $Pt–O_{chem}$ and finally to a quasi-3D lattice of $Pt^{2+}–O^{2-}$.[23]
Figure 5-4 is useful in that it allows certain trends to be identified:

- Figure 5-4 (A) shows appreciable adsorption at 0.95 V which denotes the advent of oxide formation. (The strong adsorption at 1.30 V remains unexplained but is thought to be associated with the adsorption of chlorine gas).
- Figure 5-4 (B) displays notable adsorption at the holding potential of 1.10 V.
- In Figure 5-4 (C) maximum adsorption occurs at a holding potential of 1.05 V.

In order to explain the different amounts of adsorption displayed at different holding potentials the passivity behaviour of Pt has to be considered. In Section 4.4.5.1 it was pointed out that the process of passivation is preceded by a situation in which a relatively large critical current density is required. This process leads to

etching (roughening) of the electrode surface. The roughening leads to facilitation of adsorption of ad-ions when oxide films are reduced. Holding the electrode at a potential which is favourable for passive oxide formation, will therefore eventually have the effect of increased adsorption in the positive-going part of the CV.[24]

5.4 Conclusions

The results show that in the anodic cycle of Pt in chloride-containing electrolytes the adsorption of chloride ions is favoured initially and eventually replaced by oxide species in the potential range 0.8 to ~1.1 V. The extent of the replacement of Cl^- by O species is dependent on the Cl^- concentration and is manifested by a slight change in the slopes of the EQCM curves in the anodic direction. At a relatively high concentration of 600 μM Cl^- has a pronounced influence on the shape of the CV curves in the oxide region. Oxide formation is influenced by adsorbed Cl_2 gas and the eventual evolution of chlorine at ~1.36 V. In the cathodic direction the reduction of Cl_2 to Cl^- occurs. A new insight into the electrochemistry of Pt in 0.5 M H_2SO_4 was afforded by the comparison of the EQCM mass curves with those derived from ICP Pt analyses. It became clear that the surface damaged caused by the reductive removal of Pt oxides led to an increased propensity to adsorb ions in the boundary region in the anodic part of a full voltammetric cycle. This insight places a question mark over the value of some published multi-cycle CV's.

5.5 References

1 Devivaraprasad, R., Kar, T., Leuaa, P. & Neergat, M. Recovery of Active Surface Sites of Shape-Controlled Platinum Nanoparticles Contaminated with Halide Ions and Its Effect on Surface-Structure. *Journal of The Electrochemical Society* **164**, H551-H560 (2017).

2 Li, N. & Lipkowski, J. Chronocoulometric studies of chloride adsorption at the Pt (111) electrode surface. *Journal of Electroanalytical Chemistry* **491**, 95-102 (2000).

3 Kuhn, A. T. & Wright, P. M. A study of the passivation of bright platinum electrodes during chloride evolution from concentrated sodium chloride solutions. *Electroanalytical Chemistry and Interfacial Electrochemistry* **38**, 291-311 (1972).

4 Patil, R. S., Juvekar, V. A. & Naik, V. M. Oxidation of Chloride Ion on Platinum Electrode: Dynamics of Electrode Passivation and its Effect on Oxidation Kinetics. *Industrial & Engineering Chemistry Research* **50**, 12946-12959 (2011).

5 Horanyi, G., Inzelt, G. & Szetey, E. Open circuit potential oscillations of platinum electrodes immersed in solutions of organic fuels and redox systems. Imitation of galvanostatic potentialoscillations observed in the course of electrooxidation of organic fuels. *Journal of Electroanalytical Chemistry and Interfacial Electrochemistry* **81**, 395-401 (1977).

6 Novak, D. & Conway, B. Competitive adsorption and state of charge of halide ions in monolayer oxide film growth processes at Pt anodes. *J. Chem. Soc., Faraday Trans. 1* **77**, 2341-2359 (1981).

7 Zolfaghari, A., Conway, B. E. & Jerkiewicz, G. Elucidation of the effects of competitive adsorption of Cl^- and Br^- ions on the initial stages of Pt surface oxidation by means of electrochemical nanogravimetry. *Electrochimica Acta* **47**, 1173-1187 (2002).

8 Conway, B., Zolfaghari, A., Pell, W. & Jerkiewicz, G. Voltammetry, nanogravimetry and double-layer capacitance studies on chemisorption of Cl^- and Br^-, competitive with potential-dependent electrosorption of O species at Pt electrodes. *Electrochimica Acta* **48**, 3775-3778 (2003).

9 Yadav, A., Nishikata, A. & Tsuru, T. Effect of halogen ions on platinum dissolution under potential cycling in 0.5 M H_2SO_4 solution. *Electrochimica Acta* **52**, 7444-7452 (2007).

10 Mitsushima, S., Koizumi, Y., Uzuka, S. & Ota, K.-I. Dissolution of platinum in acidic media. *Electrochimica Acta* **54**, 455-460 (2008).

11 Lam, A., Li, H., Zhang, S., Wang, H., Wilkinson, D.P., Wessel, S. & Cheng, T.T. Ex situ study of chloride contamination on carbon supported Pt catalyst. *Journal of Power Sources* **205**, 235-238 (2012).

12 Shrestha, B. R., Tada, E. & Nishikata, A. Effect of Chloride on Platinum Dissolution. *Electrochimica Acta* **143**, 161-167 (2014).

13 Wang, Z., Tada, E. & Nishikata, A. In Situ Analysis of Chloride Effect on Platinum Dissolution by a Channel-Flow Multi-Electrode System. *Journal of The Electrochemical Society* **161**, F845-F849 (2014).

14 Geiger, S., Cherevko, S. & Mayrhofer, K. J. J. Dissolution of Platinum in Presence of Chloride Traces. *Electrochimica Acta* **179**, 24-31 (2015).

15 Santos, M., Miwa, D. & Machado, S. Study of anion adsorption on polycrystalline Pt by electrochemical quartz crystal microbalance. *Electrochemistry communications* **2**, 692-696 (2000).

16 Garcia-Araez, N., Climent, V., Herrero, E., Feliu, J. M. & Lipkowski, J. Determination of the Gibbs excess of H adsorbed at a Pt (111) electrode surface in the presence of co-adsorbed chloride. *Journal of Electroanalytical Chemistry* **582**, 76-84, doi:http://dx.doi.org.nwulib.nwu.ac.za/10.1016/j.jelechem.2005.01.031 (2005).

17 Jerkiewicz, G. Electrochemical hydrogen adsorption and absorption. Part 1: Under-potential deposition of hydrogen. *Electrocatalysis* **1**, 179-199 (2010).

18 Protopopoff, E. & Marcus, P. Effect of chemisorbed sulfur on the electrochemical hydrogen adsorption and recombination reactions on Pt (111). *Journal of Vacuum Science & Technology A* **5**, 944-947 (1987).

19 Frelink, T., Visscher, W. & Van Veen, J. The third anodic hydrogen peak on platinum; Subsurface H_2 adsorption. *Electrochimica Acta* **40**, 545-549 (1995).

20 Markovic, N., Grgur, B. & Ross, P. Temperature-dependent hydrogen electrochemistry on platinum low-index single-crystal surfaces in acid solutions. *The Journal of Physical Chemistry B* **101**, 5405-5413 (1997).

21 Vilekar, S. A., Fishtik, I. & Datta, R. Kinetics of the hydrogen electrode reaction. *Journal of The Electrochemical Society* **157**, B1040-B1050 (2010).

22 Juodkazis, K., Juodkazytė, J., Šebeka, B. & Juodkazis, S. Reversible hydrogen evolution and oxidation on Pt electrode mediated by molecular ion. *Applied Surface Science* **290**, 13-17, doi:10.1016/j.apsusc.2013.10.164 (2014).

23 Jerkiewicz, G., Vatankhah, G., Lessard, J., Soriaga, M. P. & Park, Y.-S. Surface-oxide growth at platinum electrodes in aqueous H_2SO_4: Reexamination of its mechanism through combined cyclic-voltammetry, electrochemical quartz-crystal nanobalance, and Auger electron spectroscopy measurements. *Electrochimica Acta* **49**, 1451-1459 (2004).

24 Sugawara, Y., Okayasu, T., Yadav, A. P., Nishikata, A. & Tsuru, T. Dissolution mechanism of platinum in sulfuric acid solution. *Journal of The Electrochemical Society* **159**, F779-F786 (2012).

CHAPTER 6

Anodic oxide growth on platinum in sulphuric acid electrolytes containing bromide ions

6.1 Introduction

6.1.1 The nature of surface films formed on Pt during anodic polarization

It has been found that the polarizability of halide ions increases in the order:

$$F^- < Cl^- < Br^- < I^-$$

This order also reflects the strength of specific adsorption displayed by the halide ions.[1] However, in the case of oxyanions, the correlation of specific adsorption with polarizability does not hold.

There seems to be wide agreement that the formation of a surface oxide on Pt in acidic electrolytes, according to a logarithmic rate law, involves the following steps: (i) discharge of H_2O with release of two hydrated protons (H^+_{aq}) and a chemisorbed O (O_{chem}); and (ii) formation of a quasi–3D lattice comprising Pt^{2+} and O^{2-} through a "place–exchange process".[2-6] Ellipsometric studies have shown that the oxidation/reduction hysteresis in the potentials for the formation and reduction of the oxygen films on Pt is due to "place exchange", as the cathodic reduction profile can be resolved into reversible and irreversible components. The irreversible component is thought to arise from a rearrangement of the surface oxide and is already formed to a significant extent well below a monolayer of "PtOH". It is reduced at more negative potentials and gives rise to the characteristic hysteresis between oxide formation and reduction processes at Pt.[7] Because the "place–exchange" is thought to start above 1.05 V, the reaction below 1.05 V is just the simple adsorption of OH or O.[8] Four oxygen species (O_{ad}, OH_{ads}, and two types of water molecules) were distinguished by means of X–ray photoelectron spectroscopy. This provided experimental evidence that the OH_{ads} formation is the first step in anodic surface oxidation of Pt and that O_{ads} originates from the oxidation of OH_{ads}.[9]

6.1.2 The influence of bromide adsorption on the oxidation of platinum

Compared to Cl^- there is scant literature on the electrochemistry of Br^-.[10]

Halogen anions specifically adsorbed on platinum enhance several destructive electrochemical reactions, such as oxidation/reduction, metal deposition, corrosion and dissolution. Catalyst poisoning by adsorbed halide anion impurities decreases catalytic activity and is a well–known problem in batteries, electrolyzers and fuel–cells.[11] A new type of fuel cell, the regenerative fuel cell in which chemicals used in the charging cycle are stored and subsequently used as fuels during discharge to produce electricity is being studied. One such system is the H_2/Br system, which allows up to 90% of the chemical energy stored in the reactants to be converted to electricity. There is therefore renewed interest in the oxidation of Br^- to bromine and the conversion of Br^- and bromine to Br_3^-.[12] Early work brought attention to the competitive nature of halide ion adsorption in

relation to simultaneous oxide formation on platinum surfaces.[13] Reports on the amount of oxide blocking caused by Br^- vary appreciably. Almost complete blocking of the "first stage" of oxide film formation (at ~1.1 V Reversible hydrogen electrode (RHE) and $5x10^{-5}$ M Br^-), has been reported.[10,13,14] Br^- adsorption is frequently reported as Langmurian, whereas Cl^- adsorption is usually found to be linear or logarithmic.[10,13,14] It was found that a monolayer of Br^- formed between 0.5 and 1.1 V in an electrolyte with a Br^- concentration of 10^{-4} M.[15] The capacitance component of the impedance vs potential curves indicated the presence of a faradaic pseudocapacitance in the 1.0 to 1.3 V region attributed to the adsorption of Br^-.[15] In the Br adsorption process a large number of Br species may be involved, competing for the available Pt sites: Br^- [13-18], $Br^{\delta-}$ (Br displaying partial electron transfer) [13,18], radical species [10] and Br_3^- [12,19,20] have been reported. By taking advantage of the very high absorptivity of Br_3^-, the species were successfully studied quantitatively in the diffusion zone by the use of UV–vis spectroscopy.[12] Current and potential oscillations during electrochemical oxidation of bromide ions were ascribed to the formation and dissolution of Br_3^-.[19] The kinetics of Br_3^- reduction is controlled by surface dissociation of Br_2 molecules.[20] Signs of specific adsorption have been reported in the literature.[15,16] The first effects of Br^- can be detected at a concentration of 10^{-8} M.[13]

The adsorption of Br species with regard to hydrogen adsorption/desorption leads to a more complete understanding of the underlying processes. Br^- interferes with the hydrogen adsorption processes.[17] While the weak adsorption of hydrogen is affected by Br–related species, the strongly adsorbed type of hydrogen is not greatly affected.[10] The double layer is broadened with increasing Br^- concentration and Br^- was found to adsorb in the hydrogen region during anodic sweeps. With increasing Br^- concentration the H_{ads}/H_{des} region peak potentials are progressively shifted to more negative values.[15] In the presence of Br^- the peak at 0.125 V is relatively less intense than the peak at 0.127 V, and with increasing bromide concentration both peaks are shifted towards lower potentials due to concurrent adsorption/desorption of H/Br^-.[17] At low concentrations (~$5x10^{-6}$ M) Br^- adsorption seems to be associated with H_{ads}/H_{des}, resulting in the suppression of H_{upd}. With higher Br^- concentration (10^{-2} M) two separate peaks are observed in the H_{upd} region, namely a peak at 0.07 V due to adsorption/desorption of Br^- along with hydrogen and a peak at 0.15 V corresponding to the adsorption of Br^-.[15,17] The parameters of the adsorption of Br^--containing species where determined from the hydrogen adsorption/desorption region and the oxide reduction peak[10]. Underpotential deposition of Br was found at potentials as low as 0.02V.[10] A peak at ~ –0.114 V, which is related to a similar anodic peak, was attributed to underpotential deposition of bromine.[10]

Bromine evolution was found to start at 1.2 V.[17] Oxidation of Br^- proceeds via a sequence of elementary steps involving oxidative adsorption of Br^- on Pt to form Br, which can then generate Br_2 either by dimerization and/or by reacting electrochemically with Br^- in solution.[18] Recent data obtained by means of sensitive EQCN nanogravimetry measurements on the effect of halogen ions on Pt dissolution showed that adsorption of Br^- leads to net positive mass changes and that of Cl^- to net negative mass changes in the oxide region.[21]

This chapter serves to investigate and critically appraise the results of anodic oxide growth on platinum in sulphuric acid electrolytes containing bromide ions.

6.2 Experimental

Please refer to chapter 2 for a description of the appropriate techniques employed as part of this investigation. The in-house cell employed is described in section 2.3.1 (Figure 2-3) and the electrode holder is shown in Figure 2-4. The platinum quartz electrodes were pre-treated as discussed in section 2.2.2. The electrolyte of 0.5 M H_2SO_4 containing bromide ions were prepared by following section 2.2.3.3. The potentiostat and the QCM were connected as discussed in section 2.3.2. The QCM was calibrated as discussed in section 2.4.6.1. The electrochemical procedures followed section 2.4.5. The mass changes were recorded with a QCM and analyzed as discussed in section 2.4.6.2. The physical characterization of the Pt quartz after subjected to electrochemical procedures, ICP-MS was used to determine Pt content in the electrolyte as discussed in section 2.6.1.

6.3 Results and discussion

6.3.1 CV and EQCM results

The effect of bromide on the voltammetric features of Pt is easily observed by comparing the voltammograms of Pt recorded without Br^- present (Figure 6-1), and with Br^- present as shown in the annotated cyclic voltammograms (Figures 6-2 to 6-4).

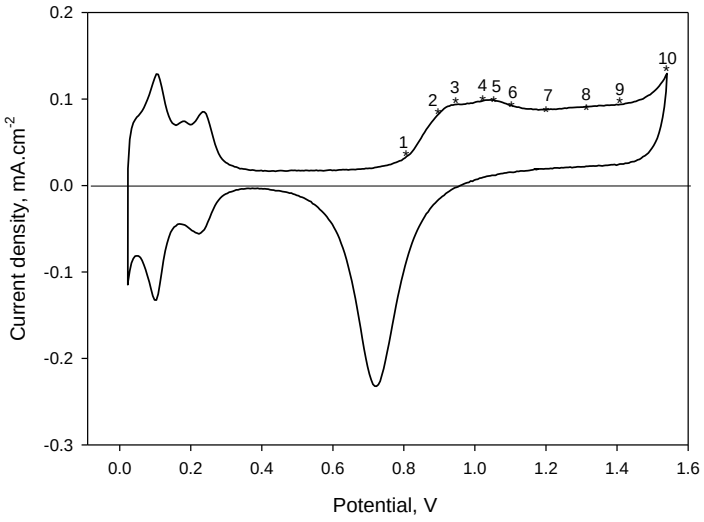

No.	E_p (V)
1	0.80
2	0.90
3	0.95
4	1.00
5	1.05
6	1.10
7	1.20
8	1.30
9	1.40
10	1.50

Figure 6-1: Typical cyclic voltammogram of Pt in deoxygenated 0.5 M H_2SO_4 (halogen ions not present) recorded at a scan rate of 50 mVs^{-1}

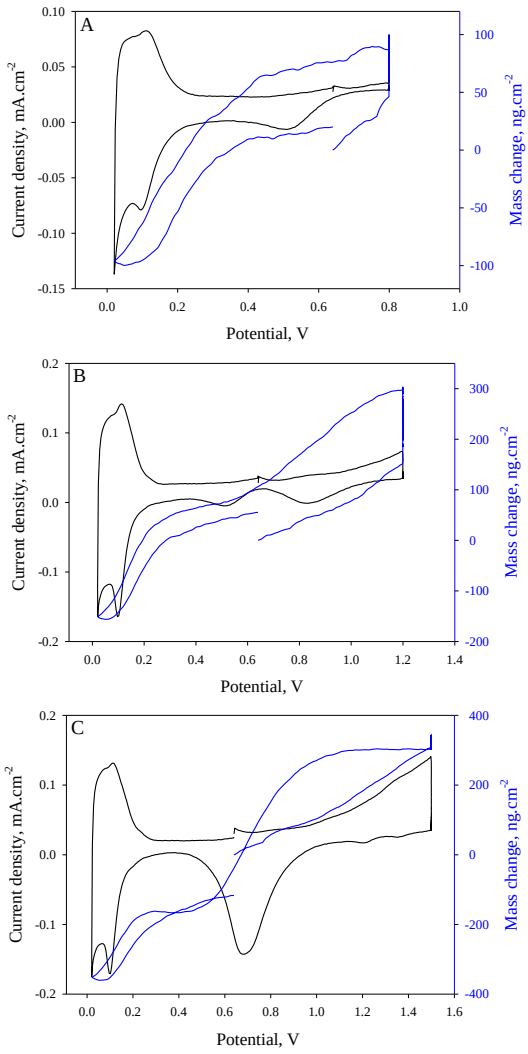

Figure 6-2: CVs and mass changes for 6 µM Br^- (E_p = (A) 0.80, (B) 1.20 and (C) 1.50 V)

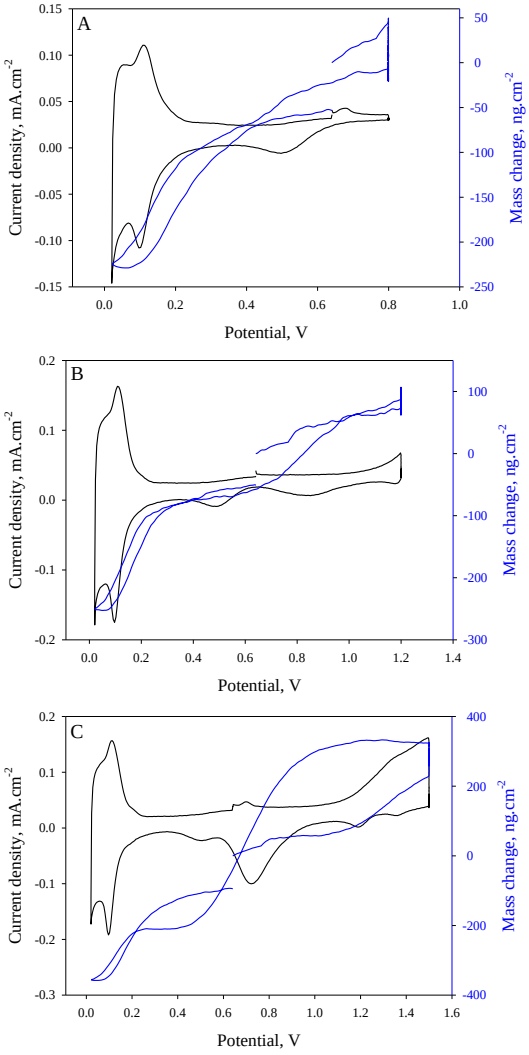

Figure 6-3: CVs and mass changes for 60 µM Br^- (E_p = (A) 0.80, (B) 1.20 and (C) 1.50 V)

Starting the anodic cycle at 0.6 V the EQCM results shown in Figures 6-2 to 6-4 point towards mass increases of ~300 ng cm^{-2} (6 µM Br^-), ~220 ng cm^{-2} (60 µM Br^-) and ~190 ng cm^{-2} (600 µM Br^-) at E_p's of 1.5 V. These results show progressive interference in the platinum oxidation process by Br^- ions with increasing Br^- concentration. An important feature of the EQCM mass increase curves is that a change in slope occurs at ~1.2 V in all instances and that this feature occurs at a mass gain of ~100 ng cm^{-2}, translating to about 50% coverage. Reference to the work of Zolfaghari *et al.*[14], using a series of voltammograms with successive addition of Br^-, reported an anodic isopotential point at ~1.3 V, which points to a situation in which oxide and Br^- species share the electrode surface. It can therefore be concluded that only adsorbed Br^- ions exist on the Pt surface from the double layer region up to about 1.2 V, whereupon O species increasingly co-occupy the surface to form oxide in the presence of Br^- ions. In a 600 µM Br^- electrolyte the mass increase when proceeding from 1.2 V to 1.5 V (~100 ng cm^{-2}) corresponds to ~2.5 ML of oxygen.

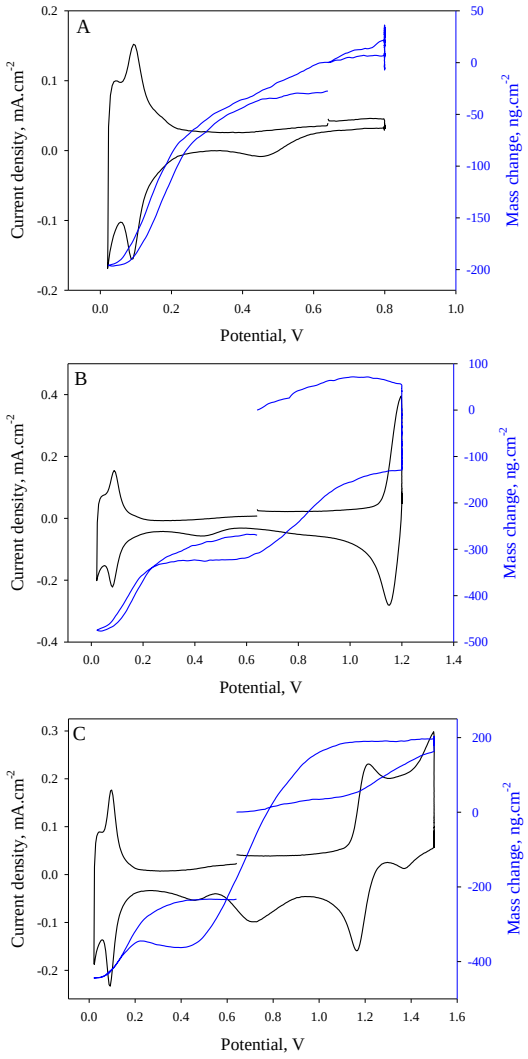

Figure 6-4: CVs and mass changes for 600 µM Br^- (E_p = (A) 0.80, (B) 1.20 and (C) 1.50 V)

Referring to Figures 6-2 and 6-4 it is clear that considerably more adsorbed Br^- accumulates on the Pt surface at E_p = 1.2 V than at an E_p of 1.5 V. For the 6 µM Br^- electrolyte the adsorbed $Br^-$is 74% less at 1.5 V and for the 600 µM Br^- electrolyte 80%. (The values for the 60 µM Br^- electrolyte are inconclusive). This phenomenon might be ascribed to increasing bromide evolution, which was reported to start at 1.2 V.[17] Comparison of the nine CVs shown in Figures 6-2 to 6-4 with the CV shown in Figure 6-1 reveals clear interference in the hydrogen adsorption/ desorption processes by Br^-, across all concentrations from 6 µM to 600 µM. The weak adsorption and desorption peak pair of hydrogen at 0.21 V disappears altogether in the presence of Br^-, clearly making way for the adsorption of Br^-. At the same time the strong adsorption and desorption peak pair of hydrogen at 0.1 V becomes more pronounced with an increase in Br^- concentration, pointing towards some synergism between the weakly bound $H_{ads/des}$ and Br^-.

As one moves down group 7 of the periodic table the dissociation strength of the acid decreases, which point towards an increasing affinity between H and bromide. This could well be explaining the disappearance of the weakly bound H that is now associated with the halide in 'acidic' form. In the case of chloride both hydrogen peaks (strongly and weakly bound H) were observed, which points towards the fact that HCl is a strong acid that dissociates completely with poor affinity between H and Cl^- (see Chapter 5).

The formation of the oxide layer starts at increasingly more anodic potentials with increasing bromide concentration. The occurrence of an anodic isopotential point at ~1.3 V, alluded to above, seems very significant. Development of Br_2 is reported to start at ~1.2 V.[22] The instantaneous drop in the current after the holding time t_p is thought to indicate the desorption of Br_3^- and can be correlated with a change in the slope of the anodic part of the CVs. The presence of Br_2 on the electrode surface creates the opportunity for reaction between Br and Br_2 to form Br_3^- (*cf.* Mastragostino & Gramellini[23]). In the present work mass losses starting at ~1.100 V seem to suggest the reduction of Br_3^-. The relatively large peak at ~0.7 V (which seems to correlate with an anodic peak at +0.7 V (see Figure 6-4 (C)) and accompanied by a small mass increase in Figure 6-4

(C)) can possibly be explained by PtO reduction. The reduction currents (*cf.* Figures 6-2 (C), 6-3 (C) and 6-4 (C)) are 0.142, 0.100 and 0.098 mA cm^{-2}, respectively. This indicated the progressive blocking of oxide formation with increasing Br^- concentration. The peak at 0.5 V is only present in the 60 and 600 µM Br^- electrolytes (*cf.* Figures 6-3 (C) and 6-4 (C)) and is accompanied by the slowing down and even stabilizing of the mass loss in the reduction cycle. This peak, associated with increasing bromide concentration, could be ascribed to the reduction of a platinum bromide complex.

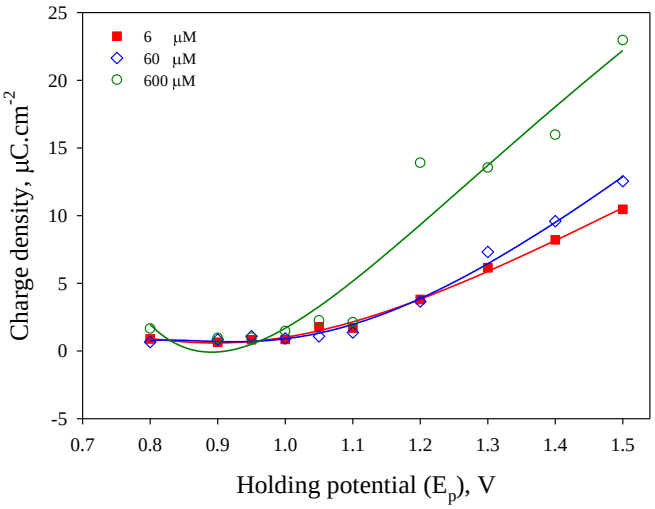

Figure 6-5: Additional charge density flow after holding for 100 s at E_p, followed by reversal of polarization direction in 6, 60 and 600 µM Br^-

Figure 6-5 depicts the charge density accumulated during the holding time of 100 s at each holding potential E_p. This figure illustrates a clear trend of increasing charge density coupled with increasing bromide concentration, which illustrates increasing platinum oxide formation, platinum dissolution, bromine evolution, and the formation of Br_3^-. This is evident in that the charge density is similar for 6, 60 and 600 µM of bromide up to 1.1 V. From 1.2 V onwards an increasing charge density is observed that correlates with increasing bromide concentration.

6.3.2 Combination of ICP and EQCM results

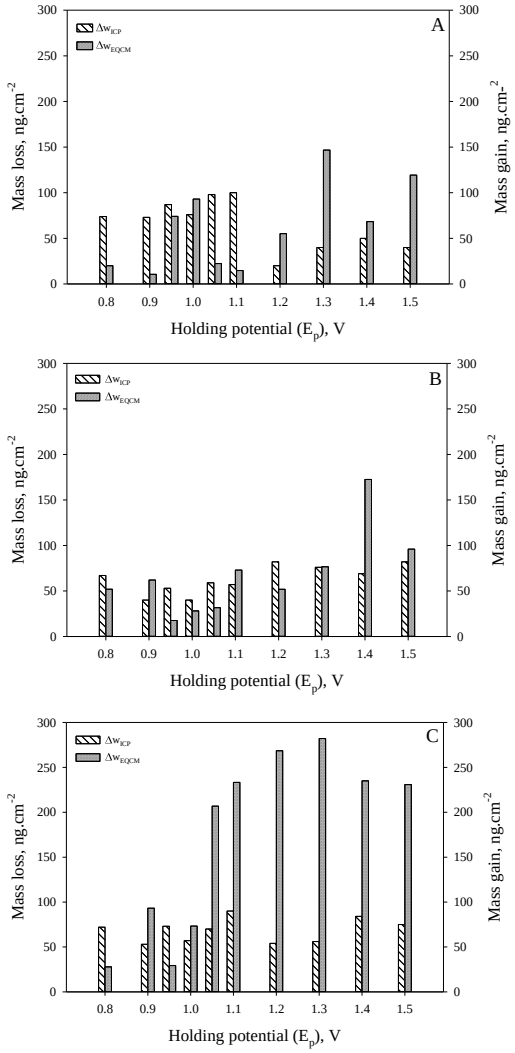

Figure 6-6: Values of mass loss $\Delta w_{(ICP)}$ and mass gain $\Delta w_{(EQCM)}$ as a function of E_p's at Br^- of (A) 6 µM, (B) 60 µM and (C) 600 µM

Without ascribing specific processes to the observations, which would be quite impossible at this stage, it is clear from Figures 6-6 (A) to (C) (where the $\Delta w_{(EQCM)}$ was calculated from Figure 2B (A), (B) and (C) in Appendix B) that an increasing bromide concentration correlates with an increase in mass from 6 to 600 µM, with an increase in mass being initiated somewhere between 60 and 600 µM. It is hypothesised that this is due to the strong adsorption of the bromide ion, which was not seen in the case of chloride. In fact, an increase in chloride concentration correlated with an increasing mass loss pointing towards an increase in platinum dissolution. This trend is more apparent in the case of the iodide ion, where an even greater increase in mass is observed, which is associated with a more pronounced adsorption of the iodide ion (see Chapter 7).

6.4 Conclusions

Results presented in this section are considered important as they contribute to new insights into the electrochemistry of the $Pt/Br^-/Br_2$ system. The strong adsorption of the bromide ion affects the adsorption of hydrogen in that the weakly adsorbed hydrogen peak, compared to that of chloride, is not observed. This is ascribed to stronger association of hydrogen with bromide leading to the 'formation' of HBr. The strong adsorption of the bromide ion (see the bar charts of Figure 6-6) coupled with the strong blocking effect of Br^- on oxide formation could be illustrated by the diminishing reduction current for oxide reduction as the Br^- concentration increases. Holding potentials (E_p) up to 1.1 V do not have any significant effect on the platinum surface in the presence of the bromide ion, whereas holding potentials in excess of 1.1 V show a clear increase in surface processes (platinum oxide formation, platinum dissolution, bromine evolution, and the formation of Br_3^-) as the bromide concentration increase. The important role played by Br_3^- and the conditions under which

it is formed and removed from the electrode surface is alluded to. Since before 1932 it has been known that relatively high concentrations of Br^- can react with Br_2 to form the Br_3^- anion.[24] It is therefore surprizing that more recent work on the electrochemistry of bromide largely ignores the possibility of its formation. Although the relevant peaks are clearly discernible in their published voltammograms many authors fail to recognize the possible presence of Br_3^-.[11,14,15]

6.5 References

1 Attard, G. A. A phenomenological theory of electrosorption. *Journal of Electroanalytical Chemistry **819**, 481-494* (2018).

2 Alsabet, M., Grden, M. & Jerkiewicz, G. Comprehensive study of the growth of thin oxide layers on Pt electrodes under well-defined temperature, potential, and time conditions. *Journal of Electroanalytical Chemistry* **589**, 120-127 (2006).

3 Harrington, D. A. Simulation of anodic Pt oxide growth. *Journal of Electroanalytical Chemistry* **420**, 101-109 (1997).

4 Birss, V. I., Chang, M. & Segal, J. Platinum oxide film formation-reduction: an in-situ mass measurement study. *Journal of Electroanalytical Chemistry* **355**, 181-191 (1993).

5 Imai, H., Izumi, K., Matsumoto, M., Kubo, Y., Kato, K. & Imai, Y. In situ and real-time monitoring of oxide growth in a few monolayers at surfaces of platinum nanoparticles in aqueous media. *Journal of the American Chemical Society* **131**, 6293-6300 (2009).

6 Saveleva, V. A. Papaefthimiou, V., Daletou, M.K., Doh., W.H., Ulhaq-Bouillet., C., Diebold, M., Zafeiratos, S. & Savinova, E.R. Operando near ambient pressure XPS (NAP-XPS) study of the Pt electrochemical oxidation in H_2O and H_2O/O_2 ambients. *The Journal of Physical Chemistry C* **120**, 15930-15940 (2016).

7 Angerstein-Kozlowska, H., Conway, B. & Sharp, W. The real condition of electrochemically oxidized platinum surfaces: Part I. Resolution of component processes. *Journal of Electroanalytical Chemistry and Interfacial Electrochemistry* **43**, 9-36 (1973).

8 Qile, G. *Platinum oxide reduction kinetics on polycrystalline platinum electrodes* MSc thesis, Victoria, (2016).

9 Wakisaka, M., Suzuki, H., Mitsui, S., Uchida, H. & Watanabe, M. Identification and quantification of oxygen species adsorbed on Pt (111) single-crystal and polycrystalline Pt electrodes by photoelectron spectroscopy. *Langmuir* **25**, 1897-1900 (2009).

10 Ferro, S. & De Battisti, A. The bromine electrode. Part I: Adsorption phenomena at polycrystalline platinum electrodes. *Journal of applied electrochemistry* **34**, 981-987 (2004).

11 Devivaraprasad, R., Kar, T., Leuaa, P. & Neergat, M. Recovery of Active Surface Sites of Shape-Controlled Platinum Nanoparticles Contaminated with Halide Ions and Its Effect on Surface-Structure. *Journal of The Electrochemical Society* **164**, H551-H560 (2017).

12 Xu, J., Georgescu, N. S. & Scherson, D. A. The Oxidation of Bromide on Platinum Electrodes in Aqueous Acidic Solutions: Electrochemical and In Situ Spectroscopic Studies. *Journal of The Electrochemical Society* **161**, H392-H398 (2014).

13 Novak, D. & Conway, B. Competitive adsorption and state of charge of halide ions in monolayer oxide film growth processes at Pt anodes. *Journal of the Chemical Society, Faraday Transactions* **77**, 2341-2359 (1981).

14 Zolfaghari, A., Conway, B. E. & Jerkiewicz, G. Elucidation of the effects of competitive adsorption of Cl^- and Br^- ions on the initial stages of Pt surface oxidation by means of electrochemical nanogravimetry. *Electrochimica Acta* **47**, 1173-1187 (2002).

15 Breiter, M. Voltammetric study of halide ion adsorption on platinum in perchloric acid solutions. *Electrochimica Acta* **8**, 925-935 (1963).

16 Marković, N. M., Lucas, C. A., Gasteiger, H. A. & Ross, P. N. Bromide adsorption on Pt (100): rotating ring-Pt (100) disk electrode and surface X-ray scattering measurements. *Surface science* **365**, 229-240 (1996).

17 Hubbard, A. T. & Anson, F. C. Study of the Electrochemistry of Chloride and Bromide Complexes of Platinum,(II) and (IV) by thin layer electrochemistry. *Analytical Chemistry* **38**, 1887-1893 (1966).

18 Conway, B. E., Phillips, Y. & Qian, S. Y. Surface electrochemistry and kinetics of anodic bromine formation at platinum. *Journal of the Chemical Society, Faraday Transactions* **91**, 283-293 (1995).

19 Bell, J. G. & Wang, J. Current and potential oscillations during the electro-oxidation of bromide ions. *Journal of Electroanalytical Chemistry* **754**, 133-137 (2015).

20 Ferro, S., Orsan, C. & De Battisti, A. The bromine electrode Part II: reaction kinetics at polycrystalline Pt. *Journal of applied electrochemistry* **35**, 273-278 (2005).

21 Conway, B., Zolfaghari, A., Pell, W. & Jerkiewicz, G. Voltammetry, nanogravimetry and double-layer capacitance studies on chemisorption of Cl− and Br−, competitive with potential-dependent electrosorption of O species at Pt electrodes. *Electrochimica Acta* **48**, 3775-3778 (2003).

22 Hubbard, A. T. Study of the kinetics of electrochemical reactions by thin-layer voltammetry: I. theory. *Journal of Electroanalytical Chemistry and Interfacial Electrochemistry* **22**, 165-174, doi:http://dx.doi.org.nwulib.nwu.ac.za/10.1016/S0022-0728(69)80247-0 (1969).

23 Mastragostino, M. & Gramellini, C. Kinetic study of the electrochemical processes of the bromine/bromine aqueous system on vitreous carbon electrodes. *Electrochimica Acta* **30**, 373-380 (1985).

24 Griffith, R. O., McKeown, A. & Winn, A. G. The bromine-bromide-tribromide equilibrium. *Transactions of the Faraday Society* **28**, 101-107 (1932).

CHAPTER 7

Anodic oxide growth on platinum in sulphuric acid electrolytes containing iodide ions

7.1 Introduction

From an iodide concentration of ~6 μM, iodide ions are present in both the hydrogen region and the oxygen region of the platinum cyclic voltammogram.[1] In view of its high polarizability it is reasonable to accept that it adsorbs specifically onto Pt surfaces by the development of strong covalent bonds.[2] The electrochemical reduction and oxidation of iodide ions on platinum electrodes follow several paths, depending, *inter alia*, on the concentration of the iodide ions and/or the presence of platinum oxides on the electrode surface.[3-7]As already mentioned, halide ions adsorb irreversibly on the platinum surface and interfere with platinum oxidation at the anode.[3] The I^-/I_2 redox system was found to be reversible at low pH in iodide solutions with concentrations below ~10 mM, with the rate determining step being charge transfer to form iodine atoms.[8] The fast reactions lead to the formation of I_2, followed by the formation of I_3^-.[4,9] The adsorption of iodine atoms occurs in a nonuniform fashion in which only about 60% of the electrode surface seems to be available. It is thought that the rest of the surface may be covered in platinum oxide.[6-8] Films of platinum oxide inhibit the oxidation of other substances at a platinum electrode. For example, the oxidation of iodide ion to iodate ion and the oxidation of iodine to iodate were reported to be prevented by platinum oxide films generated anodically.[10] However, the oxidation of I^- to I_2 is not inhibited by the formation of an oxide film on the electrode surface.[9] The involvement of platinum oxides in the reduction of IO_3^- has also been reported.[5] Reaction 7-1, the formation of I_3^- out of I_2 and I^-, is very fast in both directions.[8]

$$I_2 + I^- \rightleftharpoons I_3^- \qquad (7\text{-}1)$$

Some experimental results are consistent with a model in which I^- ions migrate or diffuse through the layer of I_2 and are oxidized at the metal/I_2 interface, while iodine is being dissolved at the I_2/solution interface, eventually reaching a steady state.[4] Initially a compact, porous film grows linearly to form a thin, compact, amorphous layer, which is subsequently penetrated by I^- ions which are then transported through the electronically conducting film, partly by a Grotthuss type mechanism.[11] The *Grotthuss mechanism* describes the process by which protons diffuse through a hydrogen bonded network of water molecules leading to the concomitant cleavage of covalent bonds. Here it is suggested that a similar type of mechanism can explain the movement of I^- ions through an I_2 film by means of I_3^- ions.

The overall processes on an electrode surface could be controlled by any one of several reactions, depending on the potential. The double layer region current involves both faradaic current and double layer charging current. Using CV and EQCN measurements, in the absence of halide ions, the molecular weights of the interfacial species were determined, which were then identified as chemisorbed O (O_{chem}) at $0.85 \leq E \leq 1.10$ V and as O^{2-} in the form of surface PtO at $1.20 \leq E \leq 1.40$ V.[12] It was found that in the 1.3 to 1.4 V region the platinum metal is fully covered by a protective PtO film.[13] This film can undergo further oxidation at 1.5 V to

form PtO_2.[14] By using an EQCM it was found that about 0.4 monolayer of iodine–containing species was adsorbed without a concomitant faradaic process.[7] The anodic oxide layers found on Pt are transient layers in the sense that they only exist while the potential is maintained. This may not necessarily apply to iodine layers as there are indications that the adsorbed iodide ions are transformed to an iodine surface film at higher potentials.[9]

This chapter serves to investigate and report on the results of the anodic oxide growth on platinum in sulphuric acid electrolytes containing iodide ions.

7.2 Experimental

Please refer to Chapter 2 for a description of the appropriate techniques employed as part of this investigation. The in-house cell employed is described in section 2.3.1 (Figure 2-3) and the electrode holder shown in Figure 2-4. The platinum quartz electrodes were pre-treated as discussed in section 2.2.2. The electrolyte of 0.5 M H_2SO_4 containing iodide ions were prepared following section 2.2.3.3. The potentiostat and the QCM were connected as discussed in section 2.3.2. The QCM was calibrated as discussed in section 2.4.6.1. The electrochemical procedures followed section 2.4.5. The mass changes were recorded with a QCM and analyzed as discussed in section 2.4.6.2. ICP-MS was used to determine Pt content in the electrolyte as discussed in section 2.6.1.

7.3 Results and discussion

7.3.1 CV and EQCM results

Figures 7-1 to 7-3 show CVs recorded in electrolytes containing 6, 60 and 600 μM iodide, with holding potentials ranging from 0.8 to 1.5 V. The CVs showed featureless double layer regions and a common feature is CVs with a severely altered (i) hydrogen adsorption/desorption region, and (ii) oxide region (compared to iodide free electrolytes). The presence of iodide is evident in both the hydrogen region and the oxygen region from iodide concentrations of 6 μM to 600 μM. Compared to chloride, and to a lesser extent bromide, no hydrogen adsorption and desorption is observed in the presence of iodide, which clearly shows (i) the very strong adsorption of iodide to the surface, and (ii) how the surface is blocked by iodide/iodine preventing any other active species from reaching and interacting with the surface (compare Figures 5-3 (C), 6-4(C), and 7-3(C)). In the presence of chloride two hydrogen adsorption/desorption peaks are observed, whereas in the case of bromide only one is observed and in the case of iodide no hydrogen adsorption/desorption peaks are observed. It seems reasonable to assign the peak at 0.68 and 0.75 V to iodide adsorption. Iodine evolution takes place at holding potentials above 1.2 V (Figures 7-1 (C), 7-2 (C), and 7-3 (C)) as per reaction 7-2. It would seem that the oxidation of iodide (I^-) to iodine (I_2), reaction 7-2, is initiated at about 1.2 V, with a prominent peak being observed at 1.35 V, which is ascribed to iodine formation.

$$2I^- \rightleftharpoons I_2 + 2e^- \qquad (7\text{-}2)$$

$$I_2 + I^- \rightleftharpoons I_3^- \qquad (7\text{-}3)$$

With iodine now being present at the surface, together with bound iodide, the formation of the tri-iodide ion (I_3^-) (reaction 7-3) is inevitable and is observed as the shoulder formed just below 1.4 V (see Figure 7-3 (C)). The adsorption of iodide initially forms a thin compact and amorphous iodine film that grows linearly, which is subsequently penetrated by I_3^- ions.[4,8,9,11,15] The passivation (decrease in current) of the platinum surface at high potentials is supported by the work of Johnson who observed that iodine coexisted with I^- in an irreversible state of adsorption.[16] On the return sweep, i.e. the cathodic sweep, the formed tri-iodide is reduced at about 1.0 V, which is followed by the reduction of the formed iodine to produce iodide, with a peak observed at 0.68 V (Figures 7-1 (C), 7-2 (C), and 7-3 (C)).

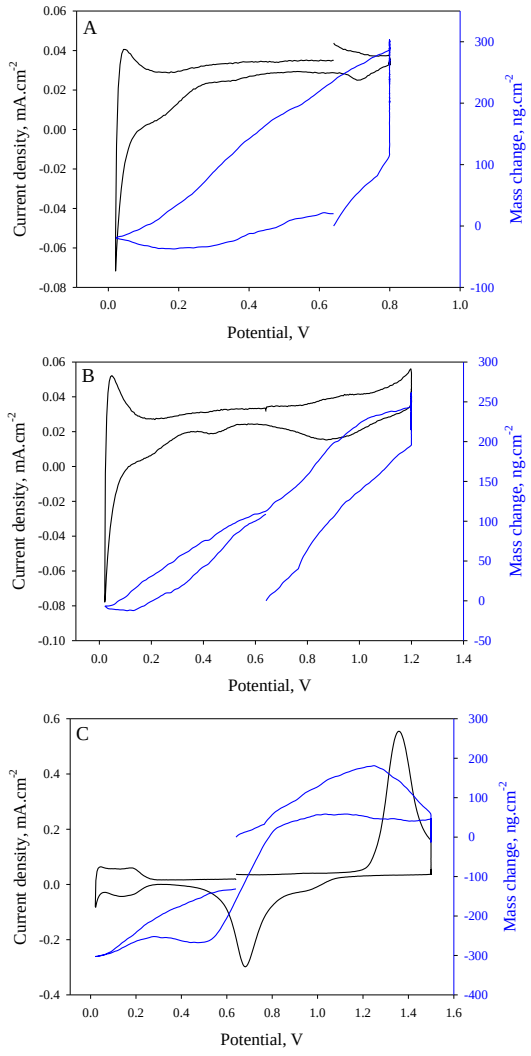

Figure 7-1: CVs and mass changes for 6 µM I^- (E_p = (A) 0.80, (B) 1.20 and (C) 1.50 V)

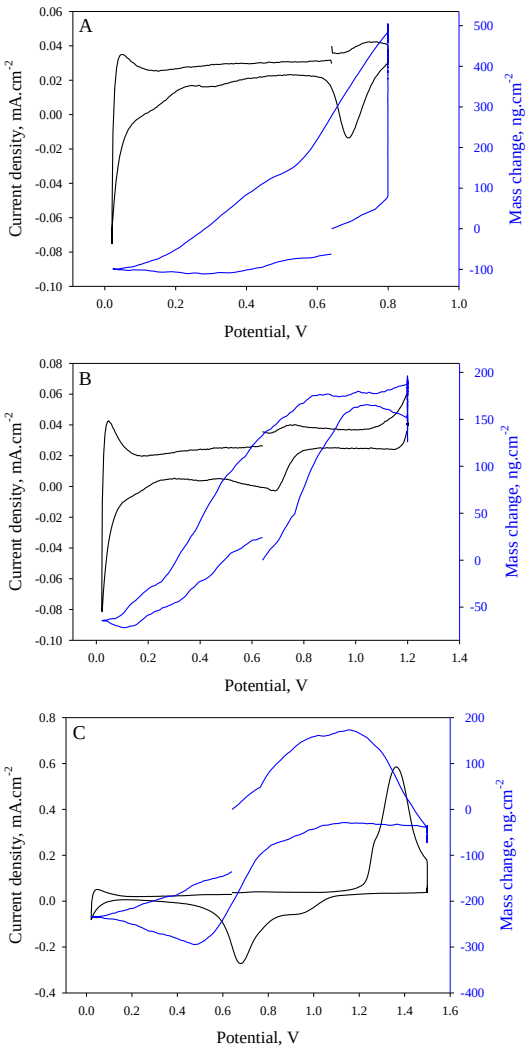

Figure 7-2: CVs and mass changes for 60 µM I^- (E_p = (A) 0.80, (B) 1.20 and (C) 1.50 V)

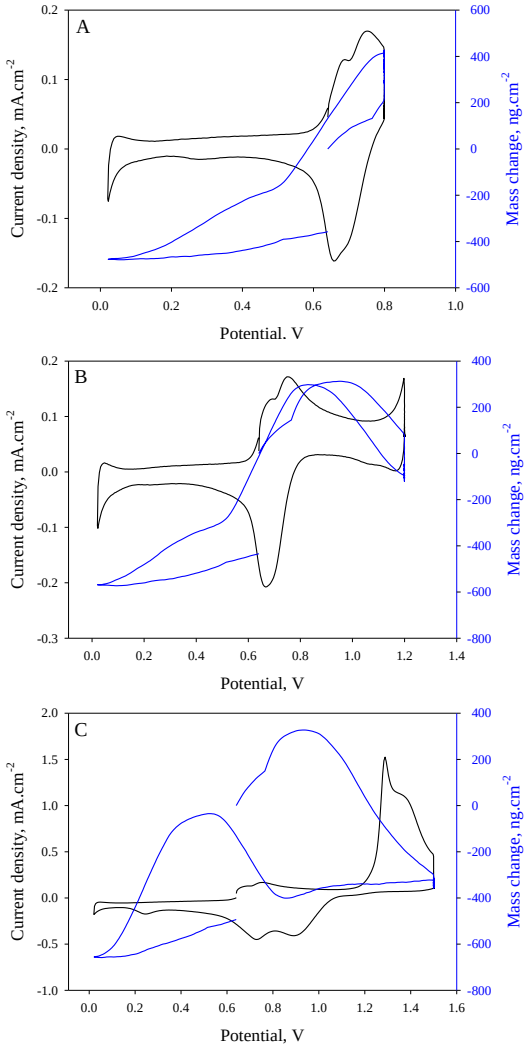

Figure 7-3: CVs and mass changes for 600 µM I^- (E_p = (A) 0.80, (B) 1.20 and (C) 1.50 V)

With regard to the observed change in mass (see Figure 7-3 (C)), the forward sweep, initiated at 0.63 V, results in an immediate increase in mass which is associated with the adsorption of iodide ions that carry substantial mass with it. This reaches a maximum and the mass then decreases as the iodide is oxidised to produce iodine. On the return sweep the mass stays relatively constant followed by an increase in mass with the formation of a platinum iodide. The mass then decreases as the platinum iodide is reduced to form a clean platinum surface (reactions 7-4, 7-5) at 0.2 – 0.4 V.[17]

$$PtI_4^{2-} + 2e^- \rightleftharpoons Pt + 4I^- \qquad (7\text{-}4)$$

$$PtI_6^{2-} + 2e^- \rightleftharpoons PtI_4^{2-} + 2I^- \qquad (7\text{-}5)$$

Figure 7-4 depicts the charge density accumulated during the holding time of 100 s at each holding potential E_p. In line with the case of bromide (Br^-), a very low and constant charge density is observed up to 1.1 V. From 1.2 V onwards the charge density increases, but goes through a maximum between 1.3 and 1.4 V subsequent to which it decreases pointing towards a passivation of the surface. The initial increase is in line with the increased availability of adsorbed iodide being converted into iodine. The iodine is a big molecule that does not move away from the surface and effectively blocks the surface from other incoming species including water, which would explain the drop in charge density that is associated with no formation of an oxide layer. This is in sharp contrast with bromide where an increase in charge density is observed, highlighting the fact that the surface is not blocked and that an oxide layer is formed (see Figure 6-5).

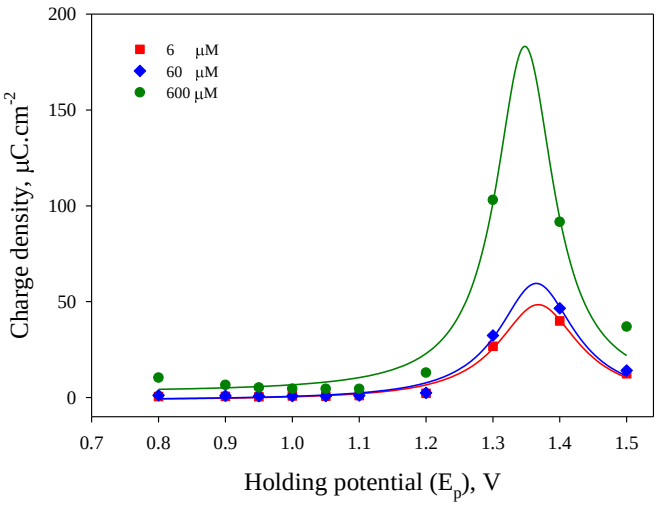

Figure 7-4: Additional charge density passed after holding at E_p for 100 s, followed by reversal of polarization direction for 6, 60 and 600 µM I^-

7.3.2 Combination of ICP and EQCM results

Similar to the observation with bromide, it is clear from Figures 7-5 (A) to (C) (where the $\Delta w_{(EQCM)}$ was calculated from Figure 2C (A), (B) and (C) in Appendix C) that an increasing iodide concentration correlates with an increase in mass from 6 to 600 µM, with an increase in mass being initiated somewhere between 60 and 600 µM. Again, this is hypothesised to be due to the strong adsorption of the iodide ion.

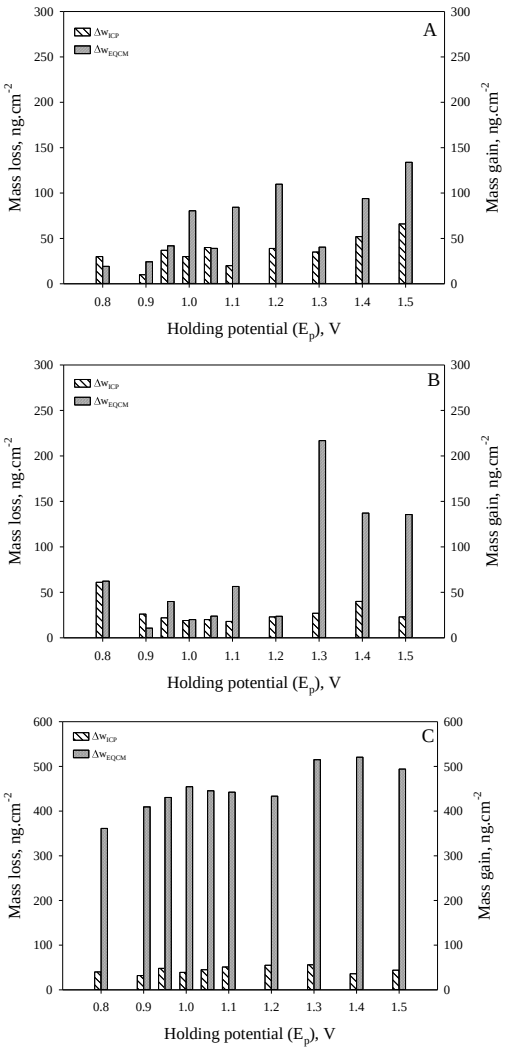

Figure 7-5: Values of mass loss $\Delta w_{(ICP)}$ and mass gain $\Delta w_{(EQCM)}$ as a function of E_p's at I^- of (A) 6 µM, (B) 60 µM and (C) 600 µM

7.4 Conclusions

The following new insights are important for a platinum surface in the presence of the iodide ion. It has been clearly shown that there is a definite tendency going from Cl^- to Br^-, to I^-, that hydrogen adsorption/desorption diminishes with two peak pairs being evident for Cl^-, one peak pair for Br^-, and no peaks for I^-. This correlates with the increasing size and adsorption strength of the halide ion. In contrast to the bromide ion, the platinum surface is passivated in the presence of the iodide ion at higher potentials resulting in no clear oxide layer being formed. This has been shown by both a decrease in current and mass. The main processes in the presence of iodide would be the formation of iodine and the tri-iodide ion, through the oxidation of the iodide ion, and the reduction of these species. No real mass loss is observed in the presence of iodide, less than 50 $ng.cm^{-2}$, compared to about 100 $ng.cm^{-2}$ in the case of bromide. In the presence of chloride, the amount of dissolved platinum was substantially higher (200 $ng.cm^{-2}$).

7.5 References

1 Breiter, M. Voltammetric study of halide ion adsorption on platinum in perchloric acid solutions. *Electrochimica Acta* **8**, 925-935 (1963).

2 Attard, G. A. A phenomenological theory of electrosorption. *Journal of Electroanalytical Chemistry* **819***, 481-494* (2018).

3 Devivaraprasad, R., Kar, T., Leuaa, P. & Neergat, M. Recovery of Active Surface Sites of Shape-Controlled Platinum Nanoparticles Contaminated with Halide Ions and Its Effect on Surface-Structure. *Journal of The Electrochemical Society* **164**, H551-H560 (2017).

4 Bejerano, T. & Gileadi, E. Formation of Thick Layers of Iodine During the Anodic Oxidation of Iodide on a RDE II. Open-Circuit Behavior. *Journal of The Electrochemical Society* **124**, 1720-1723 (1977).

5 Wels, B. R., Austin-Harrison, D. S. & Johnson, D. C. Electrocatalytic reduction of iodate at platinum electrodes in 0.5 M sulfuric acid. *Langmuir* **7**, 559-566 (1991).

6 Newson, J. & Riddiford, A. The kinetics of the iodine redox process at platinum electrodes. *Journal of the Electrochemical Society* **108**, 699-706 (1961).

7 Shu, Z. X. & Bruckenstein, S. Iodine adsorption studies at platinum. *Journal of electroanalytical chemistry and interfacial electrochemistry* **317**, 263-277 (1991).

8 Vetter, K. J. Der Einstellungsmechanismus des Jod-Jodid-Redoxpotentials an Platin auf Grund von Wechselstrompolarisation. *Zeitschrift für Physikalische Chemie* **199**, 285-299 (1952).

9 Beran, P. & Bruckenstein, S. Voltammetry of iodine (I) chloride, iodine, and iodate at rotated platinum disk and ring-disk electrodes. *Analytical Chemistry* **40**, 1044-1051 (1968).

10 Anson, F. C. & Lingane, J. J. Chemical evidence for oxide films on platinum electrometric electrodes. *Journal of the American Chemical Society* **79**, 4901-4904 (1957).

11 Swathirajan, S. & Bruckenstein, S. Ring-disk electrode studies of the formation, growth and transformation of iodine films formed during the anodic oxidation of iodide on platinum. *Journal of Electroanalytical Chemistry and Interfacial Electrochemistry* **112**, 25-38 (1980).

12 Jerkiewicz, G., Vatankhah, G., Lessard, J., Soriaga, M. P. & Park, Y.-S. Surface-oxide growth at platinum electrodes in aqueous H_2SO_4: Reexamination of its mechanism through combined cyclic-voltammetry, electrochemical quartz-crystal nanobalance, and Auger electron spectroscopy measurements. *Electrochimica Acta* **49**, 1451-1459 (2004).

13 Yadav, A. P. Stability of Platinum in Sulfuric Acid Solution Studied by Electrochemical Quartz Crystal Microbalance. *Journal of Nepal Chemical Society* **29**, 24-27 (2013).

14 You, H. *et al.* Resonance X-ray scattering from Pt (111) surfaces under water. *Physica B: Condensed Matter* **283**, 212-216 (2000).

15 Dawson, R. J. & Kelsall, G. H. Pt Dissolution and Deposition in High Concentration Aqueous Tri-Iodide/Iodide Solutions. *ECS Electrochemistry Letters* **2**, D55-D57 (2013).

16 Johnson, D. C. A study of the Adsorption and Desorption of Iodine at Platinum Electrodes in 0.1 M Sulfuric Acid. *Journal of the Electrochemical Society* **119**, 331-339 (1972).

17 Patel, A. & Dawson, R. Recovery of platinum group metal value via potassium iodide leaching. *Hydrometallurgy* **157**, 219-225 (2015).

CHAPTER 8

Concluding remarks

8.1 Conclusions

This work focused on the elucidation of aspects of the electrochemistry of polycrystalline platinum in 0.5 M sulphuric acid solution. Pt oxide is known to play a role in promoting Pt dissolution and, therefore, the investigation of its formation, structure and reduction provided the backdrop for the study of competitive reactions, such as those involving halide ions.

Prior to studying the effect of different halides on platinum, the use of glassy carbon electrodes to investigate the reduction of $[PtCl_6]^{2-}$ in HCPA electrolytes, employing numerous successive voltammetric scans, have revealed new insights into the different reactions occurring. By studying eight interrelated potential peaks (and areas) related to obtained CVs, it was ascertained that the reduction of $[PtCl_6]^{2-}$ to $[PtCl_4]^{2-}$ occurred between 0.15 and 0.03 V (SHE), followed by the incomplete reduction of $[PtCl_4]^{2-}$ to Pt. Furthermore, the simultaneous adsorption and desorption reactions of (H_2^+) and (H_3O^+) could be identified in the CVs and correlated with published results. A notable observation is the occurrence, under certain experimental conditions, of an isopotential point in the CVs, and to the knowledge of the author has not previously been reported for the electrolyte in question. The present experimental observations of the interplay between the reduction of $[PtCl_6]^{2-}/[PtCl_4]^{2-}$ and the reduction/oxidation of hydrogen-containing species perfectly fits the H_2^+/H_3O^+ model as described in chapter 3, and supports the mechanism for the HER to proceed via the adsorbed molecular hydrogen ion $(H_2^+)_{ads}$ as intermediate.

In a large number of models, depicting the electrochemical oxidation of platinum, a central generic theme is discernible. While it is generally accepted that oxidation of Pt proceeds in several overlapping stages the following basic steps in all these models comprise the following:

1. the adsorption of oxygen-containing species, i.e. $H_2O_{ads} \rightarrow OH_{ads} \rightarrow O_{ads}$, on the metal surface, and
2. place exchange between the adsorbed oxygen and platinum atoms leading to PtO, which is converted to PtO_2 at the metal electrolyte interface.

A new model based on a passivation perspective of the anodic oxidation process of Pt is presented. The build-up of a passive film (PtO/PtO_2) of the surface of the platinum gives rise to a decrease in the dissolution rate as the potential is increased.[1] The high rate of dissolution preceding oxide formation can be explained by classic metal passivation.[1] This model accounts for the changes in the surface morphology and chemical species that determine the characteristics of oxidized Pt surfaces. The possibility of oxygen entering the platinum lattice to form a solid solution was used in an attempt to cast new light on the phenomenon of hysteresis in the oxidation/reduction cycle. The continuous movement from the oxide at the oxide/Pt interface to the Pt lattice during logarithmic growth to a limiting thickness at the oxide/electrolyte interface is a central hypothesis of

the proposed model. It is argued that the locking of oxygen in tetrahedral and octahedral sites and in grain boundaries causes an imbalance in the charge density required to form and to reduce platinum oxide films resulting in these atoms being rendered electrochemically inactive, providing an explanation for the phenomenon of hysteresis in the reduction of anodic Pt films. This model furthermore allows for the oxidative and reductive dissolution of platinum that 'weakens' and dismantles the platinum surface, thereby facilitating chemical dissolution.

In the presence of chloride (Cl^-) ions, the anodic cycle of Pt revealed that the adsorption of chloride ions is favoured initially and eventually replaced by oxide species in the potential range 0.8 to ~1.1 V. The concentration of Cl^-, ranging from 6 to 600 μM, determines the extent of the replacement of Cl^- by O species and is manifested by a slight change in the slopes of the EQCM curves in the anodic direction. A higher chloride concentration of 600 μM has revealed a pronounced influence on the shape of the CV curves in the oxide region as oxide formation is influenced by adsorbed chlorine gas and the eventual evolution of chlorine at ~1.36 V. In the cathodic direction the reduction of adsorbed (and evolved) Cl_2 to Cl^- occurs. The comparison of EQCM mass curves with those derived from ICP Pt analyses afforded a new insight into the electrochemistry of Pt in 0.5 M H_2SO_4, containing chloride ions in that it became clear that surface damage caused by the reductive removal of Pt oxides led to an increased propensity to adsorb ions in the double layer region in the anodic part of a full voltammetric cycle. This insight places a question mark over the value of some published multi-cycle CVs. Alsabet *et al.*[2] subjected electrodes to a process that is referred to as "electrochemical annealing", which involved cycling electrodes 200 times between 0.05 and 1.50 V "to release any stress" before commencement of oxide growth experiments. This pretreatment inevitably caused considerable damage to the electrode surface.

In the presence of the bromide ion (Br^-) it is postulated that the tri-bromide ion (Br_3^-) plays a much more important role and more clarity has been gained on the conditions under which it is formed and removed from the electrode surface. In addition, the blocking effect of Br^- on oxide formation could be illustrated by the diminishing reduction current for oxide reduction as the Br^- concentration increases, and lastly, using mass change measurements the potential at which hydrogen adsorption starts could be determined.

In the presence of the iodide ion (I^-) an immediate observation was the disappearance of the hydrogen adsorption/desorption peaks. A clear tendency is observed in going from Cl^-, to Br^-, to I^-, in that hydrogen adsorption/desorption diminishes with two peak pairs being evident for Cl^-, one peak pair for Br^-, and no peaks for I^-. This would correlate with the increasing size and adsorption strength of the halide ion. The iodide ion, furthermore, leads to passivation of the platinum surface, in contrast to both the chloride and bromide ions. This was clearly observed in that no clear oxide layer formed at higher potentials in the presence of iodide, which was shown by both a decrease in current (CV) and mass (EQCM). It is postulated, based on these observations, that the main processes in the presence of iodide would be the formation of iodine (I_2) and the tri-iodide ion (I_3^-), through the oxidation of the iodide ion (I^-), and the reduction of these species. Lastly, in

the presence of iodide no real mass loss is observed; less than 50 ng.cm^{-2}, compared to about 100 ng.cm^{-2} in the case of bromide. In the presence of chloride, the amount of dissolved platinum was substantially higher (200 ng.cm^{-2}). This clearly shows that dissolution/leaching of platinum diminishes in the order $Cl^- > Br^- > I^-$.

This investigation is characterized by the wide-ranging topics studied. While the main focus was on the electrochemistry of platinum oxide formation, the influence of a number of factors active in the double layer, oxide, reduction and hydrogen areas received attention. It is concluded that the aims and objectives set out for this investigation have largely been met and that a number of valuable new insights gained, leading to a better understanding of Pt electrochemistry.

8.2 Recommended future work

- This study should be extended with a more in-depth investigation and critical thought given to isopotential point observed in Chapter 3 (Figure 3-1 (A)). Isopotential points were observed on a few occasions related to multiple cyclic voltammograms, however, it was difficult to reproduce multiple cyclic voltammograms exhibiting these features. This could be investigated with the use of the EQCM in order to ascertain if the isopotential point is formed in the presence or absence of the evolution of hydrogen. The potential ingress of hydrogen into platinum during hydrogen evolution, and the possible link with the third hydrogen desorption peak (see below) and the isopotential points could also be further investigated.
- A more thorough investigation could be afforded to the third hydrogen desorption peak observed in Chapter 4 (Figure 4-2), which might be linked to the isopotential point.
- The cross-overs observed in the mass changes of the hydrogen regions (Chapter 5, 6 and to a lesser extent 7), should be given more attention, as it is not known why such is observed, with literature also not being conclusive.
- Molecular modelling studies could furthermore be conducted to fully explain the formation of anodic oxide films on platinum and to elucidate the hysteresis of the oxidation/reduction cycles.
- The EQCM could also be utilized to further probe the dissolution of platinum using multiple cycle voltammograms.

8.3 References

1 Geiger, S., Cherevko, S. & Mayrhofer, K. J. J. Dissolution of Platinum in Presence of Chloride Traces. *Electrochimica Acta* **179**, 24-31 (2015).

2 Alsabet, M., Grden, M. & Jerkiewicz, G. Comprehensive study of the growth of thin oxide layers on Pt electrodes under well-defined temperature, potential, and time conditions. *Journal of Electroanalytical Chemistry* **589**, 120-127 (2006).

APPENDIX A

The following figures were used to support results obtained in Chapter 5 (Section 5.3.2).

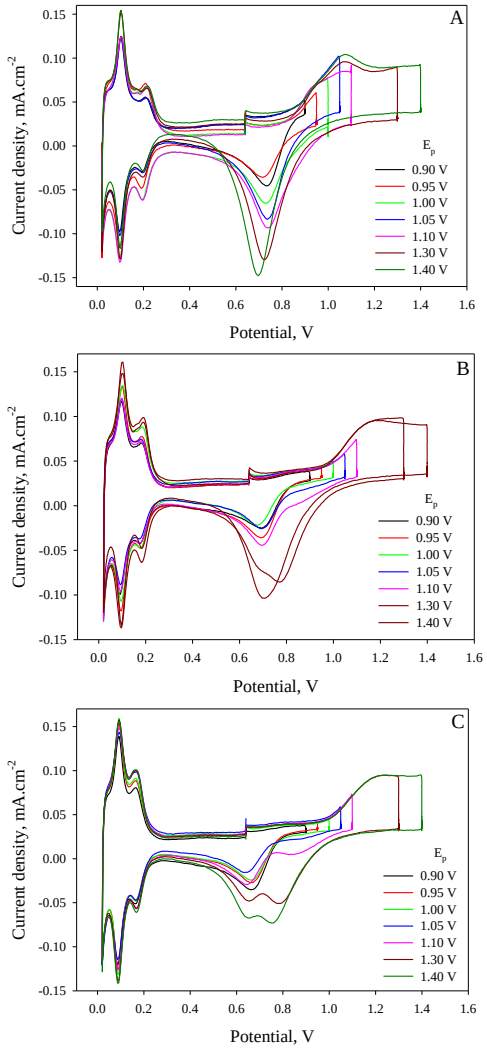

Figure 1A: CVs at different E_p's for A) 6 µM, B) 60 µM and C) 600 µM Cl^- at 50 mV s^{-1}

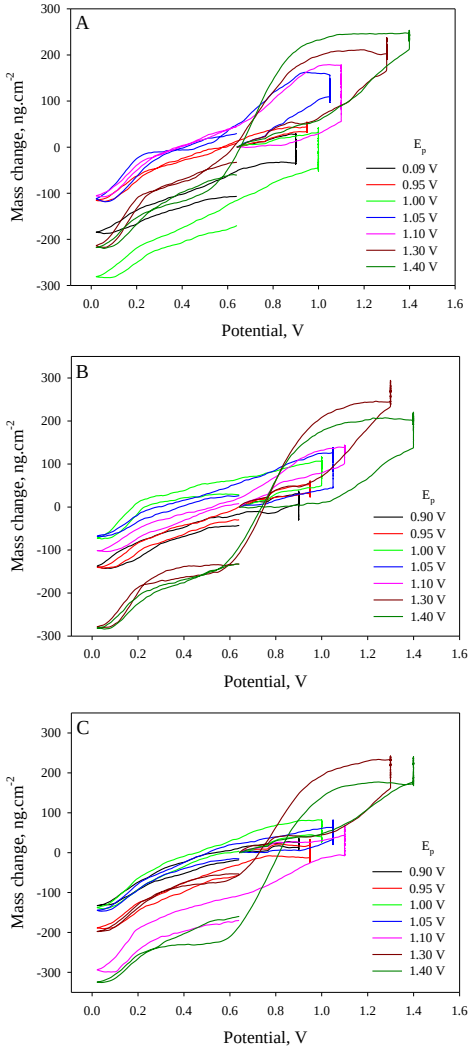

Figure 2A: Mass changes at different E_ps for A) 6 µM, B) 60 µM and C) 600 µM Cl^- at 50 mV s^{-1}

APPENDIX B

The following figures were used to support results obtained in Chapter 6 (Section 6.3.3).

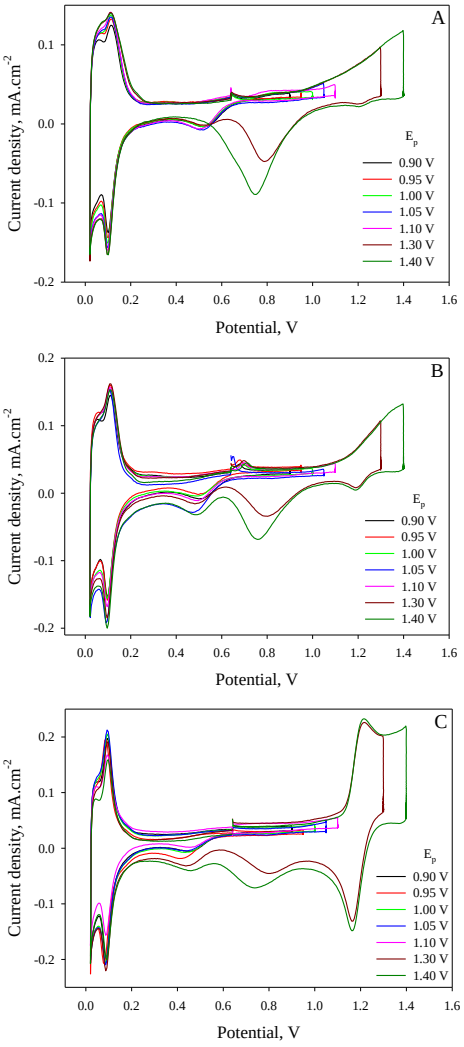

Figure 1B: CVs at different E_p's for A) 6 µM, B) 60 µM and C) 600 µM Br^- at 50 mV s^{-1}

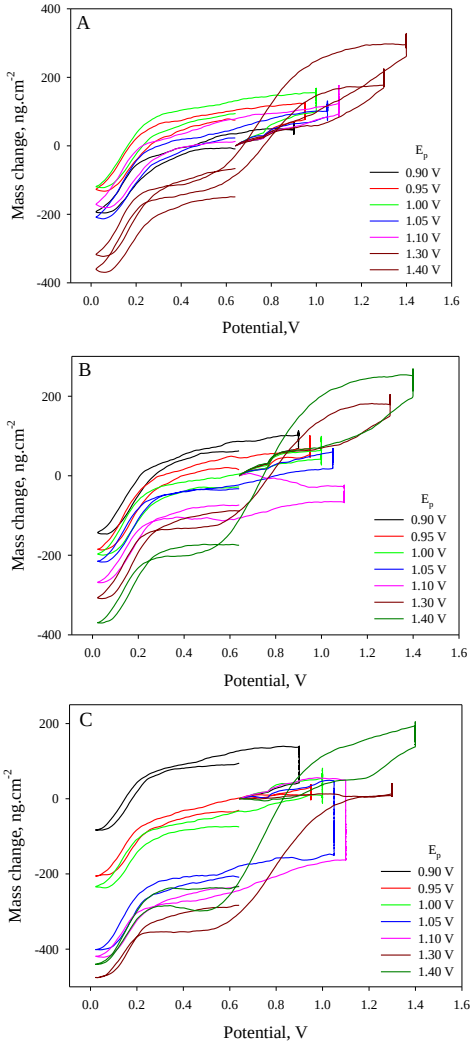

Figure 2B: Mass changes at different E_ps for A) 6 µM, B) 60 µM and C) 600 µM Br^- at 50 mV s^{-1}

APPENDIX C

The following figures were used to support results obtained in Chapter 7 (Section 7.3.2).

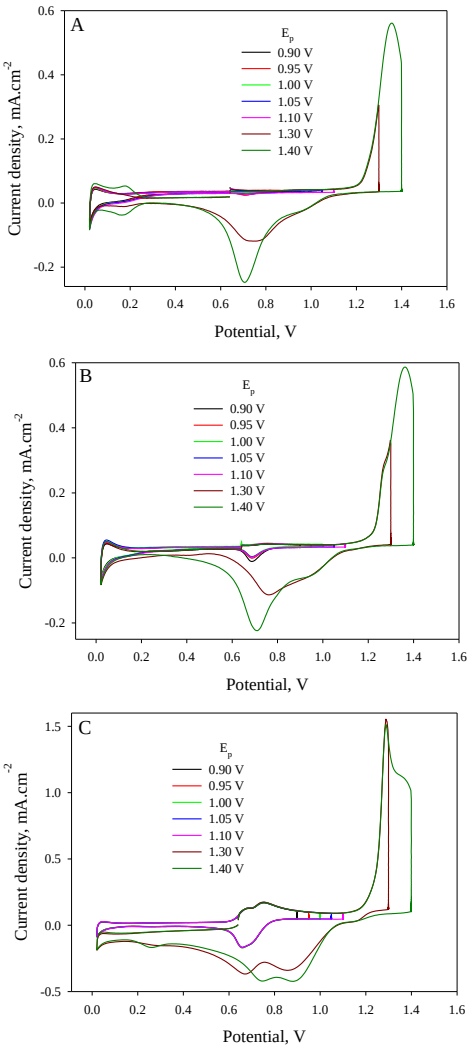

Figure 1C: CVs at different E_p's for A) 6 µM, B) 60 µM and C) 600 µM I^- at 50 mV s^{-1}

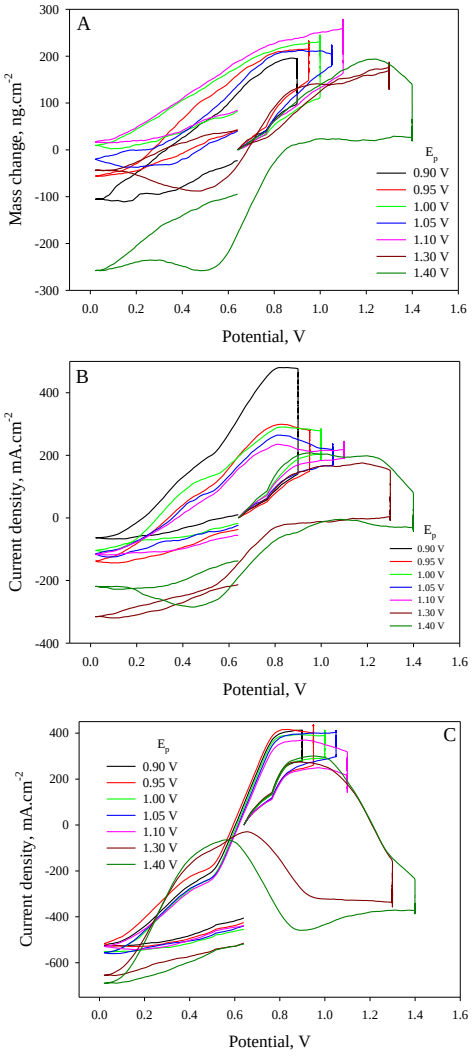

Figure 2C: Mass changes at different E_ps for A) 6 µM, B) 60 µM and C) 600 µM I^- at 50 mV s^{-1}